Mechanisms and Modeling of the Intestinal Absorption, Activation, and Systemic Availability of Gemcitabine and a Gemcitabine Prodrug for Oral Administration

by

Brian R. Thompson

A dissertation submitted in partial fulfillment
of the requirements for the degree of
Doctor of Philosophy
(Pharmaceutical Sciences)
in the University of Michigan
2020

Doctoral Committee:

Professor David E. Smith, Chair
Professor Gordon L. Amidon
Professor Kerby Shedden
Professor Emerita Donna S. Shewach
Professor Duxin Sun
Associate Professor Haojie Zhu

Brian R. Thompson

thompsbr@umich.edu

ORCID iD: 0000-0003-3055-9414

DEDICATION

To my parents, Claire and Gary,

for their unending love, support, and inspiration

ACKNOWLEDGEMENTS

With profound gratitude, I would first like to acknowledge my advisor, Dr. David E. Smith. Dr. Smith's mentorship and support were foundational not only to the successful completion of my doctoral research project, but also to my growth as a scientist. I am grateful to Dr. Smith for taking a sincere interest in my personal and professional development and encouraging me to widen my scientific training by enrolling in the Dual Master's Program in Statistics, completing internships, attending workshops, and the like. I also want to express my gratitude to Dr. Smith for demonstrating what it means to be a great mentor: being available and compassionate, valuing the input of team members, investing in the development of mentees, and providing honest feedback. The scientific knowledge and critical thinking skills instilled in me by Dr. Smith, as well as his example of great leadership, will be critical to my continued growth as I enter the next chapter of my life.

Next, I would like to recognize my dissertation committee members: Dr. Gordon L. Amidon, Dr. Kerby Shedden, Dr. Donna S. Shewach, Dr. Duxin Sun, and Dr. Haojie Zhu. Their insightful questions and comments were crucial to the completion and interpretation of my doctoral research project, specifically in understanding the implications of my work on patient care. Their time and expertise are much appreciated.

I would also like to thank past and present members of the Smith group, including Emily Briggs, Dr. Xiaomei Chen, Dr. Daniel Epling, Dr. Yongjun Hu, and Dr. Xiaoxing Wang, who made me feel welcome when first joining the lab and were generous with their

time and talents. I would like to thank Dr. Vikram M. Shenoy, Dr. Jian Shi, and Dr. Yasuhiro Tsume for their guidance and collaboration. Additionally, to the members of the College of Pharmacy who make everything possible, including Nicole Crandall, Dr. Cherie Dotson, Pat Greeley, Patrina Hardy, L.D. Hieber, Antoinette Hopper, Kylee Pulver, Carrie Vaquera, and the custodial staff, I am grateful for your hard work, availability, and patience.

During my time in graduate school I have been fortunate to develop many close friendships outside of my research. To these people, including Simon Essig Aberg, Katie L. Cavanagh, Dr. Todd A. Chan, Dr. Derek S. Frank, Billy Grant, Dr. Nicole Yadon, Dr. Nick Waltz, and many others, I am grateful for your friendship, inspiration, and empathy. I also thank you for your role in making me a more thoughtful, caring, and informed person. Additionally, I want to acknowledge Mike Chadwick, Matt Farrell, and Brett Wiebell; I am grateful for your friendship and support, despite the physical distance between us.

To my parents, Claire and Gary, and my sisters, Laura and Melissa, I am grateful for the love, support, and encouragement you have provided my entire life. I am truly fortunate for your willingness and ability to provide me with advice and reassurance, no matter the time or situation. All that I have achieved and all that I will achieve would not be possible without you.

Finally, I want to express my appreciation for the funding from the University of Michigan College of Pharmacy, the National Institutes of Health, and the Pharmacological Sciences Training Program grant that made my graduate education possible.

In closing, graduate school has been a time of great intellectual and personal growth. I want to thank everyone who helped ensure that, as my dad predicted when I first

matriculated, I will look back fondly on my time in graduate school as some of the best years of my life.

TABLE OF CONTENTS

LIST OF TABLES

LIST OF FIGURES

LIST OF APPENDICES

ABSTRACT

Gemcitabine (2'-2'-difluoro-deoxycytidine) is an intravenously administered nucleoside analogue used in the treatment of various solid tumor cancers. While oral gemcitabine administration would offer a more patient-friendly, less complex, and less expensive alternative to intravenous administration, the clinical utility of oral gemcitabine administration is hindered by a low oral bioavailability of approximately 10%. This low oral bioavailability was previously believed to be the result of gemcitabine's low intestinal permeability and oral absorption, followed by significant presystemic metabolism by the enzyme cytidine deaminase (CDA).

In one study, we sought to define the mechanisms of gemcitabine intestinal permeability, the potential for saturation of intestinal uptake, and the transporter(s) responsible for mediating the oral absorption of drug using *in situ* single-pass intestinal perfusions in mice. Concentration-dependent studies were performed for gemcitabine over 0.5 to 2000 μM, along with studies of 5 μM gemcitabine in a sodium-containing buffer ± thymidine (which can inhibit concentrative (*i.e.,* CNT1 and CNT3) and equilibrative (*i.e.,* ENT1 and ENT2) nucleoside transporters) or dilazep (which can inhibit ENT1 and ENT2), or in a sodium-free buffer (which can inhibit CNT1 and CNT3). Our findings demonstrated that gemcitabine was, in fact, a high-permeability drug in the intestine at low concentrations, that jejunal uptake of gemcitabine was saturable and mediated almost exclusively by nucleoside transporters, and that jejunal flux was mediated by both high-

affinity, low-capacity (K_m = 27.4 μM, V_{max} = 3.6 pmol/cm^2/s) and low-affinity, high-capacity (K_m = 700 μM, V_{max} = 35.9 pmol/cm^2/s) transport systems. Thus, CNT(s) and ENT(s) at the apical membrane allow for gemcitabine uptake from the lumen to enterocyte, whereas ENT(s) at the basolateral membrane allow for gemcitabine efflux from the enterocyte to portal venous blood. These results further show that systemic exposure following oral gemcitabine administration is limited by extensive CDA-mediated presystemic metabolism and potentially by saturation of nucleoside transporter-mediated intestinal uptake following oral administration of large doses (*i.e.,* doses which generate saturating gemcitabine concentrations in the intestinal lumen).

A subsequent study evaluated the *in vivo* performance of a peptide transporter 1 (PEPT1)-targeted amino acid ester prodrug of gemcitabine, 5'-L-valyl-gemcitabine (V-Gem), developed to increase gemcitabine's oral bioavailability. V-Gem was previously shown to be a substrate of the intestinally expressed PEPT1 and stable against CDA-mediated metabolism. However, earlier studies did not evaluate the *in vivo* oral performance of V-Gem as compared to parent drug. Therefore, we evaluated the pharmacokinetics and *in vivo* oral absorption of gemcitabine and V-Gem following intravenous and oral administrations in mice. These studies revealed that V-Gem undergoes rapid systemic elimination (half-life < 1 min) and has a low oral bioavailability (< 1%). Most importantly, the systemic exposure of gemcitabine was not different following oral administration of equimolar doses of gemcitabine (gemcitabine bioavailability of 18.3%) and V-Gem (gemcitabine bioavailability of 16.7%). Single-pass intestinal perfusions with portal blood sampling in mice revealed that V-Gem undergoes extensive activation (*i.e.,* conversion to gemcitabine) in intestinal epithelial cells and that

gemcitabine undergoes first-pass metabolism in intestinal epithelial cells. Thus, formulation of gemcitabine as the prodrug V-Gem does not increase systemic gemcitabine exposure following oral dosing, due, in part, to the metabolic instability of V-Gem in intestinal epithelial cells. These findings suggest that future development of gemcitabine prodrugs for oral administration should focus on prodrugs with high intestinal permeability, high presystemic stability, and complete *in vivo* conversion to gemcitabine.

CHAPTER 1

Research Objectives

Gemcitabine is a nucleoside analog with regulatory approval for use in the treatment of pancreatic, lung (in combination with cisplatin), breast (in combination with paclitaxel), and ovarian (in combination with carboplatin) cancers [1]. Furthermore, gemcitabine is extensively used off-label in combination with other medications and for the treatment of other solid tumors [2]. Gemcitabine is utilized clinically for both its cytotoxic (*i.e.,* ability to kill cancer cells) and radiosensitizing (*i.e.,* ability to make cancer cells more sensitive to radiation therapy) properties [3, 4]. Generally, gemcitabine is administered to patients via a 30-minute intravenous infusion, once per week at a dose of 1,000 – 1,250 mg/m^2 [1]. Although not currently available, an orally administrable formulation would benefit patients, providers, and payers by making gemcitabine administration more patient-friendly, safer, and cheaper. Furthermore, orally administrable gemcitabine would enable a variety of dosing regimens which may increase the efficacy and/or reduce the toxicity associated with gemcitabine therapy but are difficult to implement when the drug is administered intravenously (*e.g.,* frequent low dose administration) [5, 6].

Despite these advantages associated with oral administration, the clinical utility of orally administered gemcitabine is hampered by a low oral bioavailability of approximately 10% [7]. Although few studies have explored the mechanistic basis of this low oral bioavailability, it is generally believed to be a result of incomplete absorption from the gastrointestinal tract and first-pass metabolism in the intestinal epithelium and/or liver by the enzyme cytidine deaminase [7, 8]. While various formulation strategies may be employed to increase intestinal absorption and/or reduce first-pass metabolism, a better understanding of the barriers limiting gemcitabine's oral bioavailability is necessary for the rational application of these strategies to the design and development of gemcitabine formulations with increased oral bioavailability.

Specifically, although gemcitabine is widely considered to have low intestinal permeability, gemcitabine's intestinal absorption has not previously been systematically characterized. Furthermore, preliminary studies examining gemcitabine absorption utilized *in vitro* cell lines (*e.g.,* Caco-2 cells) which have low expression levels of intestinally expressed nucleoside transporters known to transport gemcitabine [8-11] and do not replicate important physiological aspects of intestinal drug absorption (*e.g.,* intact blood supply). Thus, studies which enhance the understanding of gemcitabine's intestinal absorption and its role in limiting oral bioavailability may provide critical information for the future development of orally administrable gemcitabine.

One such strategy to increase gemcitabine's oral bioavailability, formulating gemcitabine as the amino acid ester prodrug 5'-L-valyl-gemcitabine (V-Gem), may both increase gemcitabine's intestinal absorption and reduce gemcitabine's first-pass metabolism. First, while gemcitabine was widely believed to undergo limited intestinal

absorption, V-Gem was developed to act as a substrate of the intestinal uptake transporter peptide transporter 1 (PEPT1) (*i.e.* a PEPT1-targeted prodrug) [12]. PEPT1 is a high-capacity, low-affinity transporter extensively expressed on the apical membrane of intestinal enterocytes and has been successfully targeted to increase the intestinal uptake of low-permeability drugs via formation of PEPT1-targeted prodrugs. Such prodrugs, which are typically formulated by attaching an amino acid or dipeptide to the parent compound via an ester bond, undergo PEPT1-mediated intestinal uptake and are subsequently activated, liberating the parent compound [13]. Thus, as V-Gem was verified *in vitro* to be a PEPT1 substrate, it is expected to undergo increased intestinal absorption [10, 12]. Next, while gemcitabine undergoes cytidine deaminase-mediated first-pass metabolism in the intestine and/or liver [7], V-Gem is stable against cytidine deaminase-mediated metabolism during *in vitro* incubations with recombinant enzyme [14]. Therefore, V-Gem may protect gemcitabine against metabolism during first-pass transit through the intestine and/or liver and undergo subsequent activation. Importantly, V-Gem was shown to undergo *in vitro* activation mediated, at least in part, by the biphenyl hydrolase like enzyme [10, 15]. However, while this PEPT1-targeted prodrug V-Gem has been evaluated *in vitro* and shown promising properties for increasing gemcitabine's oral bioavailability (*e.g.,* V-Gem is a PEPT1 substrate, stable against cytidine deaminase-mediated metabolism, and enzymatically activated), this prodrug's *in vivo* pharmacokinetic performance has not previously been evaluated.

With the ultimate goal of enabling oral gemcitabine administration through increasing gemcitabine's oral bioavailability, along with the knowledge gaps detailed above, the following specific aims are proposed:

1) To characterize the mechanisms of gemcitabine oral absorption using *in situ* intestinal perfusions in mice
2) To evaluate the systemic availability and pharmacokinetic performance of gemcitabine and the valine gemcitabine prodrug, V-Gem, following oral and intravenous administrations in mice

References

[1] Gemzar [package insert]. Eli Lilly and Company, Indianapolis, IN, (2019).

[2] Conti R.M., Bernstein A.C., Villaflor V.M., Schilsky R.L., Rosenthal M.B., and Bach P.B., Prevalence of Off-Label Use and Spending in 2010 Among Patent-Protected Chemotherapies in a Population-Based Cohort of Medical Oncologists, J Clin Oncol. 31 (9) (2013) 1134-1139.

[3] Plunkett W., Huang P., Xu Y.Z., Heinemann V., Grunewald R., and Gandhi V., Gemcitabine: metabolism, mechanisms of action, and self-potentiation, Semin Oncol. 22 (4 Suppl 11) (1995) 3-10.

[4] Shewach D.S. and Lawrence T.S., Antimetabolite radiosensitizers, J Clin Oncol. 25 (26) (2007) 4043-4050.

[5] Yapp D.T., Wong M.Q., Kyle A.H., Valdez S.M., Tso J., Yung A., Kozlowski P., Owen D.A., Buczkowski A.K., and Chung S.W., The differential effects of metronomic gemcitabine and antiangiogenic treatment in patient-derived xenografts of pancreatic cancer: treatment effects on metabolism, vascular function, cell proliferation, and tumor growth, Angiogenesis. 19 (2) (2016) 229-244.

[6] Dehua Z., Mingming C., and Jisheng W., Meta-analysis of gemcitabine in brief versus prolonged low-dose infusion for advanced non-small cell lung cancer, PLoS One. 13 (3) (2018) e0193814.

[7] Veltkamp S.A., Jansen R.S., Callies S., Pluim D., Visseren-Grul C.M., Rosing H., Kloeker-Rhoades S., Andre V.A., Beijnen J.H., Slapak C.A., and Schellens J.H., Oral administration of gemcitabine in patients with refractory tumors: a clinical and pharmacologic study, Clin Cancer Res. 14 (11) (2008) 3477-3486.

[8] Chen G., Svirskis D., Lu W., Ying M., Huang Y., and Wen J., N-trimethyl chitosan nanoparticles and CSKSSDYQC peptide: N-trimethyl chitosan conjugates enhance the oral bioavailability of gemcitabine to treat breast cancer, J Control Release. 277 (2018) 142-153.

[9] Lim J.H., You S.K., Baek J.S., Hwang C.J., Na Y.G., Shin S.C., and Cho C.W., Preparation and evaluation of polymeric microparticulates for improving cellular uptake of gemcitabine, Int J Nanomed. 7 (2012) 2307-2314.

[10] Tsume Y., Incecayir T., Song X., Hilfinger J.M., and Amidon G.L., The development of orally administrable gemcitabine prodrugs with D-enantiomer amino acids: enhanced membrane permeability and enzymatic stability, Eur J Pharm Biopharm. 86 (3) (2014) 514-523.

[11] Takahashi K., Yoshisue K., Chiba M., Nakanishi T., and Tamai I., Involvement of Concentrative Nucleoside Transporter 1 in Intestinal Absorption of Trifluridine Using Human Small Intestinal Epithelial Cells, J Pharm Sci. 104 (9) (2015) 3146-3153.

[12] Song X.Q., Lorenzi P.L., Landowski C.P., Vig B.S., Hilfinger J.M., and Amidon G.L., Amino acid ester prodrugs of the anticancer agent gemcitabine: Synthesis, bioconversion, metabolic bioevasion, and hPEPT1-mediated transport, Mol Pharm. 2 (2) (2005) 157-167.

[13] Smith D.E., Clemencon B., and Hediger M.A., Proton-coupled oligopeptide transporter family SLC15: physiological, pharmacological and pathological implications, Mol Aspects Med. 34 (2-3) (2013) 323-336.

[14] Tsume Y., Drelich A.J., Smith D.E., and Amidon G.L., Potential Development of Tumor-Targeted Oral Anti-Cancer Prodrugs: Amino Acid and Dipeptide Monoester Prodrugs of Gemcitabine, Molecules. 22 (8) (2017) 1322.

[15] Kim I., Song X., Vig B.S., Mittal S., Shin H.-C., Lorenzi P.J., and Amidon G.L., A novel nucleoside prodrug-activating enzyme: substrate specificity of biphenyl hydrolase-like protein, Mol Pharm. 1 (2) (2004) 117-127.

CHAPTER 2

Background and Literature Review

2.1 Oral Route of Drug Administration

Oral administration is the most common and preferred route of drug administration as it is non-invasive, patient friendly, and cost-effective [1]. Additionally, when compared to other common routes of administration (*e.g.,* intravenous, intramuscular, subcutaneous), oral administration is associated with higher patient compliance and may offer greater flexibility in optimizing the dosing regimen [2]. For most drugs (*i.e.,* systemic-acting drugs), however, oral dosing presents additional barriers for drug activity as the active pharmaceutical ingredient (API) must be intestinally absorbed (*see Section 2.1.1*) and avoid first-pass metabolism in the gut and liver (*see Section 2.1.2)* to reach its site of action in the body. A drug's oral bioavailability (F_{oral}) is the fraction of the orally administered dose that enters systemic circulation and is a product of the fraction of the administered dose that is absorbed from the intestinal lumen (F_a), the fraction escaping first-pass intestinal metabolism (F_g), and the fraction escaping first-pass hepatic metabolism (F_h) (Eq. 1).

$$F_{oral} = F_a \, x \, F_g \, x \, F_h \qquad \text{(Eq. 1)}$$

Low oral bioavailability can preclude oral administration as therapeutic drug levels in plasma may be unachievable following oral administration and/or the high inter-individual variability in drug exposure associated with low bioavailability may be unacceptable for the given drug (*e.g.,* drugs with narrow therapeutic indices) [3]. For such drugs, either alternative administration routes are utilized or the drug is simply not developed as market forces strongly favor the development of orally administrable drugs [4].

2.1.1 Small Intestinal Drug Absorption

The small intestine is a tubular organ which functions as the main site of absorption for orally administered drugs (and nutrients). Although there is high inter- and intrasubject variability in the reported macroscopic dimensions of the small intestine, the mean diameter is approximately 2 - 4 cm [5] with reported mean lengths ranging from approximately 3 m to 7 m [6, 7]. The small intestine is subdivided into the duodenum, jejunum, and ileum, which account for approximately 5%, 40%, and 55% of the total length, respectively [8]. Although the site of drug absorption in the small intestine is dependent on many factors, most drugs are absorbed in the proximal small intestine [9]. The inner surface of the small intestine consists of a single-cell thick barrier, the intestinal epithelium, which separates the intestinal lumen from the portal blood and regulates the uptake of molecules into the body. The epithelium is comprised of intestinal epithelial cells, also known as intestinal enterocytes, connected via tight junctions. The surface area of contact between the intestinal lumen and epithelium is greatly increased by intestinal folding, as well as villi and microvilli structures present on the epithelium. This large

surface area, estimated to be ~ 30 m^2, aids in the absorption of orally ingested compounds [5].

Movement of drug from the intestinal lumen into portal blood occurs through either a paracellular and/or transcellular pathway (Figure 2.1). Paracellular absorption involves the movement of drug between intestinal epithelial cells and generally occurs only for small hydrophilic molecules with a positive charge [10, 11]. The extent of paracellular absorption is greatly limited by the presence of tight junctions between epithelial cells and the small surface area of the intestinal epithelium allowing for paracellular uptake of drug from the lumen (*i.e.,* < 0.01% of total surface area) [1]. Transcellular absorption is the major route of absorption for most drugs and involves the sequential partitioning of drug molecules across the epithelial cells' apical membranes (moving from the intestinal lumen into epithelial cells) and basolateral membranes (moving from epithelial cells into the portal blood). Drug molecules partition across these membranes mainly by passive diffusion through the membrane and/or by carrier-mediated transport [1]. Transcytosis mechanisms have also been implicated in the movement of nanocarriers and macromolecules across the intestinal membranes [12, 13]. Passive diffusion occurs mainly for lipophilic compounds which can travel directly through the lipophilic lipid bilayer comprising the epithelial cell membranes, diffusing from higher to lower concentrations. Other compounds, typically hydrophilic, are unable to travel directly through the membrane and instead are shuttled across the membrane by a transmembrane transport protein (*i.e.,* transporter) [9]. The transporters can either be facilitative, allowing only the passive transport of drug down its concentration gradient, or active, able to transport drug against the concentration gradient [14]. Intestinal enterocytes are known to express many transporters belonging to the

adenosine triphosphate-binding cassette (ABC) and solute carrier (SLC) superfamilies on both the apical and basolateral membranes. Several of these intestinally expressed transporters have been classified by the International Transporter Consortium as having a clinically important impact on oral drug absorption and systemic availability [15].

2.1.2 First-Pass Metabolism

While traversing the intestinal epithelium, moving from the intestinal lumen into the portal vein, the drug is subject to metabolism by enzymes expressed in intestinal epithelial cells [16]. The portal vein then carries the drug to the liver, the main site of metabolism in the body, where the drug is subject to metabolism by hepatic enzymes. The drug then exits the liver, entering systemic circulation (*i.e.,* hepatic vein). Drug metabolism in the intestine and/or liver that occurs prior to the drug entering systemic circulation is considered first-pass (presystemic) metabolism and can greatly limit a drug's oral bioavailability.

2.2 Transporter-Targeted Prodrugs

Traditionally, passive transcellular diffusion was considered the near exclusive mechanism of small molecule drug absorption in the intestine. This view implied that to achieve sufficient intestinal absorption an orally administered drug must achieve a hydrophilic-lipophilic "sweet spot": hydrophilic enough to be sufficiently soluble in the gastrointestinal tract but lipophilic enough to sufficiently cross the epithelial membranes. Guidelines for achieving this "sweet spot" were famously defined by Lipinski *et al.* [17]. However, numerous preclinical and clinical studies have since unequivocally demonstrated the importance of transporters in mediating the intestinal absorption and oral bioavailability of many drugs [15, 18-20]. Based on this mechanism of absorption, an oral drug

development strategy has emerged in which a drug's intestinal permeability (*i.e.,* the ability to move from the intestinal lumen into the intestinal epithelial cells) is increased by covalently linking an inactive moiety (IM) to the API, generating a prodrug that is a substrate of uptake transporters expressed on the apical membrane of intestinal epithelial cells. Following uptake, the prodrug is chemically or enzymatically activated, liberating the API (Figure 2.2) [21]. Based on the site of prodrug activation, the prodrug may also improve drug stability during first-pass transit through the gut and/or liver, reducing first-pass metabolism [22]. Thus, transporter-targeted prodrugs can increase a drug's oral bioavailability by increasing intestinal absorption and/or by decreasing first-pass metabolism.

Given market forces favoring the development of orally administrable drugs, many compounds with acceptable *in vivo* activity were/are not developed due to poor predicted oral bioavailability. Applying the transporter-targeted prodrug strategy to such compounds may improve their oral bioavailability while maintaining their *in vivo* activity. This application will likely become more relevant as toxicity and drug-drug interaction issues associated with lipophilic drugs have moved recent drug discovery to a less lipophilic space, presumably increasing the prevalence of drugs with poor intestinal absorption [23]. Additionally, applying this strategy to drugs currently administered via non-oral routes may enable their oral administration [21]. Thus, as more knowledge regarding intestinal transporters and prodrug activating enzymes is gained, the potential utilization of this technique is vast.

2.3 Proton-Coupled Oligopeptide Transporters

The family of proton-coupled oligopeptide transporters (POTs) facilitates the uptake of dipeptides, tripeptides, and molecules (including many drugs) which sterically and electrostatically resemble peptides (*i.e.,* peptidomimetics). According to the Human Genome Organization (HUGO) nomenclature, the human POTs are classified in Family 15 of the solute carrier group of transmembrane transport proteins (SLC15). The human POTs with HUGO designated *SLC encoding sequences* are peptide transporter 1 (PEPT1, *SLC15A1)*, peptide transporter 2 (PEPT2, *SLC15A2*), peptide/histidine transporter 1 (PHT1, *SLC15A4)*, and peptide/histidine transporter 2 (PHT2, *SLC15A3)* [24]. As shown in Table 2.1, comparison of amino acid length and sequence identity points to two branches in this family: peptide transporters (PEPT1, PEPT2) and peptide/histidine transporters (PHT1, PHT2).

Although PEPT1 and PEPT2 are found in several tissues throughout the body, PEPT1 is predominantly expressed on the apical membrane of small intestinal epithelial cells and contributes to nutritional absorption while PEPT2 is predominately expressed on the apical membrane of renal epithelial cells and contributes to nutritional reabsorption [24]. Both transporters generally recognize the same substrates, but PEPT2 typically binds substrates with higher affinity. This has led to the designation of PEPT2 as the "high-affinity, low-capacity" transporter and PEPT1 as the "low-affinity, high-capacity" transporter [25]. For instance, the commonly used model dipeptide glycylsarcosine (GlySar) is transported by PEPT1 and PEPT2 with Michaelis-Menten constants ranging from 500 – 1,500 μM and 50 – 150 μM, respectively [25]. Although this rule holds for most substrates (*i.e.,* PEPT2 affinity > PEPT1 affinity), there are some exceptions [26].

Comparatively little is known about PHT1 and PHT2, which are subcellular (*i.e.,* endosomal and lysosomal) transporters expressed in tissues throughout the body [24, 27, 28]. Recent work suggests that PHT1 plays an important role in neural development and histamine/histidine homeostasis in the brain [29, 30]. Furthermore, PHT1 has been demonstrated to mediate immune response [31, 32] and is believed to be involved in the pathogenesis of inflammatory bowel disease [33], lupus [34], and diabetes [35]. Likewise, PHT2 is also believed to play a critical role in mediating immune response and has been proposed as a therapeutic target for treating inflammatory bowel disease [36, 37]. The substrate specificities of PHT1 and PHT2 have not been systematically evaluated but, broadly speaking, both transport histidine and the typical POT substrates (*i.e.,* di/tripeptides and peptidomimetics) [25]. Recently, efficient cellular models to characterize PHT1 and PHT2 transport have been developed and used for preliminary evaluation of substrate specificity [38, 39].

Interestingly, peptide/peptidomimetic transporters outside of the POT family have been reported including human peptide transporter 1 (HPT1) and an opioid peptide transporter [40, 41]. Although HPT1 has been shown *in vitro* to transport peptidomimetics including bestatin, cephalexin, and valacyclovir, its *in vivo* function has not been demonstrated [25, 40, 42]. Finally, the Na^+-Cl^- coupled opioid peptide transporter, which shows no transport activity towards non-opioid peptides, is believed to influence the distribution of opioid peptides across the blood-brain barrier [41, 43].

2.4 Peptide Transporter 1 (PEPT1)

2.4.1 Localization and Function

PEPT1 protein expression has been observed in the small intestine, kidney, pancreas, bile duct, and monocyte [44-48]. Interestingly, there are conflicting reports regarding the expression of PEPT1 in the colon and the potential upregulation of colonic PEPT1 expression in inflammatory bowel disease (IBD) [49-52]. Despite expression in many tissues, the functional activity of PEPT1 is most prominent in the small intestine and kidney.

PEPT1, which is present on the apical membrane of intestinal enterocytes, serves as a "low-affinity, high-capacity" transporter of dipeptides, tripeptides, and peptidomimetics from the intestinal lumen into the enterocyte. Utilizing absolute protein quantification, Drozdzki *et al.* quantified the intestinal protein expression of 19 transporters in 9 organ donors, showing that PEPT1 accounted for 17%, 31%, 28%, and 2% of total transporter expression in the duodenum, jejunum, ileum, and colon, respectively. Furthermore, they reported the rank order of absolute intestinal PEPT1 expression as jejunum ≈ ileum > duodenum > colon [50]. This is in contrast to the rank order of intestinal PEPT1 expression in mice, which was reported as jejunum > duodenum ≈ ileum > colon [53]. The peptides transported by intestinal PEPT1 are typically formed by the digestion of dietary and endogenous proteins via peptidases and proteases secreted by the stomach/pancreas or bound to the enterocyte's apical membrane. Once inside the enterocyte, most dipeptides and tripeptides are further metabolized into their constituent amino acids which are then transported into the portal blood via basolaterally expressed amino acid transporters. However, some peptides and peptidomimetics are transported

across the basolateral membrane intact [54]. Although a basolateral peptide transporter has been shown functionally to exist in intestinal epithelial cells and was recently suggested to be the multidrug resistant protein 3 (MRP3) transporter, its identity and many crucial transport characteristics remain unknown [55, 56]. Addressing this knowledge gap in drug efflux into portal blood may aid in predicting the disposition of orally administered peptidomimetic drugs.

In the kidney, PEPT1 and its "high-affinity, low-capacity" paralog PEPT2 function to reabsorb oligopeptides from the glomerular filtrate [57]. Localization studies have shown PEPT1 and PEPT2 expression in the proximal and distal regions of the proximal tubule, respectively. It is hypothesized that the proximal "low-affinity, high-capacity" PEPT1 and distal "high-affinity, low-capacity" PEPT2 work jointly to maximize oligopeptide reabsorption [45, 58]. Interestingly, studies in wildtype and PEPT2 knockout mice showed PEPT2 accounted for 86% of the renal tubular reabsorption of GlySar [59]. The necessity for efficient peptide reabsorption is evidenced by the large contribution of peptides to the total circulating amino acid pool. Although this percentage has not been reported in human, peptides account for approximately 52%, 65%, and 78% of the total circulating amino acid pool in rat, steer, and sheep, respectively [60]. Just as in the intestine, the presence of a basolateral peptide transporter in the proximal tubule has been shown functionally but its identity and many crucial characteristics are unknown [61]. Given the role of glomerular filtrate reabsorption in renal clearance, further study into this topic may aid in predicting peptidomimetic drug disposition. More generally, appreciating the wide expression profile of PEPT1, further research into its expression/function elsewhere in the

body may also improve the prediction of drug disposition and present novel therapeutic targets.

2.4.2 Mechanism of Transport

In the mid-1980s, Ganapathy and Leibach first suggested peptides are actively cotransported with protons in the intestine and kidney [62, 63]. This was later confirmed in 1994 as the successful expression of rabbit PEPT1 in *Xenopus laevis* oocytes allowed direct investigation into the mechanism of peptide transport. Using intracellular pH monitoring and the two-electrode voltage clamp (TEVC) technique, transport of the commonly used model dipeptide GlySar was shown to be electrogenic, H^+-coupled, and saturable [64]. Utilizing this same technique, it has been demonstrated by many others that these conclusions are applicable to PEPT1 substrates regardless of their net charge [65-69]. It was thus established that PEPT1-mediated transport is coupled to and powered by the movement of protons down an intracellularly-directed proton gradient. The proton gradient is established and maintained, at least in part, by the apically expressed Na^+/H^+ antiporter NHE3. NHE3 is driven, in turn, by the intracellularly-directed Na^+ gradient established by the basolaterally expressed Na^+-K^+-ATPase [70]. Thus, as illustrated in Figure 2.3, PEPT1 is a tertiary-active transporter.

Given that PEPT1 electrogenically transports peptides regardless of their net charge, significant work has explored the stoichiometry of proton and peptide cotransport. Using rabbit PEPT1 expressed in *Xenopus laevis* oocytes, Steel *et al.* found the proton:peptide transport ratio to be 1:1, 2:1, and 1:1 for neutral, acidic, and basic dipeptides, respectively [67]. Kottra *et al.* utilized the same experimental setup and showed that peptides carrying a net negative charge at extracellular pH may be transported in their

neutral and charged states with high and low affinity, respectively. Similarly, cationic dipeptides may be transported in charged and neutral states given positioning of the charge on the carboxyl terminal amino acid. They argue that each peptide is *directly* cotransported with only one proton and the transport of a protonated peptide followed by subsequent intracellular deprotonation explains the observation that the apparent stoichiometry of transport may differ from 1:1 for charged molecules. Thus, they conclude that the observed proton:peptide stoichiometry depends on the charged:uncharged ratio of extracellular peptides as well as their relative affinities for PEPT1 [66].

2.4.3 Structure and Pharmacophore

Ever since PEPT1 was initially cloned in 1994, many techniques have been applied to elucidate its structure and key functional domains. On the basis of hydropathy plots, PEPT1 was predicted to contain 12 transmembrane domains (TMDs), a large extracellular domain (ECD) connecting TMD 9 and 10, and both termini in the cytoplasm as shown in Figure 2.4 [64]. Epitope tagging experiments confirmed the number and orientation of the TMDs from TMD 4 to the C-terminus. Information regarding the amino-terminal domains was not gathered as epitope insertions into this region interfered with PEPT1 translocation to the plasma membrane and/or altered transporter function [71]. The crystal structure of the ~190 amino acid ECD connecting TMD 9 and 10 was solved by Beale *et al.* for the *Mus musculus* (*i.e.,* house mouse) PEPT1 homologue, revealing two immunoglobulin domains which display a specific interaction with trypsin [72]. Although no complete crystal structure has been solved for PEPT1 or a mammalian homologue, crystal structures have been solved for several prokaryotic homologues including $PEPT_{Sh}$ (*Staphylococcus hominis),* $PEPT_{so}$ (*Shewanella oneidensis)*, $PEPT_{St}$ (*Streptococcus thermophiles*), GkPOT

(*Geobacillus kaustophilus*), $PEPT_{So2}$ (*Shewanella oneidensis)*, YbgH (*Escherichia coli*), and YePEPT (*Yersinia enterocolitica)* [73-79]. These crystal structures all reveal a 12 TMD structure comprised of two six-helical bundles (TMD 1-6 and TMD 7-12) forming a 'V'-shaped transporter with two additional TMDs, helix A (HA) and helix B (HB), connecting these bundles. HA and HB appear to be absent in metazoan, fungal, and plant protein sequences suggesting they are not integral to a conserved transport mechanism [74].

Biophysical and molecular modeling simulations have been performed utilizing structural knowledge obtained from the $PEPT_{So}$ and $PEPT_{St}$ crystal structures. Based on these simulations, it was proposed that peptide transport occurs via an alternating access mechanism with the periplasmic gate formed by TMD 1, 2, 7, and 8 and the cytoplasmic gate formed by TMD 4, 5, 10, and 11 [80]. Importantly, however, these simulations were based on crystal structures of prokaryotic PEPT1 homologues which have only a 20 – 30% amino acid sequence identity with PEPT1 [72]. Thus, it is possible, although unlikely given the evolutionary relationship between bacterial and human transporters, that PEPT1 transport utilizes a different mechanism.

Significant work has also gone into elucidating the proton and peptide binding sites in PEPT1. First, using site-directed mutagenesis, it has been shown that pH-dependent transport and direct proton binding is mediated mainly by H^{57} on TMD 2 [81]. Much of the current information regarding the peptide binding site is the result of co-crystallization of PEPT1 bacterial homologues with peptides/peptidomimetics. There are several common features in these crystal structures: (1) the peptide binding site is formed by residues from TMD 1, 2, 4, 5, 7, 8, 10, and 11; (2) recognition and binding occurs as distinct regions of the binding pocket interact with the peptide/peptidomimetic backbone and sidechains; and

(3) peptides/peptidomimetics interact with several residues conserved across bacterial and mammalian transporters [82, 83]. For example, the peptide binding site in $PEPT_{So}$ contains residues corresponding to the following equivalent residues in PEPT1: R^{27}, Y^{31}, R^{34}, Y^{64}, K^{140}, Y^{167}, I^{170}, W^{294}, F^{297}, E^{595}, S^{599}, W^{622}. Lending credibility to these observations, Y^{167}, W^{294}, and E^{595} had been previously implicated in peptide binding to PEPT1 via site-directed mutagenesis experiments [84]. Furthermore, the recently published crystal structure of $PEPT_{Sh}$ reports a peptide binding site including, among others, amino acids corresponding to Y^{167} and E^{595} in PEPT1 [73].

However, many questions remain regarding PEPT1's peptide binding site. While Samsudin *et al.*, utilized crystal structures of PEPT1 bacterial homologues to generate a pharmacophore model, the applicability of this pharmacophore model to PEPT1 is unclear given differences in protein sequence/structure [85]. Solving the crystal structure of PEPT1 or a mammalian homologue would aid in the creation of a more relevant pharmacophore model and ultimately aid the discovery and development of peptidomimetic drugs.

2.4.4 Substrate Specificity

PEPT1 displays wide substrate specificity as necessitated by its role in the uptake of dietary peptides. It is believed that PEPT1 transports most of the 400 dipeptides and 8,000 tripeptides arising from the 20 naturally occurring amino acids [86]. Furthermore, PEPT1 has been shown to transport modified peptides (*e.g.,* N-acetyl-L-phenylalanyl-L-tyrosine-amide) [87], bacteria-derived peptides (*e.g.,* muramyl dipeptide) [88], and many pharmaceutical peptidomimetics (*e.g.,* β-lactam antibiotics, various angiotensin-converting enzyme inhibitors, bestatin, 5-aminolevulinic acid, valacyclovir, valganciclovir) [89-94].

Interestingly, PEPT1 substrates do not require a peptide bond but instead a positive and negative charge separated by 500 - 630 pm [95]. Brandsch *et al.* reported that compounds carrying a net charge generally have lower PEPT1 affinity, compounds containing L-amino-acids generally have higher PEPT1 affinity, and sidechain hydrophobicity can influence PEPT1 affinity depending on sidechain location [96]. However, Vig *et al.* presented data showing an important distinction between binding and transport as some compounds display high PEPT1 affinity but do not undergo PEPT1-mediated transport [97]. Although the general trends reported by Brandsch *et al.* for PEPT1 binding are similar to those presented by Vig *et al.* for PEPT1 transport, both studies highlight the complexity of thoroughly characterizing PEPT1's substrate specificity without a transporter structure.

2.4.5 Regulation

PEPT1 activity is regulated by many factors including biological development, exogenous molecules (*e.g.,* diet and drugs), endogenous molecules (*e.g.,* hormones), and disease states (*e.g.,* IBD). Regulation of PEPT1 activity occurs largely via mechanisms which impact mRNA transcription, mRNA stability, translation of mRNA into PEPT1, post-translational PEPT1 modification (*e.g.,* phosphorylation), trafficking of PEPT1 to the membrane, and the transmembrane proton gradient which powers PEPT1 transport [24].

Few studies have been published on the developmental expression, or ontogeny, of PEPT1. Shen *et. al* reported that intestinal PEPT1 expression in rats is induced at birth and again during weaning [98]. Mooji *et al.* completed studies in humans, finding that intestinal PEPT1 mRNA expression was approximately 20% lower in neonates/infants (age range: 0 – 17 weeks) compared to adolescents (age range: 9 – 17 years) ($p < 0.05$). However, the

authors predicted this difference in expression would not lead to clinically relevant differences in drug absorption [99]. Alghamdi *et al.* reported that both the expression and localization of renal PEPT1 differ between young, middle-aged, and old rats [100].

Dietary consumption has been shown to impact PEPT1 activity as rat PEPT1 expression levels increase approximately 150 – 200 % following prolonged starvation (4 days), semistarvation (10 days), or total parenteral nutrition (10 days) [101]. PEPT1 upregulation was also observed in mice after fasting for as short as 16 hours [102]. Additionally, there is a strong positive correlation between dietary protein intake and PEPT1 expression in rats while high fat diets have been shown to decrease PEPT1 expression in mice [103, 104]. Interestingly, diurnal variations in PEPT1 activity have been noted in rats and appear to be driven by feeding patterns [105, 106].

Many drugs have been shown to alter PEPT1 activity both *in vitro* and *in vivo*. Various phosphodiesterase inhibitors including caffeine, pentoxifylline, and theophylline have been shown to the reduce the capacity of PEPT1 transport (V_{max}) in Caco-2 cells. It is hypothesized that phosphodiesterase inhibitors alter transport by increasing intracellular cAMP concentrations, leading to inhibition of the apically expressed NHE3 Na^+/H^+ exchanger and thus reducing the proton gradient which powers PEPT1 transport [107]. Alternatively, the α2-adrenergic agonist clonidine, which decreases intracellular cAMP, has been shown to increase the capacity of PEPT1 transport in Caco-2 3B cells. Although the precise mechanism for this effect is unknown, it may involve increased translocation of PEPT1 protein to the plasma membrane [108]. The σ1 receptor agonist pentazocine has also been shown to increase the capacity of PEPT1 transport in Caco-2 cells, likely through increasing the expression and/or stability of PEPT1 mRNA [109]. It was found that

coadministration of the calcium channel blocker nifedipine increased the absorption rate of cefixime, a PEPT1 substrate [110]. This observation may be explained by the finding that increasing/decreasing intracellular calcium concentrations decreases/increases PEPT1 mediated transport, likely by altering the activity of NHE3 and thus the proton gradient driving PEPT1 transport [111]. The anti-cancer compound 5-fluorouracil (5-FU) was shown to increase PEPT1 mRNA and protein expression in rat, an observation the authors attributed to "5-FU induced intestinal damage" [112]. Recent work suggests the commonly used excipients Solutol HS15, Tween 20, and Tween 80 inhibit PEPT1, although the mechanism was not explored [113].

There is also extensive hormonal regulation of PEPT1. Insulin and leptin increase PEPT1 V_{max} by increasing the translocation of preformed PEPT1 to the apical membrane while human growth hormone was shown to increase PEPT1 activity by increasing PEPT1 gene expression [114-116]. Conversely, thyroid hormone was shown to decrease PEPT1 mRNA levels while epidermal growth factor (EGF) was shown to decrease both mRNA and protein levels [117, 118]. However, a subsequent study reported EGF may upregulate PEPT1 mRNA expression, and, thus, further investigation is necessary to understand the effect of EGF on PEPT1 [119]. The role of hormones in regulating PEPT1 activity in certain physiological conditions has been explored, revealing potentially therapeutic roles for ghrelin in sepsis and growth hormone in oxidative stress [120, 121].

As with other biological processes, disease states may cause or result from aberrant PEPT1 activity. Specifically, it has been reported that there is increased colonic PEPT1 expression in patients with IBD and short bowel syndrome (SBS) [122-124]. Furthermore, colonic PEPT1 upregulation in IBD and the potential for IBD to cause colitis-associated

cancer (CAC) has led some to propose colonic PEPT1 as a target in treating IBD and preventing colitis-associated tumorigenesis [125]. However, in 2014 Wuensch *et al.* presented data suggesting colonic PEPT1 expression actually decreased in humans with IBD [126]. Thus, the role of PEPT1 in IBD is unclear and future work addressing this pathology could present novel therapeutic targets to address IBD, SBS, and CAC. PEPT1 has also been shown to be overexpressed in cell lines of various cancers including pancreatic, gastric, and prostate [127-129].

2.4.6 PEPT1-Targeted Prodrugs for Oral Administration

The promiscuity and extensive intestinal expression of PEPT1 have made it a common target in the development of transporter-targeted prodrugs for oral administration. Application of the PEPT1-targeted prodrug technique has been successful in increasing the intestinal permeability and oral bioavailability of many drugs both preclinically and clinically, with two such prodrugs (valacyclovir and valganciclovir) receiving regulatory approval for use in humans [130]. PEPT1-targeted prodrugs are typically generated by attaching an amino acid (or dipeptide) to the API through an ester bond [131]. Importantly, these prodrugs require *in vivo* activation to liberate the API and exert a pharmacological effect. Thus, a successful PEPT1-targeted prodrug must be a PEPT1 substrate (*see section 2.4.4 for PEPT1 substrate specificity*) that also undergoes activation following absorption. Accordingly, understanding the *in vivo* activation of PEPT1-targeted prodrugs is crucial for their rational design and development.

To identify the enzyme(s) responsible for mediating the *in vivo* activation of PEPT1-targeted prodrugs (or a subset of these prodrugs), Kim *et al*. isolated and identified an enzyme from Caco-2 cells that displays significant hydrolytic activity towards

valacyclovir and valganciclovir. This enzyme was identified as the serine hydrolase biphenyl hydrolase-like protein (BPHL) which shows high RNA expression in human liver and kidney and lower expression in intestine, heart, and skeletal muscle [132, 133]. Systematic investigation into BPHL substrate specificity revealed that, in addition to valacyclovir and valganciclovir, BPHL catalyzes the hydrolytic activation of 3'- and 5'-amino acid ester prodrugs of several nucleoside analogs including zidovudine, floxuridine, benzimidazole, and gemcitabine [134]. In general, BPHL shows a preference for prodrugs containing 5'-esters, APIs that function as a labile leaving group, and L-α-amino acids that are small, hydrophobic, and aromatic [134-136]. Furthermore, Asp-123 was shown to be crucial in dictating substrate selectivity as it forms a negatively charged area near the active site, explaining the preference of BPHL for amino acid prodrugs carrying a free and positively charged amino group. This fact, paired with the absence of peptidase activity, has led BPHL to be classified as an α-amino acid ester hydrolase [136].

However, work in wildtype and BPHL knockout mice showed conclusively that non-BPHL enzymes can also activate valacyclovir *in vivo* [137]. Subsequent work using competitive activity-based protein profiling in Caco-2 cells identified the serine hydrolase RBB9 as an activating enzyme of both valacyclovir and the PEPT1-targeted gemcitabine prodrug 5'-L-valyl-gemcitabine. The *in vivo* relevance of RBB9-mediated activation was confirmed, showing RBBP9 involvement in the intestinal activation of valacyclovir in mice [138]. However, this study was unable to conclude that valacyclovir activation is driven solely by BPHL and RBBP9, suggesting that additional enzyme(s) may be involved. Identification and characterization of these enzymes may aid in future PEPT1-targeted prodrug design and development. Importantly, however, these findings may not be

applicable to all PEPT1-targeted prodrugs as the enzymes responsible for mediating activation and their relative contributions may vary from prodrug to prodrug.

2.5 Gemcitabine

2.5.1 Structure and Physiochemical Properties

Gemcitabine is a small molecule (molecular weight = 263.2 g/mol) anti-cancer compound originally synthesized at Eli Lilly in 1988 [139]. As shown in Figure 2.5A, gemcitabine is the fluorine-containing cytidine analogue 2'2'-difluorodeoxycytidine (dFdC). Gemcitabine is a hydrophilic (log P = -1.4) weak base (pKa = 3.6) with an aqueous solubility of 22 mg/mL (84 mM) [140, 141]. When used clinically, gemcitabine is typically supplied as a hydrochloride salt (molecular weight = 299.7 g/mol) which has an aqueous solubility of 38 mg/mL (127 mM) [140].

2.5.2 Clinical Applications in Cancer Therapy

Gemcitabine received initial FDA approval in 1996 for treatment of locally advanced (nonresectable Stage II or Stage III) or metastatic (Stage IV) pancreatic adenocarcinoma. Gemcitabine has since received FDA approval for additional indications: treatment in combination with cisplatin of inoperable and locally advanced (Stage IIIA or Stage IIIB) or metastatic (Stage IV) non-small cell lung cancer (1998), treatment in combination with paclitaxel of metastatic breast cancer after failure of anthracycline-containing adjuvant chemotherapy (2004), and treatment in combination with carboplatin of advanced ovarian cancer which relapsed at least six months after platinum-based therapy (2006) [142]. Additionally, off-label gemcitabine use is quite common as one study found that in 2010 approximately 68% of total gemcitabine use was off-label [143]. Table 2.2 summarizes off-label gemcitabine applications in cancer therapy which received "strong"

recommendations for clinical use in the Elsevier Gold Standard's Clinical Pharmacology compendium [144]. Furthermore, gemcitabine therapy is often combined with radiation as gemcitabine acts as a radiosensitizer [145]. Depending upon the indication and the use of combination therapies (*i.e.,* coadministered medications), a typical gemcitabine regimen involves weekly administration of 1000 mg/m^2 – 1250 mg/m^2 over 21- or 28-day cycles via a 30-minute constant-rate intravenous (IV) infusion [142]. When used in combination with radiation therapy, gemcitabine may be administered at much lower doses [146-149].

Interestingly, there are clinical data showing that increasing the length of the infusion, while administering an equal or even lower total gemcitabine dose, can increase cellular exposure to the active gemcitabine metabolite, gemcitabine triphosphate (dFdCTP) [150, 151]. However, the clinical relevance of this is unclear as studies comparing clinical outcomes between standard 30-minute gemcitabine infusions and prolonged infusions present conflicting results [152]. For instance, a Phase II study in patients with pancreatic adenocarcinoma showed that a prolonged gemcitabine infusion performed better than a standard gemcitabine infusion in both 1-year survival (28.8% vs. 9%, $p = 0.014$) and 2-year (18.3% vs. 2.2%, $p = 0.007$) survival [151]. However, a Phase III trial in patients with pancreatic adenocarcinoma reported that prolonged infusions did not improve survival, relative to standard infusions [153]. Such discrepancies are not uncommon in the literature and may be due to differences in the patient population, the dosing regimens studied, the clinical endpoints, or a combination of these factors. Furthermore, although recent meta-analysis suggest that prolonging gemcitabine infusion may increase the overall response rate when treating non-small cell lung cancer and increase median survival when treating pancreatic adenocarcinoma, more large scale clinical trials are required to both prove the

clinical utility of prolonged gemcitabine infusions and optimize such dosing regimens (*e.g.,* dose, length of infusion, frequency of administration) [154, 155]. Thus, gemcitabine is still most frequently administered weekly as a 30-minute infusion [156].

Interestingly, although gemcitabine was first approved over 20 years ago, according to ClinicalTrials.gov (as of May 19, 2020) there are currently 73 "not yet recruiting" , 387 "recruiting" , and 207 "active" clinical trials examining gemcitabine in treating a range of cancers [157]. Thus, gemcitabine remains commonly used in the clinic and, as evidenced by the number of trials involving gemcitabine currently planned and in progress, it appears gemcitabine will remain an integral component of cancer therapy.

2.5.3 Clinical Pharmacokinetics

Absorption/Administration

Gemcitabine has an oral bioavailability of approximately 10% and is thus administered as a zero-order intravenous infusion over a 30 minute period [142, 158]. Gemcitabine plasma concentrations typically plateau 15 - 30 minutes into an infusion, with average maximum plasma concentrations (C_{max}) (*i.e.,* concentrations at the end of the infusion) ranging from 30 - 37 μM following a 1000 mg/m^2 dose and 50 - 70 μM following a 1250 mg/m^2 dose [159, 160].

Distribution

A two-compartment population pharmacokinetic (POPPK) model of gemcitabine was developed using data collected from seven studies (353 patients total). This model revealed that gemcitabine's steady-state volume of distribution (Vd_{ss}) is approximately 65 L/m^2 when administered via a "short" infusion (*i.e.,* < 70 minutes) and approximately 385 L/m^2 when administered via a "long" infusion (*i.e.,* > 70 minutes). The central compartment

volume (V_1) is 12.2 and 17.5 L/m^2 for women and men, respectively, following both "short" and "long" infusions. The peripheral compartment volume (V_2) does not show a gender-dependency and is 47.4 L/m^2 following "short" infusions and 370 L/m^2 following "long" infusions [161]. However, the clinical impact of the increased distribution seen with longer infusion times is unclear (*see Section 2.5.2)*. The major metabolite of gemcitabine, 2',2'-difluorodeoxyuridine (dFdU, Figure 2.5B), has been described using both a 2- and 3-compartment model [162, 163].

The distribution/cellular uptake of gemcitabine and dFdU is mediated by two solute carrier (SLC) transporter families: the SLC28 family of concentrative nucleoside transporters (CNTs), which are sodium-dependent and unidirectional transporters able to transport substrates against their concentration gradient (*i.e.,* from low to high concentrations), and the SLC29 family of equilibrative nucleoside transporters (ENTs), which are sodium-independent and bidirectional transporters that facilitate substrate movement down their concentration gradient (*i.e.,* from high to low concentrations) [164, 165]. Within these families, gemcitabine is a substrate of four transporters localized to the plasma membrane: CNT1 (K_m = 24 μM), CNT3 (K_m = 60 μM), ENT1 (K_m = 160 μM), and ENT2 (K_m =740 μM) [166, 167]. It is believed that ENT1 is mainly responsible for gemcitabine distribution and a recent meta-analysis of clinical data concluded that high ENT1 protein expression in pancreatic tumors is associated with increased overall survival in patients receiving gemcitabine treatment [164, 168]. A similar positive correlation between tumoral ENT1 expression and gemcitabine response was observed in patients with bladder and biliary tract cancer [169, 170]. Finally, the stark difference in Vd_{ss} seen following short and long infusions may be due, in small part, to saturation of uptake

transporters (*e.g.,* CNT1, CNT3) at the high plasma gemcitabine concentrations generated during short infusions [166, 167].

Metabolism and Excretion

The same gemcitabine POPPK model described above reported that gemcitabine clearance is gender-dependent (*i.e.,* approximately 40% higher in men than women) and age-dependent (*i.e.,* decreases approximately 55% from age 29 – 79) as shown in Table 2.3. Although no specifics were provided, the authors state that clearance is comparable following "short" and "long" infusions [161]. When administered as a standard 30-minute infusion, clearance is independent of dose from 40 – 3650 mg/m^2 but may show dose-dependency above 3650 mg/m^2 [171, 172].

Gemcitabine elimination is largely driven by cytidine deaminase (CDA)-mediated metabolism into dFdU, occurring mainly in the liver. Based on the results of an intravenous radiolabeled pharmacokinetic study in 5 patients, CDA-mediated metabolism accounts for over 90% of gemcitabine clearance while renal excretion of intact gemcitabine accounts for less than 10% [142]. This result is consistent with subsequent gemcitabine PK studies [171, 172]. According to the package insert, gemcitabine's plasma half-life ($t_{1/2}$) ranges from 42 - 94 minutes following a "short" infusion [142]. Interestingly, there is large variation in published $t_{1/2}$ values following "short" infusions as Peters *et al.* reported gemcitabine's $t_{1/2}$ ranges from 5 - 20 minutes in a widely cited 2007 paper [172]. This discrepancy may arise from difficulties in separating the distribution $t_{1/2}$ ($t_{1/2,\alpha}$) and the elimination $t_{1/2}$ ($t_{1/2,\beta}$), as a 2015 paper reported $t_{1/2,\alpha}$ values of approximately 10 minutes and $t_{1/2,\beta}$ values of approximately 60 minutes [173]. Thus, it is possible that Peters *et al.* reported $t_{1/2,\alpha}$ while the true $t_{1/2,\beta}$ is longer, as reported in the package insert. Regardless of

these discrepancies, gemcitabine's short $t_{1/2}$ prevents gemcitabine accumulation during weekly administration [174]. When administered via a "long" infusion, gemcitabine's $t_{1/2}$ increases to 295 - 638 minutes, reflecting an increased Vd_{ss} [161].

The main gemcitabine metabolite, dFdU, is eliminated unchanged in urine with a mean $t_{1/2}$ ranging from 33 – 84 hr [175]. Although dFdU is present at concentrations ranging from 1 - 6 μM one week after administration of a standard gemcitabine dose, there is no measurable dFdU accumulation with weekly gemcitabine administration [174]. While some believe dFdU may contribute to gemcitabine's cytotoxic and radiosensitizing effects *in vivo* [176-178], recent work reported very low concentrations of phosphorylated dFdU nucleotides (much lower than gemcitabine nucleotides) in peripheral blood mononuclear cell samples collected from patients receiving gemcitabine therapy [179]. This finding, paired with the higher potency of gemcitabine relative to dFdU as both a cytotoxic and radiosensitizing agent [178-180], suggests that dFdU activity may not be clinically relevant, as hypothesized by others (D. Shewach, personal communication, July 29, 2020).

2.5.4 Mechanism of Action

Intracellular Generation and Accumulation of Active Gemcitabine Metabolites

Within one week of radiolabeled gemcitabine intravenous administration, nearly all (92 – 98%) of the administered dose is recovered in urine as gemcitabine and dFdU [142]. However, additional gemcitabine metabolites are generated intracellularly *in vivo* as illustrated in Figure 2.6. Although these additional metabolites are not found at quantifiable levels in plasma or urine, they drive gemcitabine's pharmacological action. The primary active form of gemcitabine, gemcitabine triphosphate (dFdCTP), is generated intracellularly by three sequential phosphorylation events: (1) deoxycytidine kinase (dCK)-

mediated phosphorylation of gemcitabine, forming gemcitabine monophosphate (dFdCMP); (2) pyrimidine nucleoside monophosphate kinase (UMP-CMP kinase)-mediated phosphorylation of dFdCMP, forming gemcitabine diphosphate (dFdCDP); and (3) undetermined enzyme (potentially nucleoside diphosphate kinase)-mediated phosphorylation of dFdCDP forming gemcitabine triphosphate (dFdCTP). Metabolic inactivation processes are also occurring simultaneously, including CDA-mediated deamination of gemcitabine, 5'-nucleotidase (5'-NT)-mediated dephosphorylation of dFdCMP, and deoxycytidylate deaminase (dCTD)-mediated deamination of dFdCMP [181]. Furthermore, dFdU is phosphorylated forming dFdU monophosphate (dFdUMP), dFdU diphosphate (dFdUDP), and dFdU triphosphate (dFdUTP) [177, 179].

dCK-mediated gemcitabine phosphorylation is the rate limiting step of dFdCTP formation and a positive correlation between dCK expression in pancreatic cancer tissues and overall survival following gemcitabine treatment has been demonstrated [182, 183]. dCK phosphorylates gemcitabine with a K_m ranging from roughly 1 - 10 μM, depending on the source of the phosphate donor (*e.g.,* ATP, UTP, NTP mixture) [184, 185]. Clinical trial results support the relevance of dCK saturation as intracellular dFdCTP accumulation plateaus above gemcitabine plasma concentrations of 15 - 20 μM [171, 186]. Importantly, such saturating concentrations are reached following 30 minute gemcitabine infusions at 1,000 mg/m^2 (Cmax = 30-37 μM) or 1,250 mg/m^2 (Cmax = 50 - 70 μM) [159, 160]. Increasing the length of the gemcitabine infusion would increase exposure to plasma gemcitabine concentrations of $\leq 15 - 20$ μM, theoretically leading to increased intracellular dFdCTP accumulation [187]. As described in *Section 2.6.2*, longer infusion times have in

fact been shown in various clinical trials to increase intracellular dFdCTP accumulation, but the clinical relevance of this is unclear.

In various cancer cell lines, the removal of intracellular gemcitabine and gemcitabine metabolites was shown to occur mainly through the efflux of gemcitabine via SLC transporters (likely ENT1) and the efflux of dFdU via members of the ATP-binding cassette transporter subfamily C (ABCC) [177, 188]. Interestingly, the cellular retention of dFdCTP is quite long in comparison to other tri-phosphate nucleoside analogs (*e.g.,* Ara-C), which may be important for gemcitabine's cytotoxicity. For instance, in Chinese hamster ovary (CHO) cells, Ara-c triphosphate elimination is linear ($t_{1/2}$ = 0.7 hr), while dFdCTP elimination is linear at low concentrations ($t_{1/2}$ = 3.9 hr) and biphasic at high concentrations, ($t_{1/2}\,\alpha$ = 3.9 hr, $t_{1/2}\,\beta$ > 16 hr) [189]. Biphasic dFdCTP elimination was also seen in leukemic cells with $t_{1/2}\,\alpha$ values ranging from 0.6 – 1.3 hr and $t_{1/2}\,\beta$ values ranging from 5 – 43 hr, depending on dFdCTP concentration [176]. While $t_{1/2}$ values were not reported, dFdCTP was also shown to be well retained in several solid tumor cell lines. For instance, in the A2780 ovarian cancer cell line, high levels of dFdCTP remained 24 hours after removal of gemcitabine from the incubation medium (>70% of concentration seen when gemcitabine was first removed from the incubation) [190]. The long cellular retention and concentration-dependent biphasic elimination of dFdCTP is believed to result from the inhibition of various intracellular enzymes by gemcitabine metabolites, which ultimately increases the formation of dFdCTP and decreases the formation of the cellular efflux substrates dFdU and gemcitabine. This mechanism, known as self-potentiation, will be thoroughly discussed in the following subsection [176, 191].

Cytotoxic Mechanism of Action

There are many proposed mechanisms through which gemcitabine exerts its cytotoxic effect. The main mechanism involves dFdCTP incorporation into DNA in place of deoxycytidine triphosphate (dCTP), blocking cell cycle progression at the G1/S-phase boundary [192]. In a cell free system (*i.e.,* a system containing DNA polymerase but lacking the repair enzymes found in intact cells), it was demonstrated that incorporation of dFdCTP is followed by the incorporation of one additional nucleotide, at which point chain elongation is terminated. The penultimate positioning of dFdCMP prevents both DNA polymerase mediated chain elongation and the removal of dFdCMP via 3'→5' exonucleases [192]. While the relevance of this process, known as "masked-chain termination", is not known for intact cancer cells, dFdCTP incorporation into DNA has been shown to be essential for gemcitabine-induced apoptosis [193]. Several intracellular signaling pathways have been implicated in mediating gemcitabine-induced apoptosis including the caspase, p38 mitogen-activated protein kinase (MAPK), p53, NF-κβ, ERK, and Akt pathways [194-199]. It has also been shown that dFdCTP incorporation can lead to topoisomerase I poisoning, causing accumulation of strand breaks and cell death [200]. Interestingly, dFdUTP is also incorporated into DNA and both dFdCTP and dFdUTP are incorporated into RNA [177]. While some hypothesize that dFdUTP is an active metabolite [201], it is likely that dFdUTP incorporation into DNA and RNA is not clinically relevant, as described in *Section 2.3*.

The incorporation of dFdCTP into DNA, and subsequent cytotoxic effect, is enhanced by gemcitabine metabolites via a process known as self-potentiation. As shown in Figure 2.7, dFdCDP and dFdCTP increase cytotoxicity by depleting deoxycytidine

triphosphate (dCTP) pools and increasing the intracellular formation of dFdCTP, respectively, thereby increasing the likelihood of dFdCTP incorporation into DNA. First, dFdCDP irreversibly inhibits ribonucleotide reductase (RR), the enzyme responsible for conversion of nucleoside diphosphates (NDP) to deoxynucleoside diphosphates (dNDP), ultimately depleting deoxynucleoside triphosphate (dNTP) pools [202, 203]. Interestingly, while gemcitabine-mediated RR inhibition primarily depleted dCTP levels in the leukemia cell line K562, gemcitabine-mediated RR inhibition primarily depleted dATP levels in many solid tumor cell lines (*e.g.,* U251, D54, HT-29) [202, 204, 205]. dFdCTP directly inhibits dCTD, decreasing dFdCMP inactivation and increasing dFdCTP formation. These self-potentiating mechanisms are hypothesized to be responsible for the long cellular retention time and biphasic elimination of dFdCTP, as previously mentioned [176]. Furthermore, dFdUMP-mediated inhibition of thymidylate synthase may alter cellular deoxythymidine triphosphate (dTTP) pools, increasing nucleotide mis-incorporation and DNA damage [206]. Further clarification of the mechanisms underlying gemcitabine cytotoxicity and sensitivity/resistance will enable better predictions of patient efficacy and the rational design of combination therapies addressing multiple pathways.

Radiosensitizing Mechanism of Action

Gemcitabine is a potent radiosensitizer both *in vivo* and *in vitro*. Clinically, combining radiation therapy with low dose gemcitabine (often at a fraction of the standard chemotherapy dose) has shown promising results in treating various solid tumor cancers, including pancreatic bladder, head and neck, and malignant gliomas [148, 149, 207, 208]. However, toxicity concerns may severally limit the administrable gemcitabine dose when treating certain tumor types, especially when extended nodal irradiation is performed [209].

Interestingly, however, one study showed that full dose gemcitabine (1000 mg/m^2) and cisplatin (40 mg/m^2) can be safely combined with conformal radiation therapy in treating pancreatic cancer [210]. *In vitro, g*emcitabine was shown to induce radiosensitization in HT-29 cells at 10 nM. This effect increased with concentration until 1.0 μM, above which a plateau in radiosensitization is observed [204]. The radiosensitizing effect of gemcitabine was further explored in colon carcinoma cells and these results suggest that dFdCDP-mediated inhibition of ribonucleotide reductase and the resulting depletion and imbalance of deoxynucleotides, especially deoxyadenosine triphosphate (dATP), is an important factor in radiosensitization [204]. Experiments in two pancreatic cancer cell lines reported a similar conclusion [211]. The nucleotide imbalance leads to increased nucleotide mis-incorporation and radiosensitization if the mismatches are not repaired prior to irradiation. Thus, cells with decreased mismatched repair activity show greater gemcitabine induced radiosensitization [212]. On the other hand, homologous recombination repair was shown to be required for gemcitabine induced radiosensitization [213]. It was proposed that following drug washout and irradiation, major DNA damage is repaired (*i.e.* double strand breaks via homologous recombination) at the expense of repairing mismatches, leading to greater DNA damage than observed with radiation or gemcitabine treatment alone. Interestingly, upregulated homologous recombination repair (HRR) activity has been found in many cancer types and the extent of HRR activity may be an important factor in gemcitabine radiosensitization [214]. Finally, there are preliminary results suggesting that the radiosensitization effect of gemcitabine is increased by performing longer infusions, likely due to increased intracellular dFdCDP accumulation [215]. Again, however,

additional large-scale clinical studies will be needed to explore the relationship between infusion time and radiosensitization.

2.6 PEPT1-Targeted Gemcitabine Prodrugs for Oral Administration

Gemcitabine has a low oral bioavailability of approximately 10%, due, in part, to extensive first-pass metabolism by CDA [158]. Additionally, many studies assume that gemcitabine has low intestinal permeability, implying that oral bioavailability is further limited by incomplete intestinal absorption [216-219]. Gemcitabine's low oral bioavailability, paired with its narrow therapeutic index, precludes oral administration [220]. However, oral gemcitabine administration is preferable to IV administration as oral administration is more patient-friendly, reduces the cost and complexity of administration, and would enable dosing regimens that are hypothesized to improve gemcitabine efficacy (*e.g.,* dosing which mimics a prolonged infusion and metronomic dosing) [1, 154, 221]. To this end, PEPT1-targeted amino acid/dipeptide ester gemcitabine prodrugs have been developed and evaluated *in vitro* and *in situ*, showing promise in enabling oral administration. These prodrugs, 5'-L-valyl-gemcitabine (L-Val-Gem), 5'-D-valyl-gemcitabine (D-Val-Gem), 5'-L-phenylalanyl-gemcitabine (L-Phe-Gem), 5'-D-phenylalanyl-gemcitabine (D-Phe-Gem), and 5'-L-Phenylalanyl-L-tyrosyl-gemcitabine (L-Phe-L-Tyr-Gem), are shown in Figure 2.8.

Such prodrugs have been shown to address the two factors believed to limit gemcitabine oral bioavailability: (1) low intestinal permeability and (2) extensive first-pass metabolism. First, as shown in Table 2.4, all tested prodrugs displayed a higher apparent permeability (P_{app}) than gemcitabine when incubated at 100 μM with Caco-2 cell monolayers [218, 222]. Although the P_{app} of L-Phe-L-Tyr-Gem was not determined, L-

Phe-L-Tyr-Gem uptake was greater than gemcitabine uptake when incubated at 100 μM in Caco-2 cells. Interestingly, the Caco-2 uptake of all prodrugs, except L-Phe-L-Tyr-Gem, was statistically significantly reduced in the presence of a competitive PEPT1 inhibitor (10 mM glycyl-proline). This suggests that the increased uptake of L-Phe-L-Try-Gem, relative to gemcitabine, is not due to PEPT1-mediated transport [222]. Likewise, *in situ* jejunal perfusions in mice revealed increased effective intestinal permeability (P_{eff}) for all prodrugs, relative to gemcitabine, when perfused at 100 μM. The P_{eff} values for gemcitabine and the prodrugs reported in the literature by Tsume *el al.* contain a unit error [218, 222]. Interestingly, approximately 30% of the perfused gemcitabine was found in perfusion outlet samples as cytosine, signifying extensive glycosidic bond breakage (Tsume laboratory notebook). While this metabolic pathway has been reported for other nucleoside analogs, including floxuridine, it has not been reported for gemcitabine [223]. Next, as seen in Table 2.5, *in vitro* incubations of gemcitabine and gemcitabine prodrugs at 200 μM with purified CDA enzyme at 5.0 ng/μL showed that all prodrugs had increased resistance to CDA-mediated deamination, relative to gemcitabine [224]. Finally, following a 2 hr *in situ* jejunal perfusion of gemcitabine and the gemcitabine prodrugs at 100 μM, the plasma concentrations of prodrug (following prodrug perfusion), gemcitabine, and cytosine were determined. These results, presented in Figure 2.9, show a general trend that total drug concentrations in plasma are higher following prodrug perfusion and that four of the five prodrugs are found in systemic circulation intact. Importantly, while the prodrugs show promise for increasing gemcitabine oral bioavailability based on both *in vitro* and *in situ* experiments, their *in vivo* pharmacokinetic performance has not yet been evaluated.

Tables and Figures

Table 2.1 Amino acid length and sequence identity of the human proton-coupled oligopeptide transporters

Transporter	Amino Acid Length	Sequence Identity with PEPT1	Sequence Identity with PEPT2	Sequence Identity with PHT1	Sequence Identity with PHT2
PEPT1	708	-	49.2%	23.1%	23.8%
PEPT2	729	49.2%	-	25.8%	24.2%
PHT1	577	23.1%	25.8%	-	50.6%
PHT2	581	23.8%	24.2%	50.6%	-

Sequence identities were calculated using the Basic Local Alignment Search Tool (BLAST) provided by the National Center for Biotechnology Information [225]. PEPT1, peptide transporter 1; PEPT2, peptide transporter 2; PHT1, peptide/histidine transporter 1; PHT2, peptide/histidine transporter 2.

Table 2.2 Off-label uses of gemcitabine receiving a "Strong" recommendation for use from Elsevier Gold Standard's Clinical Pharmacology compendium

Indication	**Coadministered Medication**
Biliary tract cancer (advanced or metastatic)	cisplatin
Non-Hodgkin lymphoma (aggressive, in transplant eligible patients with relapsed or refractory cases)	cisplatin + dexamethasone + rituximab (for CD20-positive)
Non-small cell lung cancer (advanced or metastatic)	paclitaxel
Non-small cell lung cancer (unresectable, locally advanced or metastatic)	carboplatin
	docetaxel
Pancreatic cancer (adjuvant treatment)	none
Pancreatic cancer (advanced)	nab-paclitaxel
Pancreatic ductal adenocarcinoma (adjuvant treatment)	capecitabine
Translational-cell bladder cancer (locally advanced or metastatic)	cisplatin

Data aggregated from [144].

Table 2.3 Age- and gender-dependent population estimates of gemcitabine clearance

Age	Male	Female
29	92.2	66.0
45	75.7	54.2
56	55.1	39.5
79	40.7	29.2

Clearance presented as L/hr/m^2. Parameters from [161].

Table 2.4 Permeability of gemcitabine and gemcitabine prodrugs determined *in vitro* in Caco-2 cells and *in situ* via jejunal perfusions in mice

Drug or Prodrug	**P_{app}, Caco-2 (x 10^{-6} cm/s)**	**P_{eff}, jejunal mouse perfusion (x 10^{-5} cm/s)**
Gemcitabine	1.0 ± 0.2	0.2 ± 0.02
L-Val-Gem	4.0 ± 0.1 *	3.6 ± 0.9 *
D-Val-Gem	3.9 ± 0.1 *	1.9 ± 0.6 *
L-Phe-Gem	3.8 ± 0.9 *	3.4 ± 0.3 *
D-Phe-Gem	4.5 ± 0.9 *	2.2 ± 0.4 *
L-Phe-L-Tyr-Gem	NA	2.2 ± 0.4 *

Data obtained from Dr. Yasuhiro Tsume's notebook. Caco-2 incubations and jejunal perfusions both done with test compounds at 100 μM. Data reported as mean ± SD (n = 3). *$p < 0.05$, compared to gemcitabine. P_{app}, apparent permeability; P_{eff}, effective permeability; L-Val-Gem, 5'-L-valyl-gemcitabine; D-Val-Gem, 5'-D-valyl-gemcitabine; L-Phe-Gem, 5'-L-phenylalanyl-gemcitabine; D-Phe-Gem, 5'-D-phenylalanyl-gemcitabine; L-Phe-L-Tyr-Gem, 5'-L-phenylalanyl-L-tyrosyl-gemcitabine.

Table 2.5 Half-life of gemcitabine and gemcitabine prodrugs when incubated with cytidine deaminase

Drug or Prodrug	**$t_{1/2}$ (min)**
Gemcitabine	<3
L-Val-Gem	>120
D-Val-Gem	>120
L-Phe-Gem	44.6 ± 18.8
D-Phe-Gem	>120
L-Phe-L-Tyr-Gem	>120

Data from [224]. Incubations contained tested compounds at 200 μM and recombinant cytidine deaminase at 5.0 ng/μL. $t_{1/2}$, half-life; L-Val-Gem, 5'-L-valyl-gemcitabine; D-Val-Gem, 5'-D-valyl-gemcitabine; L-Phe-Gem, 5'-L-phenylalanyl-gemcitabine; D-Phe-Gem, 5'-D-phenylalanyl-gemcitabine; L-Phe-L-Tyr-Gem, 5'-L-phenylalanyl-L-tyrosyl-gemcitabine.

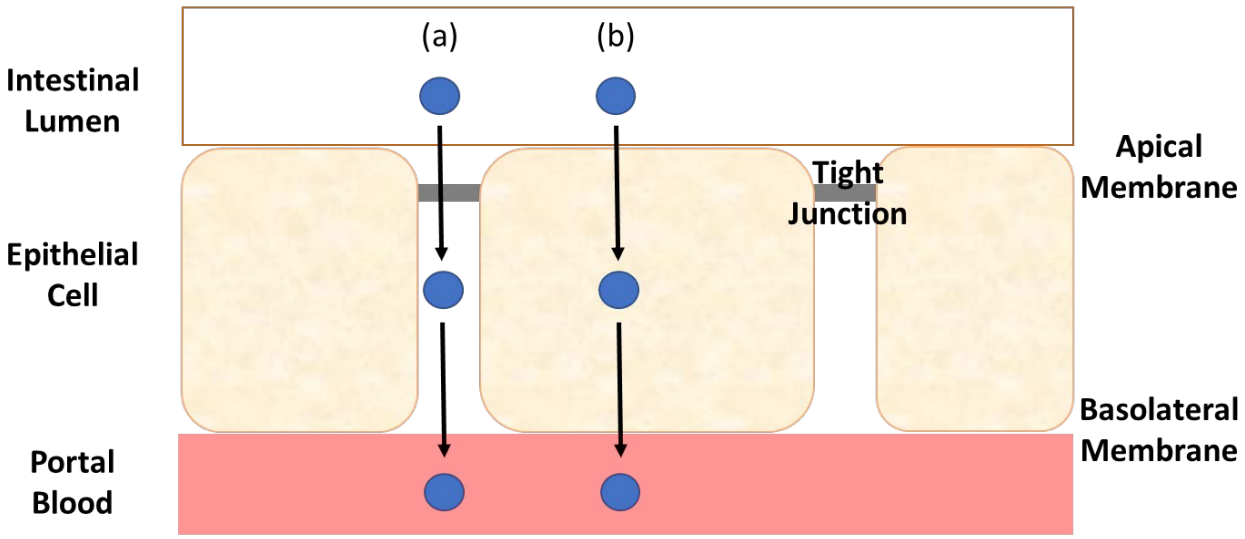

Figure 2.1 The (a) paracellular and (b) transcellular pathways of intestinal drug absorption.

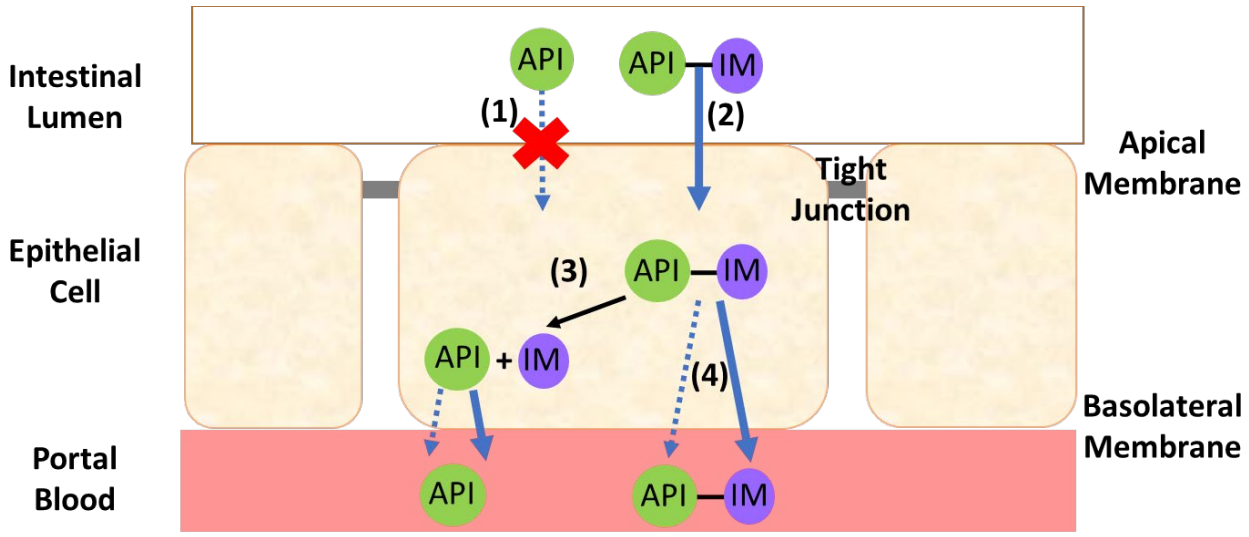

Figure 2.2 Application of the transporter-targeted prodrug strategy to increase a drug's oral bioavailability. Dashed and solid lines represent passive diffusion and transporter mediated partitioning across epithelial membranes, respectively. (1) The active pharmaceutical ingredient (API) is unable to efficiently diffuse through apical membrane. (2) The API is covalently bound to an inactive moiety (IM), generating a prodrug that undergoes transporter mediated uptake into the enterocyte. (3) Intestinal metabolism of prodrug releases the API and the API crosses the basolateral membrane through either passive diffusion or transporter mediated efflux. (4) The prodrug crosses the basolateral membrane through either passive diffusion or transporter mediated efflux.

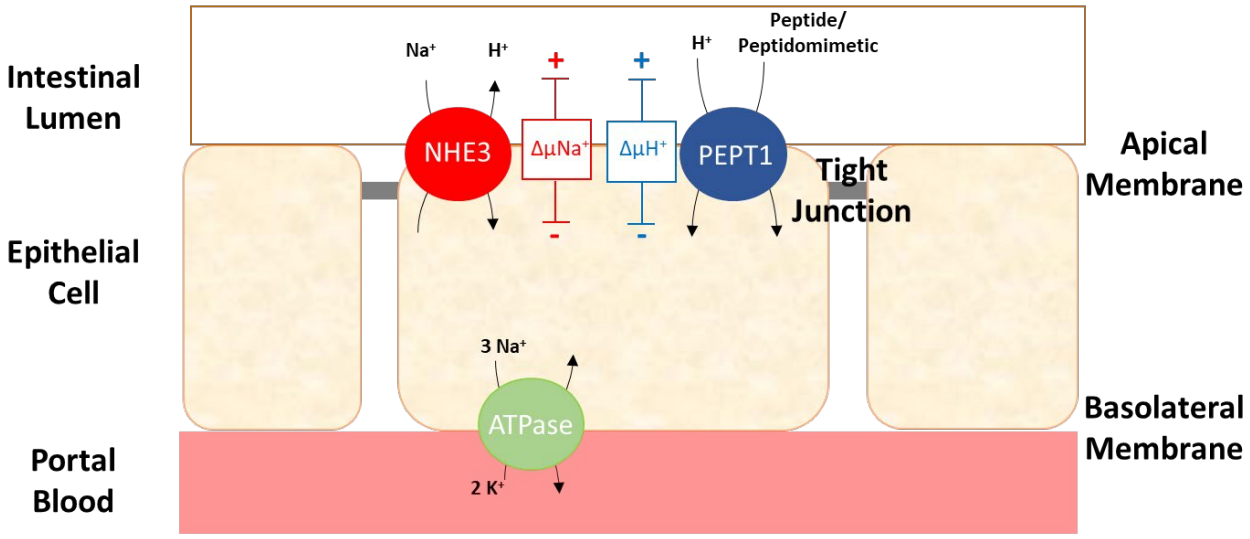

Figure 2.3 Schematic representation of the transporters (represented by large circles) involved in the PEPT1-mediated intestinal uptake of peptides/peptidomimetics. The basolaterally expressed Na^+-K^+-ATPase generates an intracellularly-directed Na^+ gradient. The apically expressed Na^+/H+ antiporter (NHE3) utilizes this Na^+ gradient to generate an intracellularly-directed H^+ gradient. The apically expressed peptide transporter 1 (PEPT1) utilizes this gradient to cotransport a proton and peptide/peptidomimetic into the enterocyte.

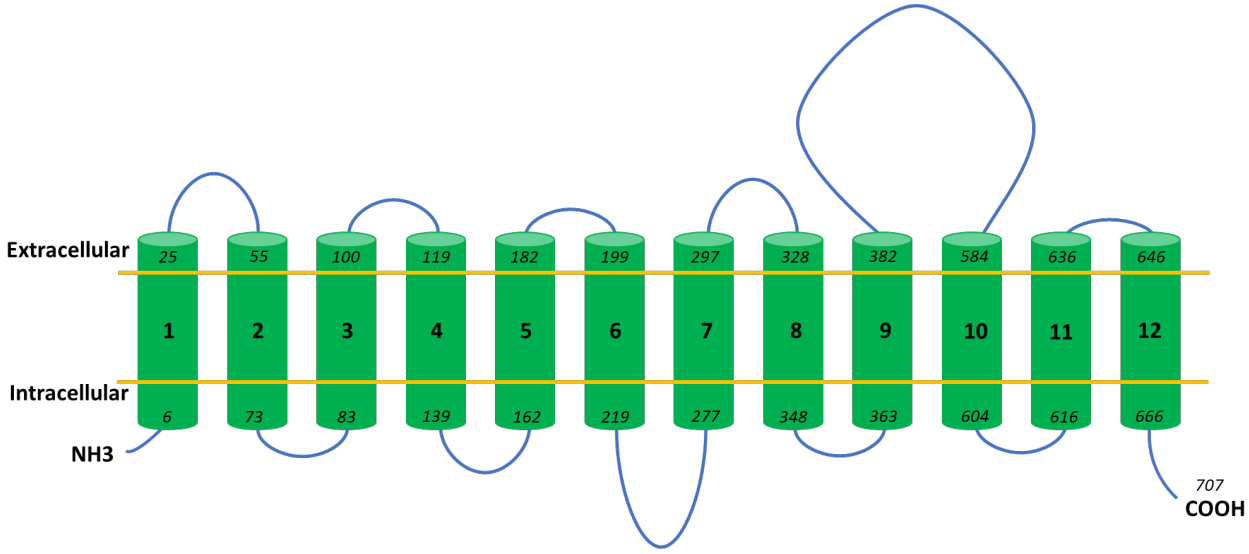

Figure 2.4 Membrane topology of PEPT1 (figure adapted from [226]).

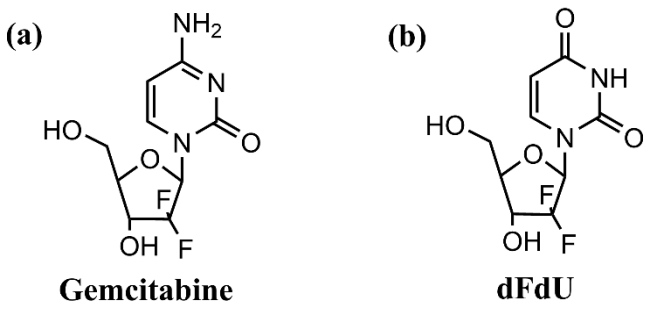

Figure 2.5 Structures of (a) gemcitabine and (b) the deaminated gemcitabine metabolite dFdU.

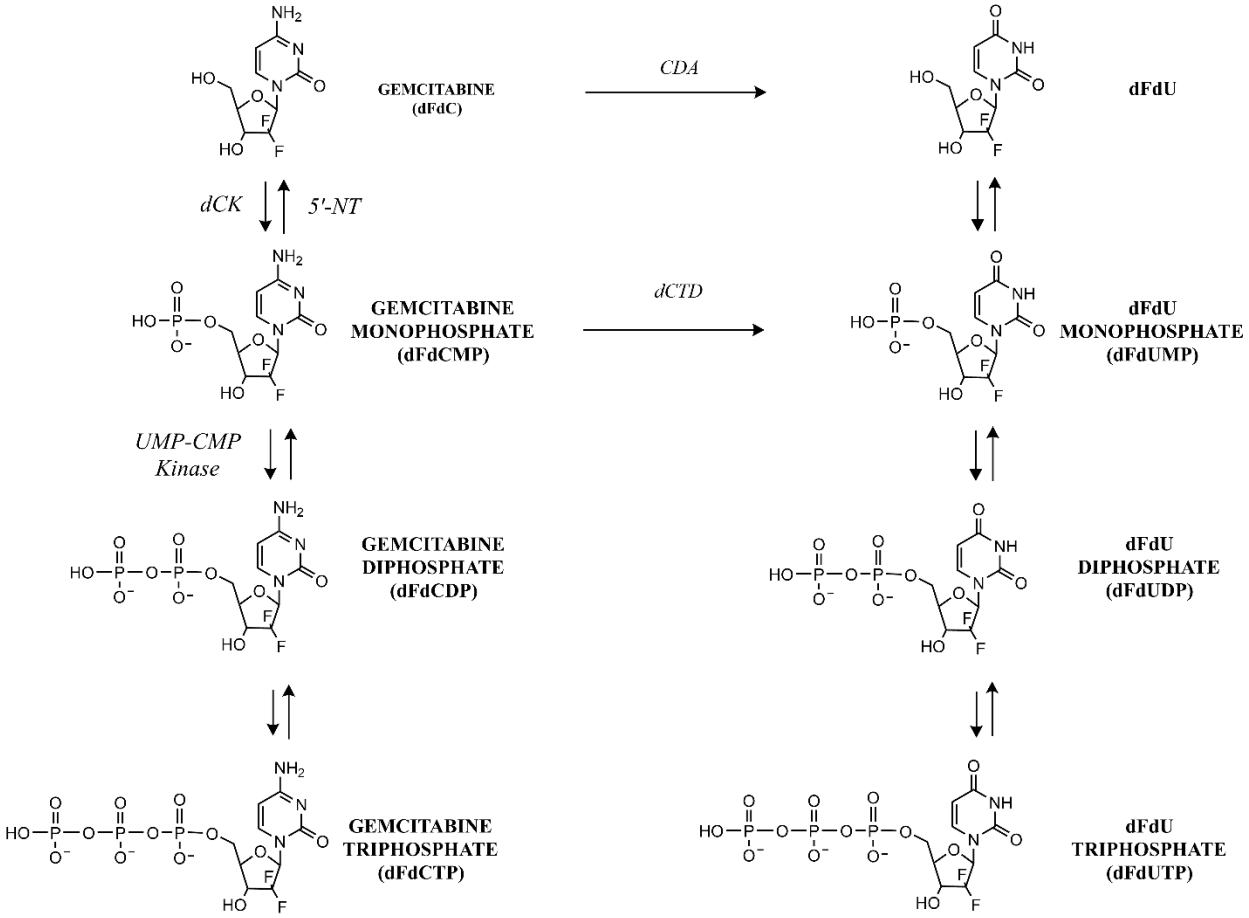

Figure 2.6 Schematic of intracellular gemcitabine activation with the enzyme mediating each step presented in *italics.* dFdU, 2',2'-difluorodeoxyuridine; CDA, cytidine deaminase; dCK, deoxycytidine kinase; 5'-NT, 5'-nucleotidase; dCTD, deoxycytidylate deaminase; UMP-CMP kinase, pyrimidine nucleoside monophosphate kinase. Figure adapted from [179].

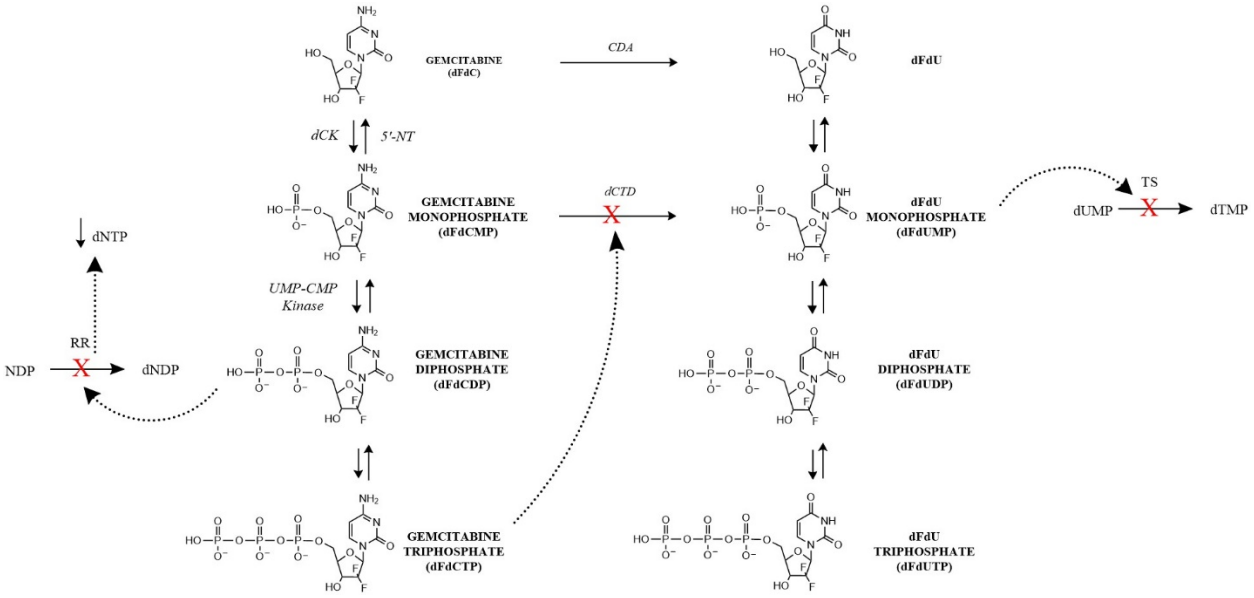

Figure 2.7 Schematic of gemcitabine self-potentiation with metabolite activity shown as a dotted arrow. dFdU, 2',2'-difluorodeoxyuridine; CDA, cytidine deaminase; dCK, deoxycytidine kinase; 5'-NT, 5'-nucleotidase; dCTD, deoxycytidylate deaminase; UMP-CMP kinase, pyrimidine nucleoside monophosphate kinase; RR, ribonucleotide reductase; NDP, nucleoside diphosphate; dNDP, deoxynucleoside diphosphate; [dNTP], intracellular concentration of deoxynucleoside triphosphates; TS, thymidylate synthase; dUMP, deoxyuridine monophosphate; dTMP deoxythymidine monophosphate. Figure adapted from [179].

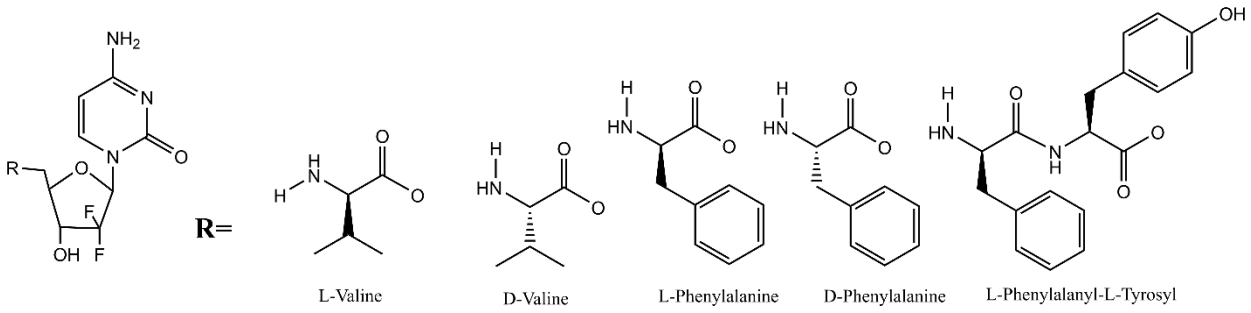

Figure 2.8 Structures of previously synthesized PEPT1-targeted amino acid and dipeptide ester gemcitabine prodrugs from the Dr. Gordon Amidon Laboratory [222, 227]

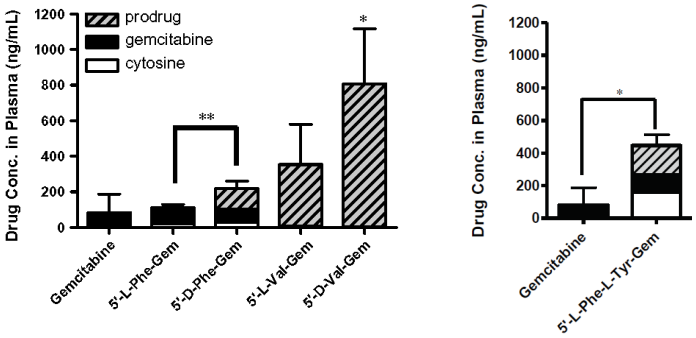

Figure 2.9 The concentrations of prodrug, gemcitabine, and cytosine in mouse plasma following a 2 hr *in situ* jejunal perfusion of gemcitabine and the gemcitabine prodrugs at 100 μM. *$p<0.05$, total drug concentration compared to gemcitabine. Amino acid ester prodrug (left panel) data taken from [218] and dipeptide ester prodrug data (right panel) taken from [222]. L-Phe-Gem, 5'-L-phenylalanyl-gemcitabine; D-Phe-Gem, 5'-D-phenylalanyl-gemcitabine; L-Val-Gem, 5'-L-valyl-gemcitabine; D-Val-Gem, 5'-D-valyl-gemcitabine; L-Phe-L-Tyr-Gem, 5'-L-phenylalanyl-L-tyrosyl-gemcitabine.

References

[1] El-Kattan A. and Varma M., *Oral absorption, intestinal metabolism and human oral bioavailability*, in *Topics on drug metabolism*, J. Paxton, Editor. 2012, InTech. p. 1-34.

[2] Homayun B., Lin X., and Choi H.J., Challenges and Recent Progress in Oral Drug Delivery Systems for Biopharmaceuticals, Pharmaceutics. 11 (3) (2019) 129.

[3] Hellriegel E.T., Bjornsson T.D., and Hauck W.W., Interpatient variability in bioavailability is related to the extent of absorption: Implications for bioavailability and bioequivalence studies, Clin Pharmacol Ther. 60 (6) (1996) 601-607.

[4] Thomas V.H., Bhattachar S., Hitchingham L., Zocharski P., Naath M., Surendran N., Stoner C.L., and El-Kattan A., The road map to oral bioavailability: an industrial perspective, Expert Opin Drug Metab Toxicol. 2 (4) (2006) 591-608.

[5] Helander H.F. and Fandriks L., Surface area of the digestive tract - revisited, Scand J Gastroenterol. 49 (6) (2014) 681-689.

[6] Fanucci A., Cerro P., and Fanucci E., Normal small-bowel measurements by enteroclysis, Scand J Gastroenterol. 23 (5) (1988) 574-576.

[7] Backman L. and Hallberg D., Small-intestinal length. An intraoperative study in obesity, Acta Chir Scand. 140 (1) (1974) 57-63.

[8] Mahadevan V., Anatomy of the small intestine, Surgery (Oxf). 35 (8) (2017) 407-412.

[9] Murakami T., Absorption sites of orally administered drugs in the small intestine, Expert Opin Drug Discov. 12 (12) (2017) 1219-1232.

[10] Artursson P., Ungell A.-L., and Löfroth J.-E., Selective Paracellular Permeability in Two Models of Intestinal Absorption: Cultured Monolayers of Human Intestinal Epithelial Cells and Rat Intestinal Segments, Pharm Res. 10 (8) (1993) 1123-1129.

[11] Karlsson J., Ungell A., Grasjo J., and Artursson P., Paracellular drug transport across intestinal epithelia: influence of charge and induced water flux, Eur J Pharm Sci. 9 (1) (1999) 47-56.

[12] Hamman J.H., Demana P.H., and Olivier E.I., Targeting receptors, transporters and site of absorption to improve oral drug delivery, Drug Target Insights. 2 (2007) 71-81.

[13] Neves A.R., Queiroz J.F., Costa Lima S.A., Figueiredo F., Fernandes R., and Reis S., Cellular uptake and transcytosis of lipid-based nanoparticles across the intestinal barrier: Relevance for oral drug delivery, J Colloid Interface Sci. 463 (2016) 258-265.

[14] Hediger M.A., Clemencon B., Burrier R.E., and Bruford E.A., The ABCs of membrane transporters in health and disease (SLC series): introduction, Mol Aspects Med. 34 (2-3) (2013) 95-107.

[15] Hillgren K.M., Keppler D., Zur A.A., Giacomini K.M., Stieger B., Cass C.E., Zhang L., and International Transporter C., Emerging transporters of clinical importance: an update from the International Transporter Consortium, Clin Pharmacol Ther. 94 (1) (2013) 52-63.

[16] Kaminsky L.S. and Zhang Q.Y., The small intestine as a xenobiotic-metabolizing organ, Drug Metab Dispos. 31 (12) (2003) 1520-1525.

[17] Lipinski C.A., Lombardo F., Dominy B.W., and Feeney P.J., Experimental and computational approaches to estimate solubility and permeability in drug discovery and development settings, Adv Drug Deliv Rev. 23 (1) (1997) 3-25.

[18] Posada M.M. and Smith D.E., Relevance of PepT1 in the intestinal permeability and oral absorption of cefadroxil, Pharm Res. 30 (4) (2013) 1017-1025.

[19] Yang B., Hu Y., and Smith D.E., Impact of peptide transporter 1 on the intestinal absorption and pharmacokinetics of valacyclovir after oral dose escalation in wild-type and PepT1 knockout mice, Drug Metab Dispos. 41 (10) (2013) 1867-1874.

[20] Imanaga J., Kotegawa T., Imai H., Tsutsumi K., Yoshizato T., Ohyama T., Shirasaka Y., Tamai I., Tateishi T., and Ohashi K., The effects of the SLCO2B1 c. 1457C> T polymorphism and apple juice on the pharmacokinetics of fexofenadine and midazolam in humans, Pharmacogenet Genomics. 21 (2) (2011) 84-93.

[21] Han H.-K. and Amidon G.L., Targeted prodrug design to optimize drug delivery, AAPS PharmSci. 2 (1) (2000) 48-58.

[22] Rautio J., Kumpulainen H., Heimbach T., Oliyai R., Oh D., Jarvinen T., and Savolainen J., Prodrugs: design and clinical applications, Nat Rev Drug Discov. 7 (3) (2008) 255-270.

[23] Varma M.V., Ambler C.M., Ullah M., Rotter C.J., Sun H., Litchfield J., Fenner K.S., and El-Kattan A.F., Targeting intestinal transporters for optimizing oral drug absorption, Curr Drug Metab. 11 (9) (2010) 730-742.

[24] Smith D.E., Clemencon B., and Hediger M.A., Proton-coupled oligopeptide transporter family SLC15: physiological, pharmacological and pathological implications, Mol Aspects Med. 34 (2-3) (2013) 323-336.

[25] Brandsch M., Knutter I., and Bosse-Doenecke E., Pharmaceutical and pharmacological importance of peptide transporters, J Pharm Pharmacol. 60 (5) (2008) 543-585.

[26] Biegel A., Knutter I., Hartrodt B., Gebauer S., Theis S., Luckner P., Kottra G., Rastetter M., Zebisch K., Thondorf I., Daniel H., Neubert K., and Brandsch M., The renal type H+/peptide symporter PEPT2: structure-affinity relationships, Amino Acids. 31 (2) (2006) 137-156.

[27] Nakamura N., Lill J.R., Phung Q., Jiang Z., Bakalarski C., de Maziere A., Klumperman J., Schlatter M., Delamarre L., and Mellman I., Endosomes are specialized platforms for bacterial sensing and NOD2 signalling, Nature. 509 (7499) (2014) 240-244.

[28] Sakata K., Yamashita T., Maeda M., Moriyama Y., Shimada S., and Tohyama M., Cloning of a lymphatic peptide/histidine transporter, Biochem J. 356 (Pt 1) (2001) 53-60.

[29] Hu Y., Xie Y., Keep R.F., and Smith D.E., Divergent developmental expression and function of the proton-coupled oligopeptide transporters PepT2 and PhT1 in regional brain slices of mouse and rat, J Neurochem. 129 (6) (2014) 955-965.

[30] Wang X.-X., Hu Y., Keep R.F., Toyama-Sorimachi N., and Smith D.E., A novel role for PHT1 in the disposition of l-histidine in brain: In vitro slice and in vivo pharmacokinetic studies in wildtype and Pht1 null mice, Biochem Pharmacol. 124 (2017) 94-102.

[31] Sasawatari S., Okamura T., Kasumi E., Tanaka-Furuyama K., Yanobu-Takanashi R., Shirasawa S., Kato N., and Toyama-Sorimachi N., The solute carrier family 15A4 regulates TLR9 and NOD1 functions in the innate immune system and promotes colitis in mice, Gastroenterology. 140 (5) (2011) 1513-1525.

[32] Hu Y., Song F., Jiang H., Nunez G., and Smith D.E., SLC15A2 and SLC15A4 Mediate the Transport of Bacterially Derived Di/Tripeptides To Enhance the Nucleotide-Binding Oligomerization Domain-Dependent Immune Response in Mouse Bone Marrow-Derived Macrophages, J Immunol. 201 (2) (2018) 652-662.

[33] Lee J., Tattoli I., Wojtal K.A., Vavricka S.R., Philpott D.J., and Girardin S.E., pH-dependent internalization of muramyl peptides from early endosomes enables Nod1 and Nod2 signaling, J Biol Chem. 284 (35) (2009) 23818-23829.

[34] Zuo X.B., Sheng Y.J., Hu S.J., Gao J.P., Li Y., Tang H.Y., Tang X.F., Cheng H., Yin X.Y., Wen L.L., Sun L.D., Yang S., Cui Y., and Zhang X.J., Variants in TNFSF4, TNFAIP3, TNIP1, BLK, SLC15A4 and UBE2L3 interact to confer risk of systemic lupus erythematosus in Chinese population, Rheumatol Int. 34 (4) (2014) 459-464.

[35] Takeuchi F., Ochiai Y., Serizawa M., Yanai K., Kuzuya N., Kajio H., Honjo S., Takeda N., Kaburagi Y., Yasuda K., Shirasawa S., Sasazuki T., and Kato N., Search for type 2 diabetes susceptibility genes on chromosomes 1q, 3q and 12q, J Hum Genet. 53 (4) (2008) 314-324.

[36] Wang Y., Hu Y., Li P., Weng Y., Kamada N., Jiang H., and Smith D.E., Expression and regulation of proton-coupled oligopeptide transporters in colonic tissue and immune cells of mice, Biochem Pharmacol. 148 (2018) 163-173.

[37] Song F., Yi Y., Li C., Hu Y., Wang J., Smith D.E., and Jiang H., Regulation and biological role of the peptide/histidine transporter SLC15A3 in Toll-like receptor-mediated inflammatory responses in macrophage, Cell Death Dis. 9 (7) (2018) 770.

[38] Song F., Hu Y., Wang Y., Smith D.E., and Jiang H., Functional Characterization of Human Peptide/Histidine Transporter 1 in Stably Transfected MDCK Cells, Mol Pharm. 15 (2) (2018) 385-393.

[39] Wang Y., Li P., Song F., Yang X., Weng Y., Ma Z., Wang L., and Jiang H., Substrate Transport Properties of the Human Peptide/Histidine Transporter PHT2 in Transfected MDCK Cells, J Pharm Sci. 108 (10) (2019) 3416-3424.

[40] Dantzig A.H., Hoskins J., Tabas L.B., Bright S., Shepard R.L., Jenkins I.L., Duckworth D.C., Sportsman J.R., Mackensen D., and Rosteck Jr P.R., Association of intestinal peptide transport with a protein related to the cadherin superfamily, Science. 264 (5157) (1994) 430-432.

[41] Huankai H., Miyauchi S., Bridges C.C., Smith S.B., and Ganapathy V., Identification of a novel Na+-and Cl−-coupled transport system for endogenous opioid peptides in retinal pigment epithelium and induction of the transport system by HIV-1 Tat, Biochem J. 375 (1) (2003) 17-22.

[42] Landowski C.P., Sun D., Foster D.R., Menon S.S., Barnett J.L., Welage L.S., Ramachandran C., and Amidon G.L., Gene expression in the human intestine and correlation with oral valacyclovir pharmacokinetic parameters, J Pharmacol Exp Ther. 306 (2) (2003) 778-786.

[43] Ganapathy V. and Miyauchi S., Transport systems for opioid peptides in mammalian tissues, AAPS J. 7 (4) (2005) E852-E856.

[44] Ogihara H., Saito H., Shin B.-C., Terada T., Takenoshita S., Nagamachi Y., Inui K.-i., and Takata K., Immuno-Localization of H+/Peptide Cotransporter in Rat Digestive Tract, Biochem Biophys Res Commun. 220 (3) (1996) 848-852.

[45] Shen H., Smith D.E., Yang T., Huang Y.G., Schnermann J.B., and Brosius F.C., 3rd, Localization of PEPT1 and PEPT2 proton-coupled oligopeptide transporter mRNA and protein in rat kidney, Am J Physiol. 276 (5 Pt 2) (1999) F658-665.

[46] Bockman D.E., Ganapathy V., Oblak T.G., and Leibach F.H., Localization of peptide transporter in nuclei and lysosomes of the pancreas, Int J Pancreatol. 22 (3) (1997) 221-225.

[47] Knutter I., Rubio-Aliaga I., Boll M., Hause G., Daniel H., Neubert K., and Brandsch M., H+-peptide cotransport in the human bile duct epithelium cell line SK-ChA-1, Am J Physiol Gastrointest Liver Physiol. 283 (1) (2002) G222-229.

[48] Charrier L., Driss A., Yan Y., Nduati V., Klapproth J.M., Sitaraman S.V., and Merlin D., hPepT1 mediates bacterial tripeptide fMLP uptake in human monocytes, Lab Invest. 86 (5) (2006) 490-503.

[49] Wuensch T., Schulz S., Ullrich S., Lill N., Stelzl T., Rubio-Aliaga I., Loh G., Chamaillard M., Haller D., and Daniel H., The peptide transporter PEPT1 is expressed in distal colon in rodents and humans and contributes to water absorption, Am J Physiol Gastrointest Liver Physiol. 305 (1) (2013) G66-G73.

[50] Drozdzik M., Busch D., Lapczuk J., Müller J., Ostrowski M., Kurzawski M., and Oswald S., Protein abundance of clinically relevant drug transporters in the human liver and intestine: a comparative analysis in paired tissue specimens, Clin Pharmacol Ther. 105 (5) (2019) 1204-1212.

[51] Groneberg D.A., Doring F., Eynott P.R., Fischer A., and Daniel H., Intestinal peptide transport: ex vivo uptake studies and localization of peptide carrier PEPT1, Am J Physiol Gastrointest Liver Physiol. 281 (3) (2001) G697-704.

[52] Viennois E., Pujada A., Zen J., and Merlin D., Function, Regulation, and Pathophysiological Relevance of the POT Superfamily, Specifically PepT1 in Inflammatory Bowel Disease, Compr Physiol. 8 (2) (2018) 731-760.

[53] Jappar D., Wu S.P., Hu Y., and Smith D.E., Significance and regional dependency of peptide transporter (PEPT) 1 in the intestinal permeability of glycylsarcosine: in situ single-pass perfusion studies in wild-type and Pept1 knockout mice, Drug Metab Dispos. 38 (10) (2010) 1740-1746.

[54] Daniel H., Molecular and integrative physiology of intestinal peptide transport, Annu Rev Physiol. 66 (2004) 361-384.

[55] Terada T., Sawada K., Saito H., Hashimoto Y., and Inui K., Functional characteristics of basolateral peptide transporter in the human intestinal cell line Caco-2, Am J Physiol. 276 (6 Pt 1) (1999) G1435-1441.

[56] Keiser M., Mangelsen E., Petrikat T., and Oswald S., Characterization of the intestinal absorption of beta-lactam antibiotics in a PEPT1/MRP3 double-transfected cell line and by using the ussing chamber technique, Drug Metab Pharmacokinet. 32 (1) (2017) S25.

[57] Adibi S.A., Renal assimilation of oligopeptides: physiological mechanisms and metabolic importance, Am J Physiol Endoc Metab. 272 (5) (1997) E723-E736.

[58] Smith D.E., Pavlova A., Berger U.V., Hediger M.A., Yang T., Huang Y.G., and Schnermann J.B., Tubular localization and tissue distribution of peptide transporters in rat kidney, Pharm Res. 15 (8) (1998) 1244-1249.

[59] Ocheltree S.M., Shen H., Hu Y., Keep R.F., and Smith D.E., Role and relevance of peptide transporter 2 (PEPT2) in the kidney and choroid plexus: in vivo studies with glycylsarcosine in wild-type and PEPT2 knockout mice, J Pharmacol Exp Ther. 315 (1) (2005) 240-247.

[60] Seal C. and Parker D., Isolation and characterization of circulating low molecular weight peptides in steer, sheep and rat portal and peripheral blood, Comp Biochem Physiol B. 99 (3) (1991) 679-685.

[61] Terada T., Sawada K., Ito T., Saito H., Hashimoto Y., and Inui K., Functional expression of novel peptide transporter in renal basolateral membranes, Am J Physiol Renal Physiol. 279 (5) (2000) F851-857.

[62] Ganapathy V. and Leibach F.H., Role of pH gradient and membrane potential in dipeptide transport in intestinal and renal brush-border membrane vesicles from the rabbit. Studies with L-carnosine and glycyl-L-proline, J Biol Chem. 258 (23) (1983) 14189-14192.

[63] Ganapathy V. and Leibach F.H., Is Intestinal Peptide-Transport Energized by a Proton Gradient, Am J Physiol. 249 (2) (1985) G153-G160.

[64] Fei Y.-J., Kanai Y., Nussberger S., Ganapathy V., Leibach F.H., Romero M.F., Singh S.K., Boron W.F., and Hediger M.A., Expression cloning of a mammalian proton-coupled oligopeptide transporter, Nature. 368 (6471) (1994) 563.

[65] Amasheh S., Wenzel U., Boll M., Dorn D., Weber W., Clauss W., and Daniel H., Transport of charged dipeptides by the intestinal H+/peptide symporter PepT1 expressed in Xenopus laevis oocytes, J Membr Biol. 155 (3) (1997) 247-256.

[66] Kottra G., Stamfort A., and Daniel H., PEPT1 as a paradigm for membrane carriers that mediate electrogenic bidirectional transport of anionic, cationic, and neutral substrates, J Biol Chem. 277 (36) (2002) 32683-32691.

[67] Steel A., Nussberger S., Romero M.F., Boron W.F., Boyd C.A., and Hediger M.A., Stoichiometry and pH dependence of the rabbit proton-dependent oligopeptide transporter PepT1, J Physiol. 498 (Pt 3) (1997) 563-569.

[68] Mackenzie B., Fei Y.J., Ganapathy V., and Leibach F.H., The human intestinal H+/oligopeptide cotransporter hPEPT1 transports differently-charged dipeptides with identical electrogenic properties, Biochim Biophys Acta. 1284 (2) (1996) 125-128.

[69] Wenzel U., Gebert I., Weintraut H., Weber W.M., Clauss W., and Daniel H., Transport characteristics of differently charged cephalosporin antibiotics in oocytes

expressing the cloned intestinal peptide transporter PepT1 and in human intestinal Caco-2 cells, J Pharmacol Exp Ther. 277 (2) (1996) 831.

[70] Thwaites D.T. and Anderson C.M., H+-coupled nutrient, micronutrient and drug transporters in the mammalian small intestine, Exp Physiol. 92 (4) (2007) 603-619.

[71] Covitz K.M., Amidon G.L., and Sadee W., Membrane topology of the human dipeptide transporter, hPEPT1, determined by epitope insertions, Biochemistry. 37 (43) (1998) 15214-15221.

[72] Beale J.H., Parker J.L., Samsudin F., Barrett A.L., Senan A., Bird L.E., Scott D., Owens R.J., Sansom M.S.P., Tucker S.J., Meredith D., Fowler P.W., and Newstead S., Crystal Structures of the Extracellular Domain from PepT1 and PepT2 Provide Novel Insights into Mammalian Peptide Transport, Structure. 23 (10) (2015) 1889-1899.

[73] Minhas G.S. and Newstead S., Structural basis for prodrug recognition by the SLC15 family of proton-coupled peptide transporters, PNAS. 116 (3) (2019) 804-809.

[74] Newstead S., Drew D., Cameron A.D., Postis V.L., Xia X., Fowler P.W., Ingram J.C., Carpenter E.P., Sansom M.S., McPherson M.J., Baldwin S.A., and Iwata S., Crystal structure of a prokaryotic homologue of the mammalian oligopeptide-proton symporters, PepT1 and PepT2, EMBO J. 30 (2) (2011) 417-426.

[75] Solcan N., Kwok J., Fowler P.W., Cameron A.D., Drew D., Iwata S., and Newstead S., Alternating access mechanism in the POT family of oligopeptide transporters, EMBO J. 31 (16) (2012) 3411-3421.

[76] Doki S., Kato H.E., Solcan N., Iwaki M., Koyama M., Hattori M., Iwase N., Tsukazaki T., Sugita Y., Kandori H., Newstead S., Ishitani R., and Nureki O., Structural basis for dynamic mechanism of proton-coupled symport by the peptide transporter POT, PNAS. 110 (28) (2013) 11343-11348.

[77] Guettou F., Quistgaard E.M., Trésaugues L., Moberg P., Jegerschöld C., Zhu L., Jong A.J.O., Nordlund P., and Löw C., Structural insights into substrate recognition in proton-dependent oligopeptide transporters, EMBO Rep. 14 (9) (2013) 804-810.

[78] Zhao Y., Mao G., Liu M., Zhang L., Wang X., and Zhang X.C., Crystal structure of the E. coli peptide transporter YbgH, Structure. 22 (8) (2014) 1152-1160.

[79] Boggavarapu R., Jeckelmann J.-M., Harder D., Ucurum Z., and Fotiadis D., Role of electrostatic interactions for ligand recognition and specificity of peptide transporters, BMC Biology. 13 (1) (2015) 58.

[80] Fowler P.W., Orwick-Rydmark M., Radestock S., Solcan N., Dijkman P.M., Lyons J.A., Kwok J., Caffrey M., Watts A., Forrest L.R., and Newstead S., Gating

topology of the proton-coupled oligopeptide symporters, Structure. 23 (2) (2015) 290-301.

[81] Uchiyama T., Kulkarni A.A., Davies D.L., and Lee V.H., Biophysical evidence for His57 as a proton-binding site in the mammalian intestinal transporter hPepT1, Pharm Res. 20 (12) (2003) 1911-1916.

[82] Newstead S., Recent advances in understanding proton coupled peptide transport via the POT family, Curr Opin Struct Biol. 45 (2017) 17-24.

[83] Newstead S., Molecular insights into proton coupled peptide transport in the PTR family of oligopeptide transporters, Biochim Biophys Acta. 1850 (3) (2015) 488-499.

[84] Bolger M.B., Haworth I.S., Yeung A.K., Ann D., von Grafenstein H., Hamm-Alvarez S., Okamoto C.T., Kim K.-J., Basu S.K., Wu S., and Lee V.H.L., Structure, Function, and Molecular Modeling Approaches to the Study of the Intestinal Dipeptide Transporter PepT1, J Pharm Sci. 87 (11) (1998) 1286-1291.

[85] Samsudin F., Parker Joanne L., Sansom Mark S.P., Newstead S., and Fowler Philip W., Accurate Prediction of Ligand Affinities for a Proton-Dependent Oligopeptide Transporter, Cell Chem Biol. 23 (2) (2016) 299-309.

[86] Ito K., Hikida A., Kawai S., Lan V.T., Motoyama T., Kitagawa S., Yoshikawa Y., Kato R., and Kawarasaki Y., Analysing the substrate multispecificity of a proton-coupled oligopeptide transporter using a dipeptide library, Nat Commun. 4 (2013) 2502.

[87] Meredith D., Temple C.S., Guha N., Sword C.J., Boyd C.A., Collier I.D., Morgan K.M., and Bailey P.D., Modified amino acids and peptides as substrates for the intestinal peptide transporter PepT1, Eur J Biochem. 267 (12) (2000) 3723-3728.

[88] Vavricka S.R., Musch M.W., Chang J.E., Nakagawa Y., Phanvijhitsiri K., Waypa T.S., Merlin D., Schneewind O., and Chang E.B., hPepT1 transports muramyl dipeptide, activating NF-kappaB and stimulating IL-8 secretion in human colonic Caco2/bbe cells, Gastroenterology. 127 (5) (2004) 1401-1409.

[89] Ganapathy M.E., Brandsch M., Prasad P.D., Ganapathy V., and Leibach F.H., Differential recognition of beta -lactam antibiotics by intestinal and renal peptide transporters, PEPT 1 and PEPT 2, J Biol Chem. 270 (43) (1995) 25672-25677.

[90] Zhu T., Chen X.-Z., Steel A., Hediger M.A., and Smith D.E., Differential Recognition of ACE Inhibitors in Xenopus Laevis Oocytes Expressing Rat PEPT1 and PEPT2, Pharm Res. 17 (5) (2000) 526-532.

[91] Ryohei H., Yoshiko T., Toshiya K., Masato Y., Ken-Ichi I., and Mikihisa T., Transport of bestatin in rat renal brush-border membrane vesicles, Biochem Pharmacol. 45 (9) (1993) 1763-1768.

[92] Xie Y., Hu Y., and Smith D.E., The proton-coupled oligopeptide transporter 1 plays a major role in the intestinal permeability and absorption of 5-aminolevulinic acid, Br J Pharmacol. 173 (1) (2016) 167-176.

[93] Ganapathy M.E., Huang W., Wang H., Ganapathy V., and Leibach F.H., Valacyclovir: a substrate for the intestinal and renal peptide transporters PEPT1 and PEPT2, Biochem Biophys Res Commun. 246 (2) (1998) 470-475.

[94] Sugawara M., Huang W., Fei Y.J., Leibach F.H., Ganapathy V., and Ganapathy M.E., Transport of valganciclovir, a ganciclovir prodrug, via peptide transporters PEPT1 and PEPT2, J Pharm Sci. 89 (6) (2000) 781-789.

[95] Döring F., Will J., Amasheh S., Clauss W., Ahlbrecht H., and Daniel H., Minimal molecular determinants of substrates for recognition by the intestinal peptide transporter, J Biol Chem. 273 (36) (1998) 23211-23218.

[96] Brandsch M., Knutter I., and Leibach F.H., The intestinal H+/peptide symporter PEPT1: structure-affinity relationships, Eur J Pharm Sci. 21 (1) (2004) 53-60.

[97] Vig B.S., Stouch T.R., Timoszyk J.K., Quan Y., Wall D.A., and Smith R.L., Human PEPT1 pharmacophore distinguishes between dipeptide transport and binding, J Med Chem. 49 (2006) 3636-3644.

[98] Shen H., Smith D.E., and Brosius F.C., Developmental Expression of PEPT1 and PEPT2 in Rat Small Intestine, Colon, and Kidney, Pediatr Res. 49 (6) (2001) 789-795.

[99] Mooij M.G., de Koning B.A., Lindenbergh-Kortleve D.J., Simons-Oosterhuis Y., van Groen B.D., Tibboel D., Samsom J.N., and de Wildt S.N., Human intestinal PEPT1 transporter expression and localization in preterm and term infants, Drug Metab Dispos. (2016) 1014–1019.

[100] Alghamdi O.A., King N., Andronicos N.M., Jones G.L., Chami B., Witting P.K., and Moens P.D.J., Molecular changes to the rat renal cotransporters PEPT1 and PEPT2 due to ageing, Mol Cell Biochem. 452 (1-2) (2019) 71-82.

[101] Ihara T., Tsujikawa T., Fujiyama Y., and Bamba T., Regulation of PepT1 Peptide Transporter Expression in the Rat Small Intestine under Malnourished Conditions, Digestion. 61 (1) (2000) 59-67.

[102] Ma K., Hu Y., and Smith D.E., Influence of Fed-Fasted State on Intestinal PEPT1 Expression and In Vivo Pharmacokinetics of Glycylsarcosine in Wild-Type and Pept1 Knockout Mice, Pharm Res. 29 (2) (2012) 535-545.

[103] Shiraga T., Miyamoto K.-I., Tanaka H., Yamamoto H., Taketani Y., Morita K., Tamai I., Tsuji A., and Takeda E., Cellular and molecular mechanisms of dietary regulation on rat intestinal H+/peptide transporter PepT1, Gastroenterology. 116 (2) (1999) 354-362.

[104] Torelli Hijo A.H., Coutinho C.P., Alba-Loureiro T.C., Moreira Leite J.S., Bargi-Souza P., and Goulart-Silva F., High fat diet modulates the protein content of nutrient transporters in the small intestine of mice: possible involvement of PKA and PKC activity, Heliyon. 5 (10) (2019) e02611.

[105] Pan X., Terada T., Okuda M., and Inui K., The diurnal rhythm of the intestinal transporters SGLT1 and PEPT1 is regulated by the feeding conditions in rats, J Nutr. 134 (9) (2004) 2211-2215.

[106] Qandeel H.G., Duenes J.A., Zheng Y., and Sarr M.G., Diurnal expression and function of peptide transporter 1 (PEPT1), J Surg Res. 156 (1) (2009) 123-128.

[107] Anderson C.M.H. and Thwaites D.T., Regulation of intestinal hPepT1 (SLC15A1) activity by phosphodiesterase inhibitors is via inhibition of NHE3 (SLC9A3), Biochim Biophys Acta. 1768 (7) (2007) 1822-1829.

[108] Berlioz F., Maoret J.-J., Paris H., Laburthe M., Farinotti R., and Rozé C., α2-Adrenergic receptors stimulate oligopeptide transport in a human intestinal cell line, J Pharmacol Exp Ther. 294 (2) (2000) 466-472.

[109] Fujita T., Majikawa Y., Umehisa S., Okada N., Yamamoto A., Ganapathy V., and Leibach F.H., sigma Receptor ligand-induced up-regulation of the H(+)/peptide transporter PEPT1 in the human intestinal cell line Caco-2, Biochem Biophys Res Commun. 261 (2) (1999) 242-246.

[110] Duverne C., Bouten A., Deslandes A., Westphal J.F., Trouvin J.H., Farinotti R., and Carbon C., Modification of cefixime bioavailability by nifedipine in humans: involvement of the dipeptide carrier system, Antimicrob Agents Chemother. 36 (11) (1992) 2462-2467.

[111] Wenzel U., Kuntz S., Diestel S., and Daniel H., PEPT1-mediated cefixime uptake into human intestinal epithelial cells is increased by Ca2+ channel blockers, Antimicrob Agents Chemother. 46 (5) (2002) 1375-1380.

[112] Yotsumoto K., Akiyoshi T., Wada N., Imaoka A., and Ohtani H., 5-Fluorouracil treatment alters the expression of intestinal transporters in rats, Biopharm Drug Dispos. 38 (9) (2017) 509-516.

[113] Otter M., Oswald S., Siegmund W., and Keiser M., Effects of frequently used pharmaceutical excipients on the organic cation transporters 1-3 and peptide transporters 1/2 stably expressed in MDCKII cells, Eur J Pharm Biopharm. (2016) 187-195.

[114] Thamotharan M., Bawani S.Z., Zhou X., and Adibi S.A., Hormonal regulation of oligopeptide transporter pept-1 in a human intestinal cell line, Am J Physiol. 276 (4 Pt 1) (1999) C821-826.

[115] Buyse M., Berlioz F., Guilmeau S., Tsocas A., Voisin T., Peranzi G., Merlin D., Laburthe M., Lewin M.J., Roze C., and Bado A., PepT1-mediated epithelial transport of dipeptides and cephalexin is enhanced by luminal leptin in the small intestine, J Clin Invest. 108 (10) (2001) 1483-1494.

[116] Sun B.W., Zhao X.C., Wang G.J., Li N., and Li J.S., Hormonal regulation of dipeptide transporter (PepT1) in Caco-2 cells with normal and anoxia/reoxygenation management, World J Gastroenterol. 9 (4) (2003) 808-812.

[117] Lu H. and Klaassen C., Tissue distribution and thyroid hormone regulation of Pept1 and Pept2 mRNA in rodents, Peptides. 27 (4) (2006) 850-857.

[118] Nielsen C.U., Amstrup J., Steffansen B., Frokjaer S., and Brodin B., Epidermal growth factor inhibits glycylsarcosine transport and hPepT1 expression in a human intestinal cell line, Am J Physiol Gastrointest Liver Physiol. 281 (1) (2001) G191-199.

[119] Iwao T., Toyota M., Miyagawa Y., Okita H., Kiyokawa N., Akutsu H., Umezawa A., Nagata K., and Matsunaga T., Differentiation of human induced pluripotent stem cells into functional enterocyte-like cells using a simple method, Drug Metab Pharmacokinet. 29 (1) (2014) 44-51.

[120] Liu J., Shi B., Shi K., Ma G., Zhang H., Lou X., Liu H., Wan S., and Liang D., Ghrelin upregulates PepT1 activity in the small intestine epithelium of rats with sepsis, Biomed Pharmacother. 86 (2017) 669-676.

[121] Alteheld B., Evans M.E., Gu L.H., Ganapathy V., Leibach F.H., Jones D.P., and Ziegler T.R., Alanylglutamine dipeptide and growth hormone maintain PepT1-mediated transport in oxidatively stressed Caco-2 cells, J Nutr. 135 (1) (2005) 19-26.

[122] Wojtal K.A., Eloranta J.J., Hruz P., Gutmann H., Drewe J., Staumann A., Beglinger C., Fried M., Kullak-Ublick G.A., and Vavricka S.R., Changes in mRNA expression levels of solute carrier transporters in inflammatory bowel disease patients, Drug Metab Dispos. 37 (9) (2009) 1871-1877.

[123] Merlin D., Si-Tahar M., Sitaraman S.V., Eastburn K., Williams I., Liu X., Hediger M.A., and Madara J.L., Colonic epithelial hPepT1 expression occurs in inflammatory bowel disease: transport of bacterial peptides influences expression of MHC class 1 molecules, Gastroenterology. 120 (7) (2001) 1666-1679.

[124] Ziegler T.R., Fernandez-Estivariz C., Gu L.H., Bazargan N., Umeakunne K., Wallace T.M., Diaz E.E., Rosado K.E., Pascal R.R., Galloway J.R., Wilcox J.N., and Leader L.M., Distribution of the H+/peptide transporter PepT1 in human intestine: up-regulated expression in the colonic mucosa of patients with short-bowel syndrome, Am J Clin Nutr. 75 (5) (2002) 922-930.

[125] Viennois E., Ingersoll S.A., Ayyadurai S., Zhao Y., Wang L., Zhang M., Han M.K., Garg P., Xiao B., and Merlin D., Critical Role of PepT1 in Promoting Colitis-Associated Cancer and Therapeutic Benefits of the Anti-inflammatory PepT1-Mediated Tripeptide KPV in a Murine Model, Cell Mol Gastroenterol Hepatol. 2 (3) (2016) 340-357.

[126] Wuensch T., Ullrich S., Schulz S., Chamaillard M., Schaltenberg N., Rath E., Goebel U., Sartor R.B., Prager M., Buning C., Bugert P., Witt H., Haller D., and Daniel H., Colonic expression of the peptide transporter PEPT1 is downregulated during intestinal inflammation and is not required for NOD2-dependent immune activation, Inflamm Bowel Dis. 20 (4) (2014) 671-684.

[127] Gonzalez D.E., Covitz K.-M.Y., Sadée W., and Mrsny R.J., An oligopeptide transporter is expressed at high levels in the pancreatic carcinoma cell lines AsPc-1 and Capan-2, Cancer Res. 58 (3) (1998) 519-525.

[128] Inoue M., Terada T., Okuda M., and Inui K.-i., Regulation of human peptide transporter 1 (PEPT1) in gastric cancer cells by anticancer drugs, Cancer Lett. 230 (1) (2005) 72-80.

[129] Tai W., Chen Z., and Cheng K., Expression profile and functional activity of peptide transporters in prostate cancer cells, Mol Pharm. 10 (2) (2013) 477-487.

[130] Murakami T., A Minireview: Usefulness of Transporter-Targeted Prodrugs in Enhancing Membrane Permeability, J Pharm Sci. 105 (9) (2016) 2515-2526.

[131] Dahan A., Zimmermann E.M., and Ben-Shabat S., Modern prodrug design for targeted oral drug delivery, Molecules. 19 (10) (2014) 16489-16505.

[132] Kim I., Chu X.Y., Kim S., Provoda C.J., Lee K.D., and Amidon G.L., Identification of a human valacyclovirase: biphenyl hydrolase-like protein as valacyclovir hydrolase, J Biol Chem. 278 (28) (2003) 25348-25356.

[133] Puente X.S. and Lopez-Otin C., Cloning and expression analysis of a novel human serine hydrolase with sequence similarity to prokaryotic enzymes involved in the degradation of aromatic compounds, J Biol Chem. 270 (21) (1995) 12926-12932.

[134] Kim I., Song X., Vig B.S., Mittal S., Shin H.-C., Lorenzi P.J., and Amidon G.L., A novel nucleoside prodrug-activating enzyme: substrate specificity of biphenyl hydrolase-like protein, Mol Pharm. 1 (2) (2004) 117-127.

[135] Sun J., Dahan A., Walls Z.F., Lai L., Lee K.-D., and Amidon G.L., Specificity of a Prodrug-Activating Enzyme hVACVase: the Leaving Group Effect, Mol Pharm. 7 (6) (2010) 2362-2368.

[136] Lai L., Xu Z., Zhou J., Lee K.-D., and Amidon G.L., Molecular Basis of Prodrug Activation by Human Valacyclovirase, an α-Amino Acid Ester Hydrolase, J Biol Chem. 283 (14) (2008) 9318-9327.

[137] Hu Y., Epling D., Shi J., Song F., Tsume Y., Zhu H.J., Amidon G.L., and Smith D.E., Effect of biphenyl hydrolase-like (BPHL) gene disruption on the intestinal stability, permeability and absorption of valacyclovir in wildtype and Bphl knockout mice, Biochem Pharmacol. 156 (2018) 147-156.

[138] Shenoy V.M., Thompson B.R., Shi J., Zhu H.-J., Smith D.E., and Amidon G.L., Chemoproteomic Identification of Serine Hydrolase RBBP9 as a Valacyclovir-Activating Enzyme, Mol Pharm. 17 (5) (2020) 1706-1714.

[139] Hertel L.W., Kroin J.S., Misner J.W., and Tustin J.M., Synthesis of 2-deoxy-2,2-difluoro-D-ribose and 2-deoxy-2,2'-difluoro-D-ribofuranosyl nucleosides, J Org Chem. 53 (11) (1988) 2406-2409.

[140] Chitkara D. and Kumar N., BSA-PLGA-based core-shell nanoparticles as carrier system for water-soluble drugs, Pharm Res. 30 (9) (2013) 2396-2409.

[141] Pili B., Bourgaux C., Meneau F., Couvreur P., and Ollivon M., Interaction of an anticancer drug, gemcitabine, with phospholipid bilayers, J Therm Anal Calorim. 98 (1) (2009) 19.

[142] Gemzar [package insert]. Eli Lilly and Company, Indianapolis, IN, (2019).

[143] Conti R.M., Bernstein A.C., Villaflor V.M., Schilsky R.L., Rosenthal M.B., and Bach P.B., Prevalence of Off-Label Use and Spending in 2010 Among Patent-Protected Chemotherapies in a Population-Based Cohort of Medical Oncologists, J Clin Oncol. 31 (9) (2013) 1134-1139.

[144] *Oncology Off-Label Indications and Recommendations*. Elsevier Gold Standard's Clinical Pharmacology Compendium [Accessed 5/19/2020]; Available from: https://www.elsevier.com/__data/assets/pdf_file/0005/174479/Els-GS-Oncology-off-label-08-2019-ll-2.pdf.

[145] Shewach D.S. and Lawrence T.S., Antimetabolite radiosensitizers, J Clin Oncol. 25 (26) (2007) 4043-4050.

[146] Wolff R.A., Evans D.B., Gravel D.M., Lenzi R., Pisters P.W.T., Lee J.E., Janjan N.A., Charnsangavej C., and Abbruzzese J.L., Phase I Trial of Gemcitabine Combined with Radiation for the Treatment of Locally Advanced Pancreatic Adenocarcinoma, Clin Cancer Res. 7 (8) (2001) 2246-2253.

[147] Metro G., Fabi A., Mirri M.A., Vidiri A., Pace A., Carosi M., Russillo M., Maschio M., Giannarelli D., and Pellegrini D., Phase II study of fixed dose rate gemcitabine as radiosensitizer for newly diagnosed glioblastoma multiforme, Cancer Chemother Pharmacol. 65 (2) (2010) 391.

[148] Eisbruch A., Shewach D.S., Bradford C.R., Littles J.F., Teknos T.N., Chepeha D.B., Marentette L.J., Terrell J.E., Hogikyan N.D., Dawson L.A., Urba S., Wolf G.T., and Lawrence T.S., Radiation Concurrent With Gemcitabine for Locally

Advanced Head and Neck Cancer: A Phase I Trial and Intracellular Drug Incorporation Study, J Clin Oncol. 19 (3) (2001) 792-799.

[149] Blackstock A.W., Bernard S.A., Richards F., Eagle K.S., Case L.D., Poole M.E., Savage P.D., and Tepper J.E., Phase I trial of twice-weekly gemcitabine and concurrent radiation in patients with advanced pancreatic cancer, J Clin Oncol. 17 (7) (1999) 2208-12.

[150] Grunewald R., Abbruzzese J.L., Tarassoff P., and Plunkett W., Saturation of 2′, 2′-difluorodeoxycytidine 5′-triphosphate accumulation by mononuclear cells during a phase I trial of gemcitabine, Cancer Chemother Pharmacol. 27 (4) (1991) 258-262.

[151] Tempero M., Plunkett W., Ruiz Van Haperen V., Hainsworth J., Hochster H., Lenzi R., and Abbruzzese J., Randomized phase II comparison of dose-intense gemcitabine: thirty-minute infusion and fixed dose rate infusion in patients with pancreatic adenocarcinoma, J Clin Oncol. 21 (18) (2003) 3402-3408.

[152] Zhao D., Chen J., Chu M., and Wang J., Prolonged low-dose infusion for gemcitabine: a systematic review, Onco Targets Ther. 12 (2019) 4859-4868.

[153] Poplin E., Feng Y., Berlin J., Rothenberg M.L., Hochster H., Mitchell E., Alberts S., O'Dwyer P., Haller D., Catalano P., Cella D., and Benson A.B., 3rd, Phase III, randomized study of gemcitabine and oxaliplatin versus gemcitabine (fixed-dose rate infusion) compared with gemcitabine (30-minute infusion) in patients with pancreatic carcinoma E6201: a trial of the Eastern Cooperative Oncology Group, J Clin Oncol. 27 (23) (2009) 3778-3785.

[154] Dehua Z., Mingming C., and Jisheng W., Meta-analysis of gemcitabine in brief versus prolonged low-dose infusion for advanced non-small cell lung cancer, PLoS One. 13 (3) (2018) e0193814.

[155] Xie J., Yuan J., and Lu L., Gemcitabine fixed-dose rate infusion for the treatment of pancreatic carcinoma: a meta-analysis of randomized controlled trials, Diagn Pathol. 9 (2014) 214.

[156] Kearns P. and Saha V., *Nucleoside Analogues*, in *New Agents for the Treatment of Acute Lymphoblastic Leukemia*, V. Saha and P. Kearns, Editors. 2011, Springer New York: New York, NY. p. 167-187.

[157] ClinicalTrials.Gov. 2017, U.S. National Library of Medicine.

[158] Veltkamp S.A., Jansen R.S., Callies S., Pluim D., Visseren-Grul C.M., Rosing H., Kloeker-Rhoades S., Andre V.A., Beijnen J.H., Slapak C.A., and Schellens J.H., Oral administration of gemcitabine in patients with refractory tumors: a clinical and pharmacologic study, Clin Cancer Res. 14 (11) (2008) 3477-3486.

[159] Kroep J.R., Giaccone G., Voorn D.A., Smit E.F., Beijnen J.H., Rosing H., van Moorsel C.J., van Groeningen C.J., Postmus P.E., Pinedo H.M., and Peters G.J.,

Gemcitabine and paclitaxel: pharmacokinetic and pharmacodynamic interactions in patients with non-small-cell lung cancer, J Clin Oncol. 17 (7) (1999) 2190-2197.

[160] Kuenen B.C., Rosen L., Smit E.F., Parson M.R.N., Levi M., Ruijter R., Huisman H., Kedde M.A., Noordhuis P., Vijgh W.J.F.v.d., Peters G.J., Cropp G.F., Scigalla P., Hoekman K., Pinedo H.M., and Giaccone G., Dose-Finding and Pharmacokinetic Study of Cisplatin, Gemcitabine, and SU5416 in Patients With Solid Tumors, J Clin Oncol. 20 (6) (2002) 1657-1667.

[161] Zhang L., Sinha V., Forgue S.T., Callies S., Ni L., Peck R., and Allerheiligen S.R., Model-based drug development: the road to quantitative pharmacology, J Pharmacokinet Pharmacodyn. 33 (3) (2006) 369-393.

[162] Sugiyama E., Kaniwa N., Kim S.R., Hasegawa R., Saito Y., Ueno H., Okusaka T., Ikeda M., Morizane C., Kondo S., Yamamoto N., Tamura T., Furuse J., Ishii H., Yoshida T., Saijo N., and Sawada J., Population pharmacokinetics of gemcitabine and its metabolite in Japanese cancer patients: impact of genetic polymorphisms, Clin Pharmacokinet. 49 (8) (2010) 549-558.

[163] Khatri A., Williams B.W., Fisher J., Brundage R.C., Gurvich V.J., Lis L.G., Skubitz K.M., Dudek A.Z., Greeno E.W., Kratzke R.A., Lamba J.K., and Kirstein M.N., SLC28A3 genotype and gemcitabine rate of infusion affect dFdCTP metabolite disposition in patients with solid tumours, Br J Cancer. 110 (2) (2014) 304-312.

[164] Mackey J.R., Mani R.S., Selner M., Mowles D., Young J.D., Belt J.A., Crawford C.R., and Cass C.E., Functional nucleoside transporters are required for gemcitabine influx and manifestation of toxicity in cancer cell lines, Cancer Res. 58 (19) (1998) 4349-4357.

[165] Young J.D., Yao S.Y., Baldwin J.M., Cass C.E., and Baldwin S.A., The human concentrative and equilibrative nucleoside transporter families, SLC28 and SLC29, Mol Aspects Med. 34 (2-3) (2013) 529-547.

[166] Mackey J.R., Yao S.Y., Smith K.M., Karpinski E., Baldwin S.A., Cass C.E., and Young J.D., Gemcitabine transport in xenopus oocytes expressing recombinant plasma membrane mammalian nucleoside transporters, J Natl Cancer Inst. 91 (21) (1999) 1876-1881.

[167] Hu H., Endres C.J., Chang C., Umapathy N.S., Lee E.W., Fei Y.J., Itagaki S., Swaan P.W., Ganapathy V., and Unadkat J.D., Electrophysiological characterization and modeling of the structure activity relationship of the human concentrative nucleoside transporter 3 (hCNT3), Mol Pharmacol. 69 (5) (2006) 1542-1553.

[168] Vos L.J., Yusuf D., Lui A., Abdelaziz Z., Ghosh S., Spratlin J.L., and Mackey J.R., Predictive and Prognostic Properties of Human Equilibrative Nucleoside Transporter 1 Expression in Gemcitabine-Treated Pancreatobiliary Cancer: A Meta-Analysis, JCO Precis Oncol. (3) (2019) 1-22.

[169] Mey V., Giovannetti E., De Braud F., Nannizzi S., Curigliano G., Verweij F., De Cobelli O., Pece S., Del Tacca M., and Danesi R., In vitro synergistic cytotoxicity of gemcitabine and pemetrexed and pharmacogenetic evaluation of response to gemcitabine in bladder cancer patients, Br J Cancer. 95 (3) (2006) 289-297.

[170] Santini D., Schiavon G., Vincenzi B., Cass C.E., Vasile E., Manazza A.D., Catalano V., Baldi G.G., Lai R., Rizzo S., Giacobino A., Chiusa L., Caraglia M., Russo A., Mackey J., Falcone A., and Tonini G., Human equilibrative nucleoside transporter 1 (hENT1) levels predict response to gemcitabine in patients with biliary tract cancer (BTC), Curr Cancer Drug Targets. 11 (1) (2011) 123-129.

[171] Abbruzzese J.L., Grunewald R., Weeks E.A., Gravel D., Adams T., Nowak B., Mineishi S., Tarassoff P., Satterlee W., and Raber M.N., A phase I clinical, plasma, and cellular pharmacology study of gemcitabine, J Clin Oncol. 9 (3) (1991) 491-498.

[172] Peters G.J., Clavel M., Noordhuis P., Geyssen G.J., Laan A.C., Guastalla J., Edzes H.T., and Vermorken J.B., Clinical phase I and pharmacology study of gemcitabine (2', 2'-difluorodeoxycytidine) administered in a two-weekly schedule, J Chemother. 19 (2) (2007) 212-221.

[173] Simon N., Romano O., Michel P., Pinçon C., Vasseur M., Lemahieu N., Barthélémy C., Hebbar M., Décaudin B., and Odou P., Influence of infusion method on gemcitabine pharmacokinetics: a controlled randomized multicenter trial, Cancer Chemother Pharmacol. 76 (4) (2015) 865-871.

[174] de Lange S.M., van der Born K., Kroep J.R., Jensen H.A., Pfeiffer P., Cleverly A., van Groeningen C.J., and Peters G.J., No evidence of gemcitabine accumulation during weekly administration, Eur J Clin Pharmacol. 61 (11) (2005) 843-849.

[175] Storniolo A.M., Allerheiligen S.R., and Pearce H.L., Preclinical, pharmacologic, and phase I studies of gemcitabine, Semin Oncol. 24 (2 Suppl 7) (1997) S2-S7.

[176] Heinemann V., Xu Y.Z., Chubb S., Sen A., Hertel L.W., Grindey G.B., and Plunkett W., Cellular elimination of 2',2'-difluorodeoxycytidine 5'-triphosphate: a mechanism of self-potentiation, Cancer Res. 52 (3) (1992) 533-539.

[177] Veltkamp S.A., Pluim D., van Eijndhoven M.A., Bolijn M.J., Ong F.H., Govindarajan R., Unadkat J.D., Beijnen J.H., and Schellens J.H., New insights into the pharmacology and cytotoxicity of gemcitabine and 2',2'-difluorodeoxyuridine, Mol Cancer Ther. 7 (8) (2008) 2415-2425.

[178] Pauwels B., Korst A.E., Lambrechts H.A., Pattyn G.G., de Pooter C.M., Lardon F., and Vermorken J.B., The radiosensitising effect of difluorodeoxyuridine, a metabolite of gemcitabine, in vitro, Cancer Chemother Pharmacol. 58 (2) (2006) 219-28.

[179] Derissen E.J.B., Huitema A.D.R., Rosing H., Schellens J.H.M., and Beijnen J.H., Intracellular pharmacokinetics of gemcitabine, its deaminated metabolite 2',2'-difluorodeoxyuridine and their nucleotides, Br J Clin Pharmacol. 84 (6) (2018) 1279-1289.

[180] Shewach D.S. and Lawrence T.S., Gemcitabine and radiosensitization in human tumor cells, Investigational New Drugs. 14 (3) (1996) 257-263.

[181] de Sousa Cavalcante L. and Monteiro G., Gemcitabine: metabolism and molecular mechanisms of action, sensitivity and chemoresistance in pancreatic cancer, Eur J Pharmacol. 741 (2014) 8-16.

[182] Sebastiani V., Ricci F., Rubio-Viquiera B., Kulesza P., Yeo C.J., Hidalgo M., Klein A., Laheru D., and Iacobuzio-Donahue C.A., Immunohistochemical and Genetic Evaluation of Deoxycytidine Kinase in Pancreatic Cancer: Relationship to Molecular Mechanisms of Gemcitabine Resistance and Survival, Clin Cancer Res. 12 (8) (2006) 2492-2497.

[183] Maréchal R., Bachet J.B., Mackey J.R., Dalban C., Demetter P., Graham K., Couvelard A., Svrcek M., Bardier–Dupas A., Hammel P., Sauvanet A., Louvet C., Paye F., Rougier P., Penna C., André T., Dumontet C., Cass C.E., Jordheim L.P., Matera E.L., Closset J., Salmon I., Devière J., Emile J.F., and Van Laethem J.L., Levels of Gemcitabine Transport and Metabolism Proteins Predict Survival Times of Patients Treated With Gemcitabine for Pancreatic Adenocarcinoma, Gastroenterology. 143 (3) (2012) 664-674.

[184] Shewach D.S., Reynolds K.K., and Hertel L., Nucleotide specificity of human deoxycytidine kinase, Mol Pharmacol. 42 (3) (1992) 518-524.

[185] Bouffard D.Y., Laliberte J., and Momparler R.L., Kinetic studies on 2',2'-difluorodeoxycytidine (Gemcitabine) with purified human deoxycytidine kinase and cytidine deaminase, Biochem Pharmacol. 45 (9) (1993) 1857-1861.

[186] Grunewald R., Kantarjian H., Du M., Faucher K., Tarassoff P., and Plunkett W., Gemcitabine in leukemia: a phase I clinical, plasma, and cellular pharmacology study, J Clin Oncol. 10 (3) (1992) 406-413.

[187] Veltkamp S.A., Beijnen J.H., and Schellens J.H., Prolonged versus standard gemcitabine infusion: translation of molecular pharmacology to new treatment strategy, Oncologist. 13 (3) (2008) 261-276.

[188] Rudin D., Li L., Niu N., Kalari K.R., Gilbert J.A., Ames M.M., and Wang L., Gemcitabine Cytotoxicity: Interaction of Efflux and Deamination, J Drug Metab Toxicol. 2 (107) (2011) 1-10.

[189] Heinemann V., Hertel L.W., Grindey G.B., and Plunkett W., Comparison of the cellular pharmacokinetics and toxicity of 2',2'-difluorodeoxycytidine and 1-beta-D-arabinofuranosylcytosine, Cancer Res. 48 (14) (1988) 4024-4031.

[190] Ruiz van Haperen V.W., Veerman G., Boven E., Noordhuis P., Vermorken J.B., and Peters G.J., Schedule dependence of sensitivity to 2',2'-difluorodeoxycytidine (Gemcitabine) in relation to accumulation and retention of its triphosphate in solid tumour cell lines and solid tumours, Biochem Pharmacol. 48 (7) (1994) 1327-39.

[191] Plunkett W., Huang P., Xu Y.Z., Heinemann V., Grunewald R., and Gandhi V., Gemcitabine: metabolism, mechanisms of action, and self-potentiation, Semin Oncol. 22 (4 Suppl 11) (1995) 3-10.

[192] Huang P., Chubb S., Hertel L.W., Grindey G.B., and Plunkett W., Action of 2',2'-difluorodeoxycytidine on DNA synthesis, Cancer Res. 51 (22) (1991) 6110-6117.

[193] Huang P. and Plunkett W., Fludarabine- and gemcitabine-induced apoptosis: incorporation of analogs into DNA is a critical event, Cancer Chemother Pharmacol. 36 (3) (1995) 181-188.

[194] Nabhan C., Gajria D., Krett N.L., Gandhi V., Ghias K., and Rosen S.T., Caspase activation is required for gemcitabine activity in multiple myeloma cell lines, Mol Cancer Ther. 1 (13) (2002) 1221-1227.

[195] Chandler N.M., Canete J.J., and Callery M.P., Caspase-3 drives apoptosis in pancreatic cancer cells after treatment with gemcitabine, J Gastrointest Surg. 8 (8) (2004) 1072-1078.

[196] Koizumi K., Tanno S., Nakano Y., Habiro A., Izawa T., Mizukami Y., Okumura T., and Kohgo Y., Activation of p38 mitogen-activated protein kinase is necessary for gemcitabine-induced cytotoxicity in human pancreatic cancer cells, Anticancer Res. 25 (5) (2005) 3347-3353.

[197] Chen M., Hough A.M., and Lawrence T.S., The role of p53 in gemcitabine-mediated cytotoxicity and radiosensitization, Cancer Chemother Pharmacol. 45 (5) (2000) 369-374.

[198] Jones D.R., Broad R.M., Comeau L.D., Parsons S.J., and Mayo M.W., Inhibition of nuclear factor kappaB chemosensitizes non-small cell lung cancer through cytochrome c release and caspase activation, J Thorac Cardiovasc Surg. 123 (2) (2002) 310-317.

[199] Chang G.C., Hsu S.L., Tsai J.R., Wu W.J., Chen C.Y., and Sheu G.T., Extracellular signal-regulated kinase activation and Bcl-2 downregulation mediate apoptosis after gemcitabine treatment partly via a p53-independent pathway, Eur J Pharmacol. 502 (3) (2004) 169-183.

[200] Pourquier P., Gioffre C., Kohlhagen G., Urasaki Y., Goldwasser F., Hertel L.W., Yu S., Pon R.T., Gmeiner W.H., and Pommier Y., Gemcitabine (2′, 2′-difluoro-2′-deoxycytidine), an antimetabolite that poisons topoisomerase I, Clin Cancer Res. 8 (8) (2002) 2499-2504.

[201] Jansen R.S., Rosing H., Schellens J.H., and Beijnen J.H., Deoxyuridine analog nucleotides in deoxycytidine analog treatment: secondary active metabolites?, Fundam Clin Pharmacol. 25 (2) (2011) 172-185.

[202] Heinemann V., Xu Y.Z., Chubb S., Sen A., Hertel L.W., Grindey G.B., and Plunkett W., Inhibition of ribonucleotide reduction in CCRF-CEM cells by 2',2'-difluorodeoxycytidine, Mol Pharmacol. 38 (4) (1990) 567-572.

[203] Wang J., Lohman G.J.S., and Stubbe J., Enhanced subunit interactions with gemcitabine-5′-diphosphate inhibit ribonucleotide reductases, PNAS. 104 (36) (2007) 14324-14329.

[204] Shewach D.S., Hahn T.M., Chang E., Hertel L.W., and Lawrence T.S., Metabolism of 2′, 2′-difluoro-2′-deoxycytidine and radiation sensitization of human colon carcinoma cells, Cancer Res. 54 (12) (1994) 3218-3223.

[205] Ostruszka L.J. and Shewach D.S., The role of DNA synthesis inhibition in the cytotoxicity of 2',2'-difluoro-2'-deoxycytidine, Cancer Chemother Pharmacol. 52 (4) (2003) 325-32.

[206] Honeywell R.J., Ruiz van Haperen V.W., Veerman G., Smid K., and Peters G.J., Inhibition of thymidylate synthase by 2',2'-difluoro-2'-deoxycytidine (Gemcitabine) and its metabolite 2',2'-difluoro-2'-deoxyuridine, Int J Biochem Cell Biol. 60 (2015) 73-81.

[207] Kent E., Sandler H., Montie J., Lee C., Herman J., Esper P., Fardig J., and Smith D.C., Combined-modality therapy with gemcitabine and radiotherapy as a bladder preservation strategy: results of a phase I trial, J Clin Oncol. 22 (13) (2004) 2540-5.

[208] Kim M.M., Camelo-Piragua S., Schipper M., Tao Y., Normolle D., Junck L., Mammoser A., Betz B.L., Cao Y., Kim C.J., Heth J., Sagher O., Lawrence T.S., and Tsien C.I., Gemcitabine Plus Radiation Therapy for High-Grade Glioma: Long-Term Results of a Phase 1 Dose-Escalation Study, Int J Radiat Oncol Biol Phys. 94 (2) (2016) 305-11.

[209] Spalding A.C. and Lawrence T.S., New and Emerging Radiosensitizers and Radioprotectors, Cancer Investigation. 24 (4) (2006) 444-456.

[210] Muler J.H., McGinn C.J., Normolle D., Lawrence T., Brown D., Hejna G., and Zalupski M.M., Phase I trial using a time-to-event continual reassessment strategy for dose escalation of cisplatin combined with gemcitabine and radiation therapy in pancreatic cancer, J Clin Oncol. 22 (2) (2004) 238-43.

[211] Lawrence T.S., Chang E.Y., Hahn T.M., Hertel L.W., and Shewach D.S., Radiosensitization of pancreatic cancer cells by 2',2'-difluoro-2'-deoxycytidine, Int J Radiat Oncol Biol Phys. 34 (4) (1996) 867-872.

[212] Flanagan S.A., Robinson B.W., Krokosky C.M., and Shewach D.S., Mismatched nucleotides as the lesions responsible for radiosensitization with gemcitabine: a new paradigm for antimetabolite radiosensitizers, Mol Cancer Ther. 6 (6) (2007) 1858-1868.

[213] Im M.M., Flanagan S.A., Ackroyd J.J., and Shewach D.S., Drug Metabolism and Homologous Recombination Repair in Radiosensitization with Gemcitabine, Radiat Res. 183 (1) (2015) 114-123.

[214] Im M.M., Flanagan S.A., Ackroyd J.J., Knapp B., Kramer A., and Shewach D.S., Late DNA Damage Mediated by Homologous Recombination Repair Results in Radiosensitization with Gemcitabine, Radiat Res. 186 (5) (2016) 466-477.

[215] Morgan M., El Shaikh M.A., Abu-Isa E., Davis M.A., and Lawrence T.S., Radiosensitization By Gemcitabine Fixed-Dose-Rate Infusion Versus Bolus Injection in a Pancreatic Cancer Model, Transl Oncol. 1 (1) (2008) 44-49.

[216] Derakhshandeh K. and Fathi S., Role of chitosan nanoparticles in the oral absorption of Gemcitabine, Int J Pharm. 437 (1) (2012) 172-177.

[217] Lim J.H., You S.K., Baek J.S., Hwang C.J., Na Y.G., Shin S.C., and Cho C.W., Preparation and evaluation of polymeric microparticulates for improving cellular uptake of gemcitabine, Int J Nanomed. 7 (2012) 2307-2314.

[218] Tsume Y., Incecayir T., Song X., Hilfinger J.M., and Amidon G.L., The development of orally administrable gemcitabine prodrugs with D-enantiomer amino acids: enhanced membrane permeability and enzymatic stability, Eur J Pharm Biopharm. 86 (3) (2014) 514-523.

[219] Chen G., Svirskis D., Lu W., Ying M., Huang Y., and Wen J., N-trimethyl chitosan nanoparticles and CSKSSDYQC peptide: N-trimethyl chitosan conjugates enhance the oral bioavailability of gemcitabine to treat breast cancer, J Control Release. 277 (2018) 142-153.

[220] Wang Y., Fan W., Dai X., Katragadda U., McKinley D., Teng Q., and Tan C., Enhanced tumor delivery of gemcitabine via PEG-DSPE/TPGS mixed micelles, Mol Pharm. 11 (4) (2014) 1140-1150.

[221] Cham K., Baker J., Takhar K., Flexman J., Wong M., Owen D., Yung A., Kozlowski P., Reinsberg S., and Chu E., Metronomic gemcitabine suppresses tumour growth, improves perfusion, and reduces hypoxia in human pancreatic ductal adenocarcinoma, Br J Cancer. 103 (1) (2010) 52-60.

[222] Tsume Y., Borras Bermejo B., and Amidon G.L., The dipeptide monoester prodrugs of floxuridine and gemcitabine-feasibility of orally administrable nucleoside analogs, Pharmaceuticals. 7 (2) (2014) 169-191.

[223] Landowski C.P., Song X., Lorenzi P.L., Hilfinger J.M., and Amidon G.L., Floxuridine Amino Acid Ester Prodrugs: Enhancing Caco-2 Permeability and Resistance to Glycosidic Bond Metabolism, Pharm Res. 22 (9) (2005) 1510-1518.

[224] Tsume Y., Drelich A.J., Smith D.E., and Amidon G.L., Potential Development of Tumor-Targeted Oral Anti-Cancer Prodrugs: Amino Acid and Dipeptide Monoester Prodrugs of Gemcitabine, Molecules. 22 (8) (2017) 1322.

[225] Database resources of the National Center for Biotechnology Information, Nucleic Acids Res. 44 (D1) (2016) D7-19.

[226] Chen X.Z., Steel A., and Hediger M.A., Functional roles of histidine and tyrosine residues in the H(+)-peptide transporter PepT1, Biochem Biophys Res Commun. 272 (3) (2000) 726-730.

[227] Song X.Q., Lorenzi P.L., Landowski C.P., Vig B.S., Hilfinger J.M., and Amidon G.L., Amino acid ester prodrugs of the anticancer agent gemcitabine: Synthesis, bioconversion, metabolic bioevasion, and hPEPT1-mediated transport, Mol Pharm. 2 (2) (2005) 157-167.

CHAPTER 3

Mechanisms of Gemcitabine Oral Absorption as determined by In Situ Intestinal Perfusions in Mice

3.1 Abstract

Gemcitabine is a widely used chemotherapeutic drug that is administered via intravenous infusion due to a low oral bioavailability of only 10%. This low oral bioavailability is believed to be the result of gemcitabine's low intestinal permeability and oral absorption, followed by significant presystemic metabolism. In the present study, we sought to define the mechanisms of gemcitabine intestinal permeability, the potential for saturation of intestinal uptake, and the transporter(s) responsible for mediating the oral absorption of drug using *in situ* single-pass intestinal perfusions in mice. Concentration-dependent studies were performed for gemcitabine over 0.5 to 2000 μM, along with studies of 5 μM gemcitabine in a sodium-containing buffer ± thymidine (which can inhibit concentrative (*i.e.,* CNT1 and CNT3) and equilibrative (*i.e.,* ENT1 and ENT2) nucleoside transporters) or dilazep (which can inhibit ENT1 and ENT2), or in a sodium-free buffer (which can inhibit CNT1 and CNT3). Our findings demonstrated that gemcitabine was, in fact, a high-permeability drug in the intestine at low concentrations, that jejunal uptake of gemcitabine was saturable and mediated almost exclusively by nucleoside transporters, and that jejunal flux was mediated by both high-affinity, low-capacity (K_m = 27.4 μM, V_{max} = 3.6

pmol/cm^2/s) and low-affinity, high-capacity (K_m = 700 μM, V_{max} = 35.9 pmol/cm^2/s) transport systems. Thus, CNTs and ENTs at the apical membrane allow for gemcitabine uptake from the lumen to enterocyte, whereas ENTs at the basolateral membrane allow for gemcitabine efflux from the enterocyte to portal venous blood.

3.2 Introduction

Gemcitabine (2′,2′-difluoro-2′-deoxycytidine; dFdC) is a pyrimidine nucleoside analogue used in the treatment of various solid tumors [1-4]. Gemcitabine distribution and cellular uptake is mediated by the action of two evolutionarily unrelated transmembrane transporter families: the concentrative nucleoside transporters (CNTs) and the equilibrative nucleoside transporters (ENTs), belonging to the solute carrier (SLC) families 28 and 29, respectively [5, 6]. Specifically, gemcitabine is a substrate of the pyrimidine selective transporter CNT1 and the broadly selective purine and pyrimidine transporters CNT3, ENT1, and ENT2 [7, 8]. CNT1 and CNT3 function as concentrative and unidirectional sodium:substrate cotransporters, whereas ENT1 and ENT2 function as equilibrative and bidirectional sodium-independent transporters [9]. It has also been demonstrated that CNT3 can function as a proton:substrate cotransporter, albeit with altered transport activity and substrate specificity [10].

Following cellular uptake, gemcitabine undergoes phosphorylation events forming the active metabolites gemcitabine diphosphate (dFdCDP) and triphosphate (dFdCTP) [11]. dFdCTP is incorporated into DNA in place of the natural substrate deoxycytidine triphosphate, preventing chain elongation [12] and leading to apoptosis [13]. dFdCDP inhibits ribonucleotide reductase, depleting the pool of deoxynucleotide triphosphates and increasing dFdCTP incorporation into DNA [14]. Additional self-potentiating mechanisms have also been described [15].

Due to a low oral bioavailability of only 10% [16], gemcitabine is administered as an intravenous infusion, typically over 30 min at a dose of 1000 – 1250 mg/m^2 once per week [17]. The factors limiting gemcitabine's oral bioavailability have been explored in humans

and mice. One study in humans highlighted the extensive first-pass metabolism of gemcitabine to 2′,2′-difluoro-2′-deoxyuridine (dFdU), via cytidine deaminase, after oral dosing of drug [16]. This study, however, quantified neither the fraction of drug absorbed from the intestinal lumen nor the fraction of drug that escaped presystemic metabolism in the gastrointestinal tract and/or liver. Studies in mice showed that tetrahydrouridine, a potent inhibitor of cytidine deaminase, could increase the oral bioavailability of gemcitabine from 10% to 40% [18]. However, while showing an improvement in the systemic availability of orally administered gemcitabine due to enzymatic inactivation, the intestinal permeability and mechanism of oral drug absorption were not studied.

Clearly, an orally administrable form of gemcitabine would benefit patients by providing a noninvasive, patient friendly, and cost-effective alternative to intravenous drug infusions while enabling greater flexibility in optimization of the dosing regimen. In particular, the intestinal absorption of gemcitabine has never been investigated systematically, even though gemcitabine is a substrate of several intestinally expressed nucleoside transporters [5]. Moreover, many *in vitro* systems (*e.g.,* Caco-2 cells) used for perfunctory evaluation of gemcitabine intestinal permeability will likely provide misleading results as low expression levels of nucleoside transporters in these cells prevent an accurate evaluation of potential transporter-mediated uptake [19]. On the other hand, mice and humans show similar intestinal expression of nucleoside transporters [20], suggesting that appropriate mouse models (*e.g., in situ* intestinal perfusions) would better reflect the oral absorption of gemcitabine in humans as compared to cell culture systems.

With this knowledge gap in mind, the primary goals of this study were to characterize the mechanisms of gemcitabine intestinal permeability, the potential for saturation of

intestinal gemcitabine uptake, and the transporter(s) responsible for mediating the oral absorption of gemcitabine using *in situ* single-pass intestinal perfusions in mice.

3.3 Materials and Methods

3.3.1 Chemicals

Gemcitabine, dilazep hydrochloride, thymidine, and high-performance liquid chromatography (HPLC) grade acetonitrile and trifluoroacetic acid (TFA) were purchased from Thermo Fisher Scientific (Waltham, MA). The deaminated gemcitabine metabolite dFdU was purchased from Sigma-Aldrich (St. Louis, MO). Radiolabeled gemcitabine (cytosine-2-^{14}C) (55.0 mCi/mmol), subsequently referred to as [^{14}C]-gemcitabine, was purchased from Moravek, Inc. (Brea, CA). CytoScint™ scintillation solution was purchased from MP Biomedicals, LLC (Solon, OH). Hyamine hydroxide was purchased from PerkinElmer (Waltham, MA). All other chemicals were obtained from standard commercial sources.

3.3.2 Animals

Studies were performed on 8- to 12-week old gender matched C57BL/6 mice. The mice were housed and bred in a temperature-controlled room with 12-hour light/dark cycles and *ad libitum* access to water and a standard diet (Unit for Laboratory Animal Medicine, University of Michigan, Ann Arbor, MI). Limited validation studies were also performed in 8- to 12-week old female BALB/c mice (Charles River Laboratories, Wilmington, MA). All animal studies were conducted in accordance with the Guide for the Care and Use of Laboratory Animals.

3.3.3 In situ single-pass intestinal perfusions

Intestinal perfusions in C57BL/6 and BALB/c mice were performed identically and as previously described [21-23]. Prior to experimentation, mice were fasted overnight (~

16 hr) with free access to water. The mice were then anesthetized with sodium pentobarbital (40 - 60 mg/kg intraperitoneal) and placed on a heating pad to maintain body temperature. The abdominal region was sterilized with 70% ethanol and the intestines exposed via a mid-line abdominal incision. An 8 cm jejunal segment, beginning 2 cm distal from the Ligament of Treitz, was isolated and glass cannulas (2.0 mm outer diameter) were inserted into each end of the segment and secured with silk sutures. The cannulated segment was rinsed with isotonic saline solution (or distilled water in experiments using sodium-free buffer) to remove debris. The mice were then transferred to a 31°C temperature controlled chamber and their abdomen covered with saline-wetted gauze and parafilm to prevent dehydration. Inlet tubing connected the proximal cannula to a 20 mL syringe containing the perfusion solution and positioned in a perfusion pump (PHD Ultra, Harvard Apparatus, South Natick, MA). Outlet tubing connected the distal cannula to a collection vial.

The perfusion solution (pH 6.0) contained 145 mM NaCl, 0.5 mM $MgCl_2$, 1 mM NaH_2PO_4, 1 mM $CaCl_2$, 3 mM KCl, 5 mM glucose, 5 mM 2-morpholinoethanesulfonic acid (MES), and a given concentration of gemcitabine or [^{14}C]-gemcitabine. This solution was perfused through the cannulated jejunal segment at 0.1 ml/min for a total of 90 min. After perfusing for 30 min to achieve steady-state conditions, samples of the exiting perfusate were collected at 10 min intervals for the remaining 60 min. Following experimentation, the precise length of the perfused jejunal segment was determined. Inlet and outlet samples collected during perfusion of gemcitabine were then analyzed using ultra-performance liquid chromatography (UPLC), as described and validated below. Samples collected during perfusion of [^{14}C]-gemcitabine were analyzed by adding 100 µl

aliquots to scintillation vials containing 6.0 mL of scintillation solution and quantifying radioactivity using a dual-channel liquid scintillation counter (Beckman LS 6000 SC, Beckman Coulter Inc., Fullerton, CA).

Perfusions of 100 μM gemcitabine and 100 μM [^{14}C]-gemcitabine (0.5 μCi) were performed in C57BL/6 mice and perfusions of 100 μM gemcitabine were performed in BALB/c mice. Concentration-dependent uptake studies were conducted in C57BL/6 mice by perfusing gemcitabine at concentrations ranging from 0.5 - 2000 μM. Specificity (*i.e.*, inhibition) studies, also in C57BL/6 mice, were performed by perfusing 5 μM gemcitabine in the absence and presence of 2 mM thymidine or dilazep. An additional specificity study was performed in C57BL/6 mice by perfusing 5 μM gemcitabine in sodium-free buffer, prepared by replacing NaCl and NaH_2PO_4 in the perfusion solution with equimolar concentrations of N-methyl-D-glucamine and KH_2PO_4, respectively. Finally, concentration-dependent inhibition studies were performed in C57BL/6 mice where 5 μM gemcitabine was coperfused over a wide range of inhibitor concentrations for thymidine (0.1 - 2000 μM) and dilazep (0.1 - 2500 μM).

3.3.4 Blood and intestinal tissue collections

Portal venous blood and intestinal tissue samples were collected from C57BL/6 mice following a standard 90 min perfusion of 5 μM [^{14}C]-gemcitabine (0.5 μCi) alone and in the presence of 2 mM dilazep. Radioactivity was determined in portal venous plasma (nM levels) by adapting a previously described method [22]. Thus, immediately following the perfusion, portal venous blood was collected into tubes containing K3-EDTA and centrifuged for 3 min at 3000 rpm. A 30 μl plasma aliquot was then combined with 6.0 mL of scintillation solution and 20 μL of 0.5 N acetic acid and analyzed using a dual-channel

liquid scintillation counter (Beckman LS 6500 SC, Beckman Coulter Inc., Fullerton, CA). Likewise, radioactivity in intestinal tissue (pmol/mg) was determined by adapting a previously described method [24]. Following collection of portal venous blood, a jejunal segment was excised, washed with saline for 20 sec, blotted dry on filter paper, weighed, and soaked for 2 days in 0.33 mL of hyamine hydroxide at 37°C. Subsequently, 40 µL of 30% H_2O_2 was added to the tissue sample which was then incubated for 30 min at 60°C. After cooling to room temperature, 6.0 mL of scintillation solution and 20 µL of 0.5 N acetic acid were added to the sample which was then analyzed using a dual-channel liquid scintillation counter (Beckman LS 6500 SC, Beckman Coulter Inc., Fullerton, CA).

3.3.5 UPLC analytical method and validation

Inlet and outlet perfusate samples, other than those containing [^{14}C]-gemcitabine, were assayed for gemcitabine, dFdU, and cytosine using a Waters Acquity H-Class UPLC system (Milford, MA) equipped with a photodiode array detector. dFdU was assayed since it is the primary metabolite of gemcitabine [25], whereas cytosine was reported to be formed as a gemcitabine metabolite during mouse intestinal perfusions [26]. The analytes were resolved at 40°C on an Acquity HSS T3 column (2.1 x 100 mm), fitted with an HSS T3 VanGuard precolumn (2.1 x 5 mm). Separation was achieved using a gradient elution method combining water (plus 0.1% TFA) and acetonitrile (plus 0.1% TFA) at a flow rate of 0.4 ml/min. The solvent gradient was initiated at 100% water, decreased to 94% water linearly from 0.0 - 3.0 min, decreased to 85% water linearly from 3.0 – 5.0 min, increased to 100% water linearly from 5.0 – 6.0 min, and held at 100% water until the end of the run (8.0 min). Prior to analysis, perfusate samples were centrifuged for 15 min at 15000 rpm and 5 µl of the supernatant was subsequently injected onto the column via an autosampler.

Under these conditions, gemcitabine (detection wavelength = 284 nm) eluted at ~ 3.0 min, dFdU (detection wavelength = 265 nm) at ~ 4.2 min, and cytosine (detection wavelength = 284 nm) at ~ 1.0 min.

Selectivity of the assay was evaluated by analyzing perfusion outlet samples, collected following perfusion of blank perfusion buffer, with the three analytes at their lower limits of quantitation (*i.e.,* 0.25 µM gemcitabine, 0.25 µM dFdU, and 1 µM cytosine) to assess for potential interferences. Linearity was evaluated by developing standard curves for gemcitabine (concentration range: 0.25 µM - 100 µM), dFdU (concentration range: 0.25 µM - 5 µM), and cytosine (concentration range: 1 µM - 100 µM). Intra- and inter-day accuracy and precision were evaluated by analyzing quality control samples of gemcitabine (0.25 µM, 25 µM, and 100 µM), dFdU (0.25 µM, 1 µM, and 5 µM), and cytosine (1 µM, 50 µM, and 100 µM) in triplicate on three separate days.

3.3.6 Data analysis

The effective permeability (P_{eff}) of gemcitabine was calculated according to the parallel tube complete radial mixing model [27]:

$$P_{eff} = \frac{-Q_{in} \cdot \ln\left(\frac{C'_{out}}{C_{in}}\right)}{2\pi RL} \qquad \text{(Eq 3.1)}$$

where Q_{in} represents the inlet flow rate of perfusion buffer (0.1 ml/min), C'_{out} the total outlet concentration of all drug species, after correcting for intestinal water flux, C_{in} the inlet gemcitabine concentration, R the intestinal radius of the perfused segment (0.1 cm), and L the length of the perfused segment. Using the gravimetrically determined outlet flow

rate (Q_{out}), and the measured outlet concentrations of gemcitabine ($C_{out,gemcitabine}$) and $dFdU$ ($C_{out,dFdU}$), C'_{out} was calculated according to Eq 3.2 [28].

$$C'_{out} = (C_{out,gemcitabine} + C_{out,dFdU}) \cdot \left(\frac{Q_{out}}{Q_{in}}\right) \quad \text{(Eq 3.2)}$$

Importantly, when calculating gemcitabine P_{eff} following [^{14}C]-gemcitabine perfusion, C_{in} corresponded to the inlet radioactivity concentration and C'_{out} the outlet radioactivity concentration, after correcting for intestinal water flux as described above.

The steady-state flux (J) of gemcitabine was calculated as:

$$J = P_{eff} \cdot C_{in} \quad \text{(Eq 3.3)}$$

The concentration-dependent flux of gemcitabine was best fit to an equation consisting of two Michaelis-Menten (*i.e.*, saturable) terms:

$$J = \frac{V_{max,1} \cdot C_{in}}{K_{m,1} + C_{in}} + \frac{V_{max,2} \cdot C_{in}}{K_{m,2} + C_{in}} \quad \text{(Eq 3.4)}$$

where $V_{max,1}$ and $V_{max,2}$ correspond to the maximum uptake rates for transport systems 1 and 2, and $K_{m,1}$ and $K_{m,2}$ correspond to the Michaelis constants for transport systems 1 and 2, referenced to inlet drug concentrations.

Concentration-dependent inhibition data were normalized (*i.e.,* gemcitabine flux expressed as percent of control) and fit to Eq 3.5 for thymidine inhibition or to Eq 3.6 for dilazep inhibition:

$$Y = 100 \times \left(\frac{IC50}{IC50 + I}\right) \quad \text{(Eq 3.5)}$$

$$Y = Bottom + (100 - Bottom) \times \left(\frac{IC50}{IC50 + I}\right) \quad \text{(Eq 3.6)}$$

where $IC50$ corresponds to the half maximal inhibitory concentration, I to the inhibitor concentration of thymidine or dilazep, and $Bottom$ to the residual flux of 5 μM gemcitabine at maximum inhibition.

Data were reported as mean ± SE. When comparing two groups, statistical differences were evaluated using an unpaired t-test. Statistical differences between three or more groups were evaluated by one-way ANOVA followed by Dunnett's test for pairwise comparisons (Prism version 7, GraphPad Software, La Jolla, California). A p value ≤ 0.05 was considered significant. Nonlinear regression was performed using GraphPad Prism software and the quality of fits was evaluated using the coefficient of determination (r^2), visual inspection of the residuals, variation of the parameter estimates, and the corrected Akaike information criterion (AICc) [29].

3.4 Results

3.4.1 UPLC method validation

Selectivity of the assay was confirmed by analyzing outlet perfusate samples collected during perfusion of drug-free perfusion solution, showing no significant interference of co-eluting peaks on analysis of the three analytes at their lower limits of quantitation. Next, standard curve linearity was confirmed for gemcitabine ($r^2 = 1.000$), dFdU ($r^2 > 0.999$), and cytosine ($r^2 > 0.999$). Finally, as seen in Table 3.1, the assay showed excellent intra- and inter-day accuracy and precision.

3.4.2 Verification of experimentally-determined intestinal permeability

Following the intestinal perfusion of 100 μM gemcitabine in C57BL/6 and BALB/c mice, outlet perfusate samples contained gemcitabine and low concentrations of dFdU (< 3%). Cytosine was absent in outlet samples following perfusion in both strains (Figure 3.1). To further support our results (*i.e.,* no other metabolites were being formed), additional intestinal perfusions were performed with 100 μM [^{14}C]-gemcitabine in C57BL/6 mice. As shown in Figure 3.2, the effective permeability (P_{eff}) of 100 μM gemcitabine in C57BL/6 mice was not different between the two analytical methods, with average P_{eff} values of 1.14 x 10^{-4} cm/s when analyzed by UPLC and 1.05 x 10^{-4} cm/s when analyzed by radioactivity. These results validate the analytical methods applied in the current study and demonstrate that gemcitabine metabolites are not confounding the findings.

3.4.3 Concentration-dependent uptake studies

To explore the potential for saturation of gemcitabine intestinal uptake, *in situ* jejunal perfusions were performed in C57BL/6 mice at 14 concentrations ranging from 0.5 μM to

2 mM. As shown in Figure 3.3, gemcitabine displayed saturable kinetics, where the flux was best described by two Michaelis-Menten terms (Table 3.2). Thus, a high-affinity, low-capacity transport system was identified ($V_{max,1}$ and $K_{m,1}$) along with a low-affinity, high-capacity transport system ($V_{max,2}$ and $K_{m,2}$). Examination of the data using a Wolf-Augustinsson-Hofstee plot (Figure 3.4) shows clear deviation from linearity, providing further evidence that two distinct absorption mechanisms are mediating the intestinal uptake of gemcitabine. As a result, subsequent studies were performed using inlet gemcitabine concentrations of 5 μM to ensure linear conditions.

3.4.4 Inhibition Studies

To elucidate the transporter(s) responsible for mediating the intestinal permeability of gemcitabine in C57BL/6 mice, 5 μM gemcitabine was perfused in a sodium-containing buffer with either 2 mM thymidine (which can broadly inhibit the nucleoside transporters) or dilazep (which can inhibit the nucleoside transporters ENT1 and ENT2), or in a sodium-free buffer (which can inhibit the nucleoside transporters CNT1 and CNT3). As shown in Figure 3.5, the jejunal permeability of gemcitabine was reduced by about 95% when coperfused with 2 mM thymidine (*i.e.,* residual permeability = 4.6%) and by > 65% when perfused in a sodium-free buffer (*i.e.,* residual permeability = 31.7%). Moreover, 2 mM dilazep coperfusion reduced the jejunal permeability of gemcitabine by about 50% (*i.e.,* residual permeability = 50.2%). Additional studies were performed in C57BL/6 mice to examine the concentration-dependent inhibition of 5 μM gemcitabine flux by thymidine and dilazep. As shown in Figure 3.6, thymidine and dilazep inhibited gemcitabine flux with IC50 values of 98.5 μM and 212 μM, respectively. Taken together, these results

demonstrate that the intestinal permeability of gemcitabine is mediated almost exclusively by nucleoside transporters, with contributions by both the CNTs and ENTs.

3.4.5 Accumulation of gemcitabine in intestinal tissue and portal venous plasma

In this study, 5 μM [^{14}C]-gemcitabine was perfused in both the absence and presence of 2 mM dilazep (*i.e.,* an ENT1 and ENT2 inhibitor) for 90 min in C57BL/6 mice, at which time jejunal tissue and portal venous blood samples were obtained. As shown in Figure 3.7, total gemcitabine radioactivity in intestinal tissue was not altered by coperfusion with dilazep. However, total gemcitabine radioactivity in portal venous plasma decreased by > 65% (*i.e.,* % control = 32.5%).

3.5 Discussion

Various delivery techniques have been explored to increase the oral bioavailability of gemcitabine including the drug's formulation as a prodrug [26, 30-32], its incorporation into polymeric microparticulates [33], nanoparticles [34, 35], and a self-microemulsifying drug delivery system [36], and its coadministration with a cytidine deaminase inhibitor [18]. Many of these studies aimed to increase the oral bioavailability of gemcitabine, at least partly, by increasing the drug's purported low intestinal permeability [26, 30, 32-35]. Our studies indicated that the tenet of gemcitabine having low intestinal permeability was unfounded and, as a result, we decided to systematically characterize the drug's mechanism of intestinal absorption, its potential for saturable intestinal uptake, and the mechanism(s) by which gemcitabine may transit through enterocytes. In doing so, our studies revealed several major findings, for the first time, including that: 1) at low concentrations, gemcitabine was a high-permeability drug in the intestine; 2) the jejunal uptake of gemcitabine was saturable and mediated almost exclusively by nucleoside transporters (> 95%); 3) the jejunal flux of gemcitabine was mediated by two distinct transport systems, one being of high-affinity and low-capacity (*i.e.,* CNTs) and the other being of low-affinity and high-capacity (*i.e.,* ENTs); and 4) apically-expressed CNT(s) and ENT(s) mediate the uptake of gemcitabine into enterocytes, whereas basolaterally-expressed ENT(s) mediate the efflux of gemcitabine from enterocytes into portal venous blood.

The *in situ* jejunal permeability (P_{eff}) of gemcitabine was high in C57BL/6 mice (i.e., 1.5 - 1.9 x 10^{-4} cm/s at 5 μM, Figure 3.5; and 1.1 x 10^{-4} cm/s at 100 μM, Figure 3.2) and on the order of other compounds we studied with high intestinal permeability. For example, previous work from our group utilizing the same experimental setup reported the P_{eff} of

glycylsarcosine was 1.7 x 10^{-4} cm/s [37], the P_{eff} of cefadroxil was 0.6-0.8 x 10^{-4} cm/s [21, 22], the P_{eff} of valacyclovir was 0.9 x 10^{-4} cm/s [23], and the P_{eff} of 5-aminolevulinic acid was 1.9 x 10^{-4} cm/s [38]. To place these results in context, Escribano *et al*. reported that P_{eff} values of about > 0.7 x 10^{-4} cm/s in mice will result in a fraction absorbed of > 90% following oral dosing in human [39]. The discrepancy between our current results with gemcitabine using *in situ* mouse perfusions (*i.e.,* high permeability) and those using *in vitro* Caco-2 cells (*i.e.,* low permeability) probably reflects the low expression of nucleoside transporters in these cell cultures [19] as well as the unphysiologic nature of *in vitro* systems lacking a blood supply. Interestingly, Tsume *et al*. [26] performed similar *in situ* jejunal perfusion studies with 100 μM gemcitabine in female BALB/c mice, but reported the drug to have low intestinal permeability. Specifically, their reported P_{eff} value of 0.02 x 10^{-4} cm/s for gemcitabine was >50-fold lower than the value observed in our current study at the same drug concentration in mixed-gender C57BL/6 mice (no gender bias noted). Potential strain differences in gemcitabine P_{eff} were evaluated in the current study, where the P_{eff} of 100 μM gemcitabine was not different between C57BL/6 mice (1.14 ± 0.08 x 10^{-4} cm/s) and BALB/c mice (1.09 ± 0.13 x 10^{-4} cm/s). Thus, we attribute this "apparent" discrepancy between the current work and the previously published work to the fact that previous investigators [26] corrected gemcitabine P_{eff} for the cytosine metabolite found in their outlet samples. In contrast, no evidence of cytosine was observed in the outlet samples during our jejunal perfusions of gemcitabine in both C57BL/6 and BALB/c mice (Figure 3.1).

To further validate the UPLC analytical technique used in the current work (*i.e.,* verify all drug related metabolites were being correctly quantified), perfusions were

performed in C57BL/6 mice using radiolabeled gemcitabine (*i.e.,* [^{14}C]-gemcitabine). Thus, the total concentration of drug and drug-related species in the inlet and outlet samples could be determined by simply measuring total radioactivity, without the need to specify and quantify all potential gemcitabine metabolites(s) individually. The [^{14}C]-label was present on the cytosine moiety of gemcitabine, thereby ensuring detection of any perfused gemcitabine present in the outlet as cytosine. We found no significant difference in the jejunal permeability when samples were analyzed via radioactivity and UPLC (*i.e.,* <10%, Figure 3.2), indicating that the UPLC assay was correctly identifying all relevant gemcitabine metabolites and that gemcitabine is, in fact, highly permeable in the intestine. Thus, it appears that previous investigators [26] reported an HPLC peak that was incorrectly identified as a gemcitabine metabolite, causing a substantial underestimation of gemcitabine permeability. No such peak was observed in our assay for gemcitabine and metabolites using UPLC, which has improved resolution over HPLC.

The potential for saturation of gemcitabine's intestinal uptake along with the drug's transport kinetics were explored by evaluating the flux of gemcitabine over a large range of perfusate concentrations (*i.e.,* 0.5 μM to 2 mM) in C57BL/6 mice. These experiments showed a clear saturation of intestinal flux (Figure 3.3), which was best described by two Michaelis-Menten terms. This mathematical fit (Table 3.2) suggested that both high-affinity, low-capacity (K_m = 27.4 μM, V_{max} = 3.6 pmol/cm^2/s) and low-affinity, high-capacity (K_m = 700 μM, V_{max} = 35.9 pmol/cm^2/s) transport systems mediated the intestinal uptake of gemcitabine. The existence of two distinct transport systems was further supported by clear nonlinearity in a Wolf-Augustinsson-Hofstee analysis of the concentration-dependent flux (Figure 3.4). Based on intrinsic clearance calculations,

V_{max}/K_m, the high- and low-affinity transport systems were predicted to account for 72% and 28% of the uptake, respectively, under linear conditions. However, as shown in Figure 3.8, whereas the high-affinity transport system or CNTs dominated uptake at lower micromolar concentrations, the low-affinity transport system or ENTs dominated uptake at higher millimolar concentrations.

Broad inhibition of nucleoside transporters via coperfusion of 2 mM thymidine (IC50 = 98.5 μM) reduced gemcitabine permeability by about 95% in C57BL/6 mice, showing that gemcitabine uptake is mediated almost exclusively via nucleoside transporters. Experiments in *Xenopus laevis* oocytes have reported K_m values for gemcitabine transport via hCNT1 (Km ≈ 25 μM), hCNT3 (Km ≈ 60 μM), hENT1 (Km ≈ 160 μM), and hENT2 (Km ≈ 750 μM) [7, 8]. These published K_m values, along with our findings showing the presence of high- and low-affinity transport systems for gemcitabine (Table 3.2) and that both CNTs and ENTs mediate the intestinal uptake of gemcitabine (Figure 3.5), suggest that the high-affinity transport system in the current study corresponds to uptake via CNTs and the low-affinity transport system to uptake via ENTs. Furthermore, inhibition of CNTs in C57BL/6 mice (via perfusion with sodium-free buffer) reduced the intestinal permeability of gemcitabine by 68%, matching closely our predicted contribution of the high-affinity transport system (*i.e.,* 72% of the total transport). Inhibition of ENTs in C57BL/6 mice, via coperfusion with 2 mM dilazep (IC50 = 212 μM), reduced the intestinal permeability of gemcitabine by about 50%, matching closely the predicted maximum dilazep mediated reduction in gemcitabine flux, based upon fitting the concentration-dependent inhibition data (Figure 3.6). Still, dilazep's reduction in gemcitabine flux was

greater than our predicted contribution of the low-affinity transport system (*i.e.,* 28% of total transport), with the source of this disparity remaining unclear at present.

It is widely accepted that CNT1 and CNT3 are expressed apically in the small intestine, but there is some debate regarding the localization of ENT1 and ENT2 [5]. It has been reported that ENT2 is expressed primarily on the apical membrane of Caco-2 cells [40], that ENT1 and ENT2 are expressed on both the apical and basolateral membranes of human small intestine [41], and that ENT1 is expressed only on the basolateral membrane of human intestine [5]. It is important to consider that, although a low-affinity transport system was observed in the concentration-dependent flux data and that dilazep reduced gemcitabine's intestinal permeability, this does not necessarily imply apical expression of ENT(s). Saturation/inhibition of basolateral ENT(s) could increase intracellular gemcitabine concentrations, leading to increased repartitioning of drug from the enterocyte to lumen, thereby reducing the intestinal permeability of drug. This possibility, however, seems improbable as gemcitabine possesses very low passive permeability (Figure 3.5) and thus is unlikely to repartition into the lumen to a significant extent without apical expression of the bidirectional ENT(s).

Previous studies have explored the duodenal expression of nucleoside transporter mRNA in ICR mice [20] and the longitudinal expression (*i.e.,* stomach, duodenum, jejunum, ileum, large intestine) of nucleoside transporter mRNA in C57BL/6 mice [42]. These studies showed that the gene expression of CNTs and ENTs was similar between mouse and human, that CNTs were expressed primarily in small intestine, and that ENTs were expressed in both the small and large intestines, but at much lower levels than CNTs. To further address the localization of ENTs and to better understand their role in mediating

the intestinal uptake (*i.e.,* lumen to enterocyte) and efflux (*i.e.,* enterocyte to portal blood) of gemcitabine, intestinal perfusions of 5 μM [^{14}C]-gemcitabine were performed in C57BL/6 mice (± the ENT inhibitor dilazep), after which total radioactivity was determined in jejunal tissue and portal venous plasma. Coperfusions with 2 mM dilazep reduced the intestinal permeability of gemcitabine by about 50% (Figure 3.5), showed no change in the cellular accumulation of gemcitabine radioactivity, and reduced the portal venous plasma concentration of gemcitabine radioactivity by 68% (Figure 3.7). These observations demonstrate that ENTs mediate, at least in part, the basolateral transport of gemcitabine into portal venous blood as gemcitabine's efflux from enterocytes was substantially decreased by ENT inhibition. Still, despite the reduction of gemcitabine in portal venous plasma, the intracellular jejunal concentration of gemcitabine was not increased when coperfused with dilazep. This shows that gemcitabine's reduction in intestinal permeability after ENT inhibition is not due to increased accumulation of gemcitabine in the intestinal tissue and passive repartitioning back into lumen, but a reduction in drug uptake into epithelial cells because of apically-expressed ENTs. A proposed schematic for the transepithelial flux of gemcitabine in the small intestine is presented in Figure 3.9.

There are currently no oral dosage forms of gemcitabine. Nonetheless, it is anticipated that typical intravenous doses of 1000 - 1250 mg/m^2, given orally, would produce millimolar levels of drug in the intestinal lumen, favoring uptake by the ENTs. However, controlled-release or divided doses would serve to reduce the luminal concentrations of drug, thereby, taking advantage of both the CNTs and ENTs. Still, it would be important to determine how gemcitabine oral formulations and/or dose rates

might influence the drug's presystemic metabolism in the gastrointestinal tract and/or liver, along with drug absorption.

In conclusion, novel approaches to develop orally-administered formulations of gemcitabine have been challenged by the drug's perceived low intestinal permeability and significant presystemic metabolism. Our studies conclusively demonstrate that gemcitabine has, in fact, high permeability in the small intestine via CNT and ENT nucleoside transporters. Although gemcitabine should have low systemic availability after oral dosing, vectorial transport systems identified in the current study suggest that oral dosing (at the appropriate rate) may be advantageous for the selective targeting of gemcitabine to cancers of the intestine and liver. Furthermore, the demonstrated saturability of gemcitabine intestinal uptake highlights the importance of oral dosing rate in determining the fraction absorbed from the intestinal lumen, an important consideration for implementation of strategies aiming to enable oral gemcitabine administration by coadministration of a cytidine deaminase inhibitor.

Tables and Figures

Table 3.1 Summary of intra- and inter-day accuracy and precision of the UPLC assay for quantification of gemcitabine, dFdU, and cytosine

		Intra-day (n=3)		Inter-day (n=9)	
Analyte	**Concentration (μM)**	**Accuracy (%)**	**Precision (CV%)**	**Accuracy (%)**	**Precision (CV%)**
Gemcitabine	0.25 / 25 / 100	106 / 100 / 100	1.2 / 0.1 / 0.2	98.1 / 100 / 100	8.7 / 0.3 / 0.5
dFdU	0.25 / 1 / 5	98.4 / 101 / 100	4.1 / 0.8 / 0.5	98.9 / 100 / 100	3.8 / 0.8 / 0.8
Cytosine	1 / 50 / 100	101 / 100 / 100	2.5 / 0.1 / 0.2	105 / 100 / 100	4.8 / 0.2 / 0.2

Table 3.2 Transport kinetics of gemcitabine during *in situ* jejunal perfusions in C57BL/6 mice

Parameter	**Estimate (mean ± SE)**
$V_{max,1}$ (pmol/cm^2/s)	3.6 ± 2.1
$K_{m,1}$ (μM)	27.4 ± 13.9
$V_{max,2}$ (pmol/cm^2/s)	35.9 ± 5.5
$K_{m,2}$ (μM)	700 ± 330
r^2	0.951

Gemcitabine flux was best fit to two saturable Michaelis-Menten terms where $V_{max,1}$ and $V_{max,2}$ correspond to the maximum uptake rates for transport systems 1 and 2, and $K_{m,1}$ and $K_{m,2}$ correspond to the Michaelis constants for transport systems 1 and 2 (see Eq 3.4).

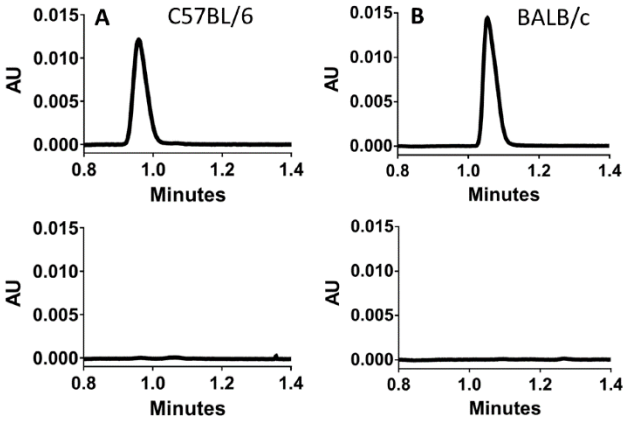

Figure 3.1 Representative chromatograms demonstrating the absence of cytosine in outlet samples following *in situ* jejunal perfusion of 100 μM gemcitabine in (A) C57BL/6 mice and (B) BALB/c mice. The top panels show 5 μM cytosine standards and the bottom panels show perfusion outlet samples.

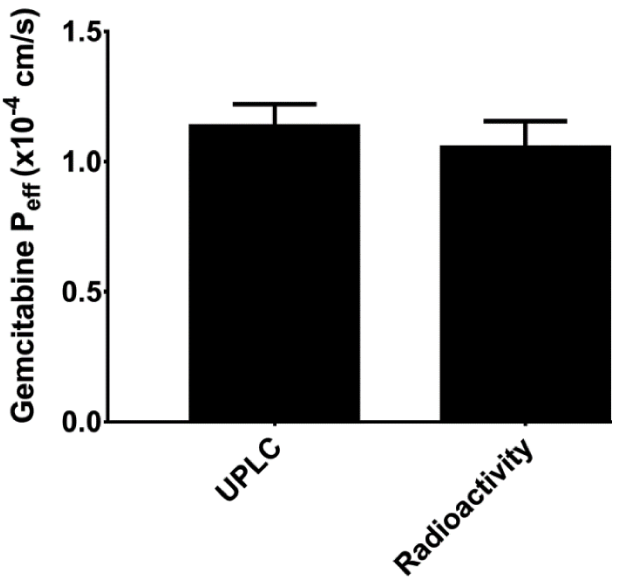

Figure 3.2 *In situ* jejunal permeability of gemcitabine in C57BL/6 mice when inlet and outlet concentrations of drug were measured by UPLC (after perfusions of 100 μM unlabeled gemcitabine) or total radioactivity (after perfusions of 100 μM [^{14}C]-gemcitabine). Data are expressed as mean ± SE, n=4. There was no significant difference between the two groups, as determined by unpaired t-test.

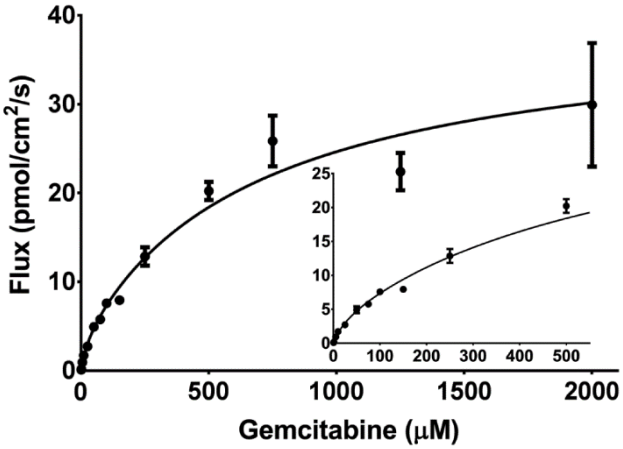

Figure 3.3 Concentration-dependent flux of gemcitabine during 0.5 μM - 2 mM *in situ* jejunal perfusions of drug in C57BL/6 mice. The solid line represents the predicted flux when data were fitted to two Michaelis-Menten terms. The inset shows the plot at low concentrations of gemcitabine. Data are expressed as mean ± SE, n=4 (error bars may be hidden by the symbol).

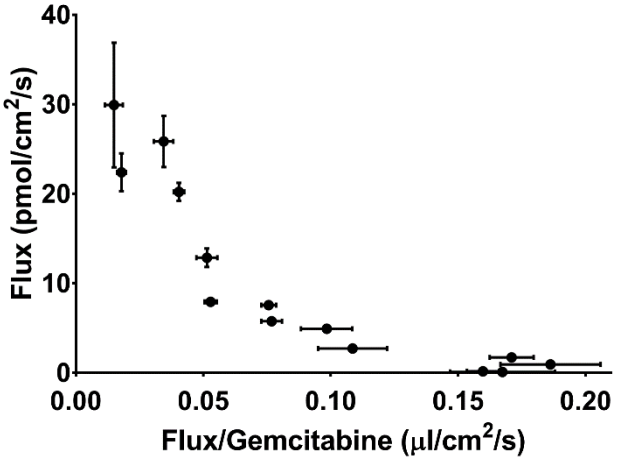

Figure 3.4 Wolf-Augustinsson-Hofstee analysis of the concentration-dependent flux of gemcitabine during 0.5 µM - 2 mM *in situ* jejunal perfusions of drug in C57BL/6 mice. Data are expressed as mean ± SE, n=4 (error bars may be hidden by the symbol).

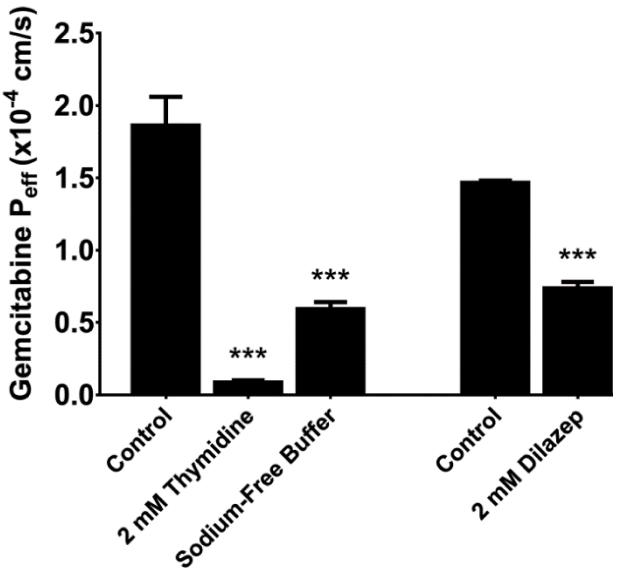

Figure 3.5 Effect of inhibitors on the intestinal permeability of 5 μM gemcitabine during *in situ* jejunal perfusions of drug in C57BL/6 mice. Experiments with 2 mM thymidine and sodium-free buffer were performed several months before those with 2 mM dilazep and, as a result, control values were reported for each set of experiments. Data are expressed as mean ± SE, n=4. *** $p<0.001$ relative to control, as determined by ANOVA followed by Dunnett's test for thymidine and sodium-free buffer data; and by unpaired t-test for dilazep data. There was no significant difference between the two control groups, as determined by unpaired t-test.

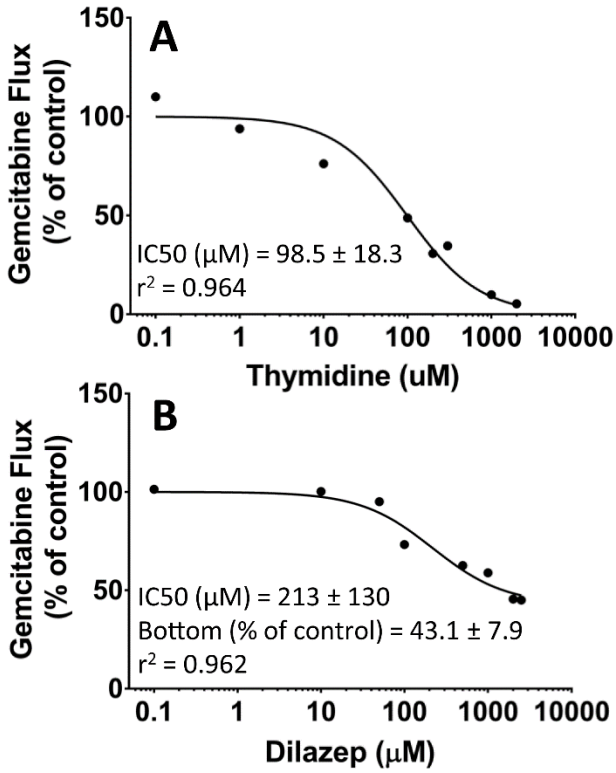

Figure 3.6 Concentration-dependent inhibition of gemcitabine flux in C57BL/6 mice during *in situ* jejunal perfusions of 5 μM drug alone and in the presence of (A) 0.1-2000 μM thymidine or (B) 0.1-2500 μM dilazep. The solid line represents the predicted flux when data were fitted to Eq 3.5 for thymidine and to Eq 3.6 for dilazep. Data are expressed as mean, n=1-4.

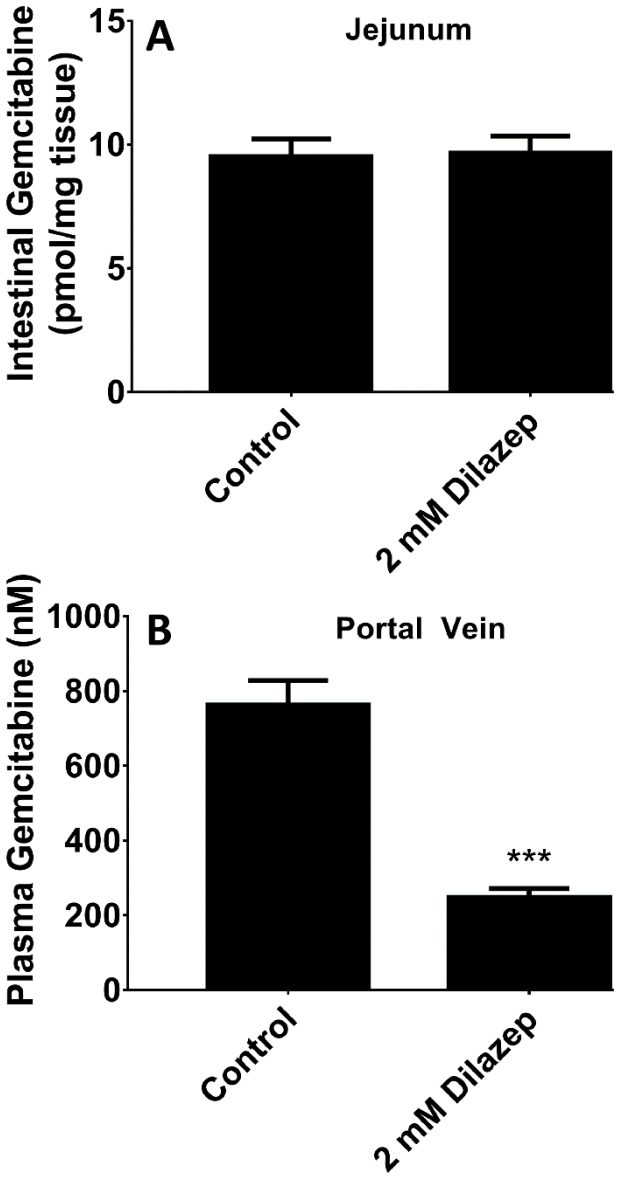

Figure 3.7 Total radioactivity of gemcitabine and drug-related species in (A) jejunal tissue and (B) portal venous plasma following *in situ* jejunal perfusions of 5 μM [^{14}C]-gemcitabine in the absence and presence of 2 mM dilazep in C57BL/6 mice. Data are expressed as mean ± SE, n=4. ***p<0.001, as determined by unpaired t-test. There was so significant difference detected in jejunal tissue radioactivity, as determined by an unpaired t-test.

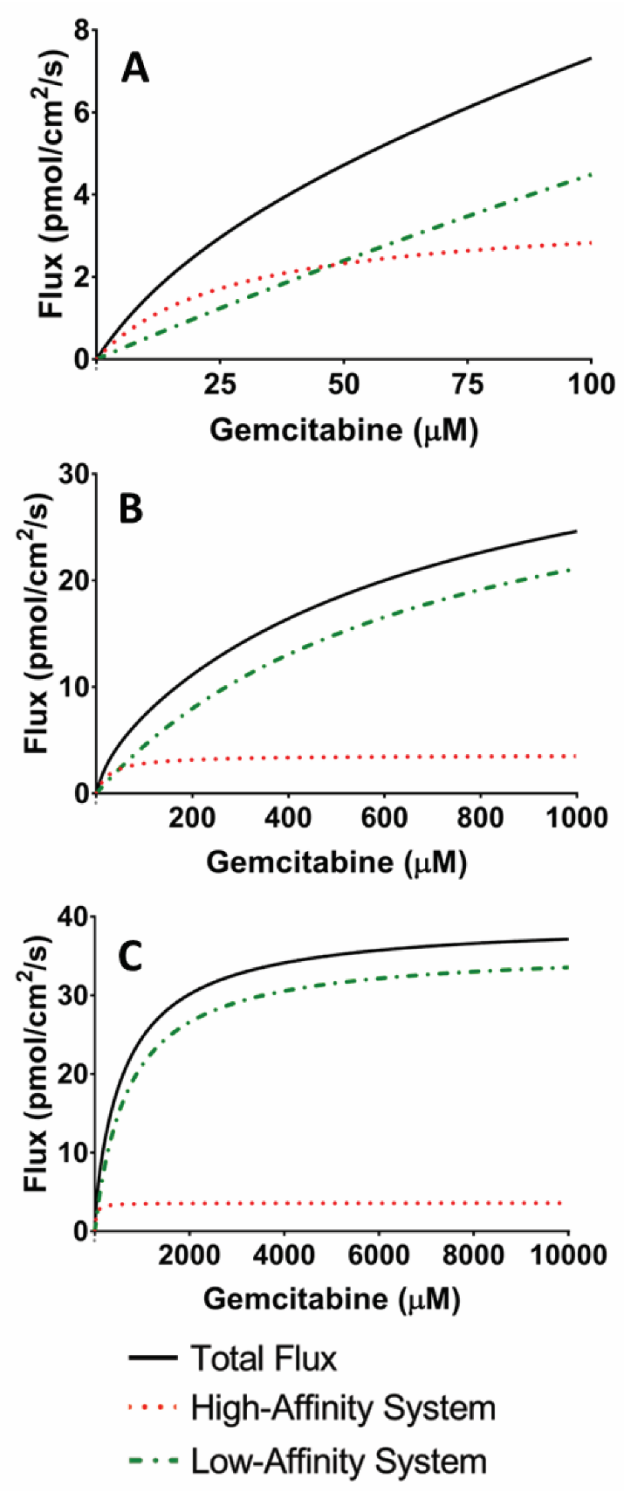

Figure 3.8 Contribution of the high-affinity (CNTs) and low-affinity (ENTs) transport systems toward gemcitabine flux, visualized over the three intestinal concentration ranges of (A) 0 – 100 μM, (B) 0 – 1,000 μM, and (C) 0 – 10,000 μM.

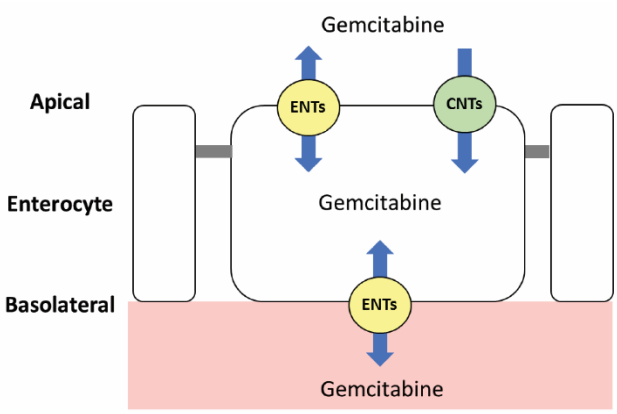

Figure 3.9 Proposed mechanism for the absorption of gemcitabine in small intestine. The apical uptake of gemcitabine (i.e., from lumen to enterocytes) is mediated by CNTs and ENTs, whereas the basolateral efflux of gemcitabine and/or gemcitabine metabolites (i.e., from enterocytes to portal venous blood) is mediated by ENTs.

References

[1] Burris H.A., Moore M.J., Andersen J., Green M.R., Rothenberg M.L., Modiano M.R., Cripps M.C., Portenoy R.K., Storniolo A.M., Tarassoff P., Nelson R., Dorr F.A., Stephens C.D., and Von Hoff D.D., Improvements in survival and clinical benefit with gemcitabine as first-line therapy for patients with advanced pancreas cancer: a randomized trial, J Clin Oncol. 15 (1997) 2403-2413.

[2] Pfisterer J., Plante M., Vergote I., du Bois A., Hirte H., Lacave A.J., Wagner U., Stahle A., Stuart G., Kimmig R., Olbricht S., Le T., Emerich J., Kuhn W., Bentley J., Jackisch C., Luck H.J., Rochon J., Zimmermann A.H., and Eisenhauer E., Gemcitabine plus carboplatin compared with carboplatin in patients with platinum-sensitive recurrent ovarian cancer: an intergroup trial of the AGO-OVAR, the NCIC CTG, and the EORTC GCG, J Clin Oncol. 24 (29) (2006) 4699-4707.

[3] Albain K.S., Nag S.M., Calderillo-Ruiz G., Jordaan J.P., Llombart A.C., Pluzanska A., Rolski J., Melemed A.S., Reyes-Vidal J.M., Sekhon J.S., Simms L., and O'Shaughnessy J., Gemcitabine plus Paclitaxel versus Paclitaxel monotherapy in patients with metastatic breast cancer and prior anthracycline treatment, J Clin Oncol. 26 (24) (2008) 3950-3957.

[4] Sandler A.B., Nemunaitis J., Denham C., von Pawel J., Cormier Y., Gatzemeier U., Mattson K., Manegold C., Palmer M.C., Gregor A., Nguyen B., Niyikiza C., and Einhorn L.H., Phase III Trial of Gemcitabine Plus Cisplatin Versus Cisplatin Alone in Patients With Locally Advanced or Metastatic Non–Small-Cell Lung Cancer, J Clin Oncol. 18 (1) (2000) 122-130.

[5] Young J.D., Yao S.Y., Baldwin J.M., Cass C.E., and Baldwin S.A., The human concentrative and equilibrative nucleoside transporter families, SLC28 and SLC29, Mol Aspects Med. 34 (2-3) (2013) 529-547.

[6] Mackey J.R., Mani R.S., Selner M., Mowles D., Young J.D., Belt J.A., Crawford C.R., and Cass C.E., Functional nucleoside transporters are required for gemcitabine influx and manifestation of toxicity in cancer cell lines, Cancer Res. 58 (19) (1998) 4349-4357.

[7] Mackey J.R., Yao S.Y., Smith K.M., Karpinski E., Baldwin S.A., Cass C.E., and Young J.D., Gemcitabine transport in xenopus oocytes expressing recombinant plasma membrane mammalian nucleoside transporters, J Natl Cancer Inst. 91 (21) (1999) 1876-1881.

[8] Hu H., Endres C.J., Chang C., Umapathy N.S., Lee E.W., Fei Y.J., Itagaki S., Swaan P.W., Ganapathy V., and Unadkat J.D., Electrophysiological characterization and modeling of the structure activity relationship of the human concentrative nucleoside transporter 3 (hCNT3), Mol Pharmacol. 69 (5) (2006) 1542-1553.

[9] Parkinson F.E., Damaraju V.L., Graham K., Yao S.Y., Baldwin S.A., Cass C.E., and Young J.D., Molecular biology of nucleoside transporters and their distributions and functions in the brain, Curr Top Med Chem. 11 (8) (2011) 948-972.

[10] Smith K.M., Slugoski M.D., Loewen S.K., Ng A.M., Yao S.Y., Chen X.Z., Karpinski E., Cass C.E., Baldwin S.A., and Young J.D., The broadly selective human Na+/nucleoside cotransporter (hCNT3) exhibits novel cation-coupled nucleoside transport characteristics, J Biol Chem. 280 (27) (2005) 25436-25449.

[11] Heinemann V., Hertel L.W., Grindey G.B., and Plunkett W., Comparison of the cellular pharmacokinetics and toxicity of 2',2'-difluorodeoxycytidine and 1-beta-D-arabinofuranosylcytosine, Cancer Res. 48 (14) (1988) 4024-4031.

[12] Huang P., Chubb S., Hertel L.W., Grindey G.B., and Plunkett W., Action of 2',2'-difluorodeoxycytidine on DNA synthesis, Cancer Res. 51 (22) (1991) 6110-6117.

[13] Huang P. and Plunkett W., Fludarabine- and gemcitabine-induced apoptosis: incorporation of analogs into DNA is a critical event, Cancer Chemother Pharmacol. 36 (3) (1995) 181-188.

[14] Heinemann V., Xu Y.Z., Chubb S., Sen A., Hertel L.W., Grindey G.B., and Plunkett W., Inhibition of ribonucleotide reduction in CCRF-CEM cells by 2',2'-difluorodeoxycytidine, Mol Pharmacol. 38 (4) (1990) 567-572.

[15] Plunkett W., Huang P., Xu Y.-Z., Heinemann V., Grunewald R., and Gandhi V., Gemcitabine: metabolism, mechanisms of action, and self-potentiation, Semin Oncol. 22 (1995) 3-10.

[16] Veltkamp S.A., Jansen R.S., Callies S., Pluim D., Visseren-Grul C.M., Rosing H., Kloeker-Rhoades S., Andre V.A., Beijnen J.H., Slapak C.A., and Schellens J.H., Oral administration of gemcitabine in patients with refractory tumors: a clinical and pharmacologic study, Clin Cancer Res. 14 (11) (2008) 3477-3486.

[17] Gemzar [package insert]. Eli Lilly and Company, Indianapolis, IN, (2014).

[18] Beumer J.H., Eiseman J.L., Parise R.A., Joseph E., Covey J.M., and Egorin M.J., Modulation of Gemcitabine (2′,2′-Difluoro-2′-Deoxycytidine) Pharmacokinetics, Metabolism, and Bioavailability in Mice by 3,4,5,6-Tetrahydrouridine, Clin Cancer Res. 14 (11) (2008) 3529-3535.

[19] Takahashi K., Yoshisue K., Chiba M., Nakanishi T., and Tamai I., Involvement of Concentrative Nucleoside Transporter 1 in Intestinal Absorption of Trifluridine Using Human Small Intestinal Epithelial Cells, J Pharm Sci. 104 (9) (2015) 3146-3153.

[20] Kim H.-R., Park S.-W., Cho H.-J., Chae K.-A., Sung J.-M., Kim J.-S., Landowski C.P., Sun D., Abd El-Aty A.M., Amidon G.L., and Shin H.-C., Comparative gene

expression profiles of intestinal transporters in mice, rats and humans, Pharmacol Res. 56 (3) (2007) 224-236.

[21] Posada M.M. and Smith D.E., Relevance of PepT1 in the intestinal permeability and oral absorption of cefadroxil, Pharm Res. 30 (4) (2013) 1017-1025.

[22] Hu Y. and Smith D.E., Species differences in the pharmacokinetics of cefadroxil as determined in wildtype and humanized PepT1 mice, Biochem Pharmacol. 107 (2016) 81-90.

[23] Epling D., Hu Y., and Smith D.E., Evaluating the intestinal and oral absorption of the prodrug valacyclovir in wildtype and huPepT1 transgenic mice, Biochem Pharmacol. 155 (2018) 1-7.

[24] Ma K., Hu Y., and Smith D.E., Peptide transporter 1 is responsible for intestinal uptake of the dipeptide glycylsarcosine: studies in everted jejunal rings from wild-type and Pept1 null mice, J Pharm Sci. 100 (2) (2011) 767-774.

[25] Abbruzzese J.L., Grunewald R., Weeks E.A., Gravel D., Adams T., Nowak B., Mineishi S., Tarassoff P., Satterlee W., and Raber M.N., A phase I clinical, plasma, and cellular pharmacology study of gemcitabine, J Clin Oncol. 9 (3) (1991) 491-498.

[26] Tsume Y., Borras Bermejo B., and Amidon G.L., The dipeptide monoester prodrugs of floxuridine and gemcitabine-feasibility of orally administrable nucleoside analogs, Pharmaceuticals. 7 (2) (2014) 169-191.

[27] Ho N.F. and Higuchi W.I., Theoretical model studies of intestinal drug absorption. IV. Bile acid transport at premicellar concentrations across diffusion layer-membrane barrier, J Pharm Sci. 63 (5) (1974) 686-690.

[28] Sutton S.C., Rinaldi M.T.S., and Vukovinsky K.E., Comparison of the gravimetric, phenol red, and 14C-PEG-3350 methods to determine water absorption in the rat single-pass intestinal perfusion model, AAPS PharmSci. 3 (3) (2001) 93-98.

[29] Hurvich C.M. and Tsai C.-L., Regression and time series model selection in small samples, Biometrika. 76 (2) (1989) 297-307.

[30] Tsume Y., Incecayir T., Song X., Hilfinger J.M., and Amidon G.L., The development of orally administrable gemcitabine prodrugs with D-enantiomer amino acids: enhanced membrane permeability and enzymatic stability, Eur J Pharm Biopharm. 86 (3) (2014) 514-523.

[31] Wickremsinhe E., Bao J., Smith R., Burton R., Dow S., and Perkins E., Preclinical absorption, distribution, metabolism, and excretion of an oral amide prodrug of gemcitabine designed to deliver prolonged systemic exposure, Pharmaceutics. 5 (2) (2013) 261-276.

[32] Wang G., Chen H., Zhao D., Ding D., Sun M., Kou L., Luo C., Zhang D., Yi X., Dong J., Wang J., Liu X., He Z., and Sun J., Combination of l-Carnitine with Lipophilic Linkage-Donating Gemcitabine Derivatives as Intestinal Novel Organic Cation Transporter 2-Targeting Oral Prodrugs, J Med Chem. 60 (6) (2017) 2552-2561.

[33] Lim J.H., You S.K., Baek J.S., Hwang C.J., Na Y.G., Shin S.C., and Cho C.W., Preparation and evaluation of polymeric microparticulates for improving cellular uptake of gemcitabine, Int J Nanomed. 7 (2012) 2307-2314.

[34] Derakhshandeh K. and Fathi S., Role of chitosan nanoparticles in the oral absorption of Gemcitabine, Int J Pharm. 437 (1) (2012) 172-177.

[35] Chen G., Svirskis D., Lu W., Ying M., Huang Y., and Wen J., N-trimethyl chitosan nanoparticles and CSKSSDYQC peptide: N-trimethyl chitosan conjugates enhance the oral bioavailability of gemcitabine to treat breast cancer, J Control Release. 277 (2018) 142-153.

[36] Hao W.H., Wang J.J., Hsueh S.P., Hsu P.J., Chang L.C., Hsu C.S., and Hsu K.Y., In vitro and in vivo studies of pharmacokinetics and antitumor efficacy of D07001-F4, an oral gemcitabine formulation, Cancer Chemother Pharmacol. 71 (2) (2013) 379-388.

[37] Jappar D., Wu S.P., Hu Y., and Smith D.E., Significance and regional dependency of peptide transporter (PEPT) 1 in the intestinal permeability of glycylsarcosine: in situ single-pass perfusion studies in wild-type and Pept1 knockout mice, Drug Metab Dispos. 38 (10) (2010) 1740-1746.

[38] Xie Y., Hu Y., and Smith D.E., The proton-coupled oligopeptide transporter 1 plays a major role in the intestinal permeability and absorption of 5-aminolevulinic acid, Br J Pharmacol. 173 (1) (2016) 167-176.

[39] Escribano E., Sala X.G., Salamanca J., Navarro C.R., and Regue J.Q., Single-pass intestinal perfusion to establish the intestinal permeability of model drugs in mouse, Int J Pharm. 436 (1-2) (2012) 472-477.

[40] Morote–Garcia J.C., Rosenberger P., Nivillac N.M., Coe I.R., and Eltzschig H.K., Hypoxia-inducible factor–dependent repression of equilibrative nucleoside transporter 2 attenuates mucosal inflammation during intestinal hypoxia, Gastroenterology. 136 (2) (2009) 607-618.

[41] Govindarajan R., Bakken A.H., Hudkins K.L., Lai Y., Casado F.J., Pastor-Anglada M., Tse C.M., Hayashi J., and Unadkat J.D., In situ hybridization and immunolocalization of concentrative and equilibrative nucleoside transporters in the human intestine, liver, kidneys, and placenta, Am J Physiol Regul Integr Comp Physiol. 293 (5) (2007) R1809-1822.

[42] Lu H., Chen C., and Klaassen C., Tissue distribution of concentrative and equilibrative nucleoside transporters in male and female rats and mice, Drug Metab Dispos. 32 (12) (2004) 1455-1461.

CHAPTER 4

Pharmacokinetics of Gemcitabine and its Amino Acid Ester Prodrug following Intravenous and Oral Administrations in Mice

4.1 Abstract

Gemcitabine is an intravenously administered anti-cancer nucleoside analogue. Systemic exposure following oral administration of gemcitabine is limited by extensive first-pass metabolism via cytidine deaminase (CDA) and potentially by saturation of nucleoside transporter-mediated intestinal uptake. An amino acid ester prodrug of gemcitabine, 5'-L-valyl-gemcitabine (V-Gem), was previously shown to be a substrate of the intestinally expressed peptide transporter 1 (PEPT1) and stable against CDA-mediated metabolism. However, preliminary studies did not evaluate the *in vivo* oral performance of V-Gem as compared to parent drug. In the present study, we evaluated the pharmacokinetics and *in vivo* oral absorption of gemcitabine and V-Gem following intravenous and oral administrations in mice. These studies revealed that V-Gem undergoes rapid systemic elimination (half-life < 1 min) and has a low oral bioavailability (< 1%). Most importantly, the systemic exposure of gemcitabine was not different following oral administration of equimolar doses of gemcitabine (gemcitabine bioavailability of 18.3%) and V-Gem (gemcitabine bioavailability of 16.7%). Single-pass intestinal perfusions with portal blood sampling in mice revealed that V-Gem undergoes extensive activation in intestinal epithelial cells and that gemcitabine undergoes first-pass metabolism in intestinal epithelial cells. Thus, formulation of

gemcitabine as the prodrug V-Gem does not increase systemic gemcitabine exposure following oral dosing, due, in part, to the instability of V-Gem in intestinal epithelial cells.

4.2 Introduction

Gemcitabine (2',2'-difluoro-2'-deoxycytidine; dFdC) is a nucleoside analogue approved for use in the treatment of pancreatic, non-small cell lung, ovarian, and breast cancer [1]. It is also used off-label for treatment of other cancer types such as biliary tract and bladder cancer [2-4]. Gemcitabine exerts its anti-cancer activity through incorporation of gemcitabine triphosphate into growing DNA strands, inhibiting DNA synthesis [5] and leading to apoptosis [6]. Various self-potentiating mechanisms, including gemcitabine diphosphate inhibition of ribonucleotide reductase [7], have been reported to augment gemcitabine cytotoxicity [8]. Gemcitabine is rapidly cleared from plasma (half-life = 42 – 94 min), mainly via cytidine deaminase (CDA)-mediated deamination of gemcitabine to 2',2'-difluoro-2'-deoxyuridine (dFdU) [9]. The *in vivo* activity of dFdU is currently unclear, although some work has suggested it may contribute to gemcitabine cytotoxicity [10, 11] and radiosensitization [12].

Gemcitabine has a low oral bioavailability of about 10% [13] and is, thus, administered via intravenous infusion, typically once per week at a dose of 1000 – 1250 mg/m^2 [1]. However, oral administration is generally preferred as it is more patient friendly, less invasive, and reduces the costs and complications associated with intravenous drug administration. Furthermore, oral gemcitabine administration would allow for greater flexibility in designing dosing schedules, enabling both metronomic gemcitabine dosing (*i.e.,* frequent low dose administration) and dosing which replicates gemcitabine pharmacokinetics following a prolonged intravenous infusion. There is evidence that such dosing schedules may lead to improvements in efficacy and/or reductions in toxicity [14-17].

Given the advantages of oral gemcitabine administration, much work has been dedicated to understanding the mechanistic basis of gemcitabine's low oral bioavailability. Recent work using

in situ intestinal perfusions in mice demonstrated that gemcitabine intestinal uptake is saturable and driven almost exclusively by nucleoside transporters (NT), and that gemcitabine has high effective permeability in the intestine, implying that first-pass metabolism drives gemcitabine's low oral bioavailability [18]. This conclusion is further supported by the observation that following oral administration, gemcitabine undergoes extensive first-pass metabolism via CDA, forming dFdU [13]. Moreover, gemcitabine intestinal uptake is rapidly saturated with increasing concentration, which may further limit gemcitabine bioavailability following oral administration of larger and perhaps more clinically relevant doses [18].

In hopes of both increasing gemcitabine oral bioavailability by decreasing first-pass metabolism and enabling the oral administration of larger gemcitabine doses through reducing the saturability of gemcitabine intestinal absorption, several peptide transporter 1 (PEPT1)-targeted gemcitabine prodrugs were previously synthesized [19]. PEPT1 (SLC15A1) is a transmembrane transporter that is extensively expressed on the apical membrane of intestinal enterocytes [20]. Given that PEPT1 generally functions as a high-capacity, low-affinity intestinal transporter, it is frequently targeted to increase intestinal drug uptake via administration of a PEPT1-targeted prodrug. These prodrugs, often formed by addition of an amino acid to the parent molecule via an ester bond, undergo PEPT1-mediated uptake and are subsequently activated, releasing the active parent compound [21]. One such PEPT1-targeted gemcitabine prodrug, 5'-L-valyl-gemcitabine (V-Gem), was generated by linking l-valine to gemcitabine via an ester bond [19]. Previous *in vitro* work confirmed that V-Gem was stable against CDA-mediated deamination [19, 22] and was a PEPT1 substrate [19, 23].

With this in mind, the primary objective of this study was to characterize the *in vivo* pharmacokinetics of gemcitabine and V-Gem following intravenous and oral administrations in

mice. The secondary objective, using *in situ* intestinal perfusions in mice, was to evaluate the ability of V-Gem to reduce first-pass metabolism and increase intestinal drug absorption, relative to gemcitabine.

4.3 Materials and Methods

4.3.1 Chemicals

Gemcitabine (Gem), high-performance liquid chromatography (HPLC) grade acetonitrile, and HPLC grade trifluoroacetic acid (TFA) were purchased from Thermo Fisher Scientific (Waltham, MA). Tetrahydrouridine (THU) and the deaminated gemcitabine metabolite 2',2'-difluorodeoxyuridine (dFdU) were purchased from Sigma-Aldrich (St. Louis, MO). $^{13}C,^{15}N_2$-Gem and $^{13}C,^{15}N_2$-dFdU internal standards were purchased from Toronto Research Chemicals (Toronto, Canada). The 5'-L-valyl-gemcitabine prodrug (V-Gem) was synthesized by AAPharmaSyn, LLC (Ann Arbor, MI). All other chemicals were obtained from standard commercial sources. See Figure 4.1 for the chemical structures of Gem, dFdU, and V-Gem.

4.3.2 Animals

Studies were performed on 8- to 12-week old gender-matched C57BL/6 mice purchased from Charles River Laboratories (Wilmington, MA). The mice were housed in a temperature-controlled room with 12-hour light/dark cycles and were provided a standard diet with *ad libitum* access to water (Unit for Laboratory Animal Medicine, University of Michigan, Ann Arbor, MI). All animal studies were conducted in accordance with the Guide for the Care and Use of Laboratory Animals.

4.3.3 Intravenous and oral pharmacokinetic studies of Gem and V-Gem

For intravenous studies, mice were administered 76 nmol/g body weight of Gem or V-Gem (in 0.1 mL saline per 25 g body weight) via bolus tail vein injection (n=4). For oral studies, mice were fasted overnight (~ 16 hr) and subsequently administered 228 nmol/g body weight of Gem or V-Gem (in 0.2 mL water per 25 g body weight) via oral gavage (n=4). Following both intravenous and oral dosing, blood samples were collected via distal tail transection at 2, 5, 15, 30,

45, 60, 90, 120, 180, 240, 300, and 360 min. At each sampling time point, approximately 20 µL of blood was collected with a pipette, added to a 0.2 mL PCR tube containing EDTA-K3 and THU (the latter included to prevent *ex vivo* Gem deamination by CDA), and centrifuged at 3000 rpm for 4 min at 4°C. A 5 µL plasma aliquot was then mixed with 200 µL ice-cold acetonitrile, containing 0.1 µM $^{13}C,^{15}N_2$-Gem and 0.25 µM $^{13}C,^{15}N_2$-dFdU as internal standards (IS), and placed in the -20°C freezer until all samples for the given mouse were collected. Samples were then centrifuged at 17,000 g for 10 min at 4 °C and a 60 µL aliquot of the supernatant stored at -80°C until analysis.

Afterwards, the supernatants were dried in a SpeedVac concentrator for two hours (with heating at 45 °C during the first hour) and reconstituted in 90 µL water (plus 0.1% formic acid). The reconstituted samples were centrifuged at 17,000 g for 10 min at 4°C and the supernatants were analyzed via liquid chromatography-tandem mass spectrometry (LC-MS/MS), as described below.

4.3.4 LC-MS/MS assay conditions for pharmacokinetic study samples

The concentrations of Gem, dFdU, and V-Gem were determined in mouse plasma samples using a novel LC-MS/MS method utilizing a Shimadzu HPLC system (Shimazu, Kyoto, Japan) coupled with an Applied Biosystems API 4000 triple quadrupole/linear ion trap (QTRAP) mass spectrometer (Foster City, CA). Following plasma sample collection and preparation (see above), 8 µL of supernatant was injected onto an Agilent Poroshell 120 EC-C18 column (2.7 µm, 2.1 x 50 mm, Santa Clara, CA). Analyte separation was achieved using a gradient elution method combining water (plus 0.1% formic acid) and acetonitrile (plus 0.1% formic acid) at a flow rate of 0.35 mL/min. The gradient was initiated and held at 1% acetonitrile for 0.5 min, increased to 90% acetonitrile linearly from 0.5 – 1.0 min, held at 90% acetonitrile from 1.0 - 3.0 min, decreased to 1% acetonitrile linearly from 3.0 - 3.1 min, and held at 1% acetonitrile until the end of the run (5.1

min). To minimize and monitor for carryover, injections of blank water were performed between all sample injections.

The MS was operated in a positive multiple reaction monitoring (MRM) mode using turbo electrospray ionization. The source-dependent parameters were set as follows: curtain gas 30 psi, ionspray voltage 5500 V, temperature 500 °C, gas1 50 psi and gas2 50 psi. The analyte-specific MS parameters are summarized in Table 4.1.

4.3.5 Validation of LC-MS/MS assay for pharmacokinetic study samples

Calibrator, quality control (QC), and stability samples were prepared by performing a 10x dilution of aqueous drug solutions into blank mouse plasma. For all three analytes (*i.e.,* Gem, dFdU, and V-Gem), calibrator samples were prepared at final concentrations of 0.05, 0.1, 0.25, 1, 5, 20, 50, and 100 μM, QC samples at 0.1, 5, and 50 μM, and stability samples at 0.1, 2, 5, 50, and 100 μM. The calibrator, QC, and stability samples were processed for analysis identically with plasma samples collected from the pharmacokinetic study (*i.e.,* plasma quenched in acetonitrile containing IS, supernatant dried, dried sample reconstituted in water, supernatant analyzed).

Selectivity of the assay was evaluated by injecting blank plasma samples prepared from multiple mice, blank plasma spiked with IS, and blank plasma spiked with the three analytes at 0.05 μM to assess potential interferences. Linearity was evaluated by developing standard curves ranging from 0.05 – 100 μM for all three analytes. $^{13}C,^{15}N_2$-dFdU was used as the IS for dFdU and $^{13}C,^{15}N_2$-Gem was used as the IS for both Gem and V-Gem. Assay accuracy and precision were determined by analyzing QC samples in triplicate in three independent runs. Finally, sample stability was assessed during long-term storage by analyzing stability samples (2, 100 μM) after storage at -80 ℃ for 30 days. Autosampler stability was assessed by analyzing stability samples (0.1, 5, and 50 μM) after storage in the autosampler (4℃) for 24 hr.

4.3.6 In situ single-pass intestinal perfusions of Gem and V-Gem

Intestinal perfusions in mice were performed as previously described [18, 24]. In brief, mice were fasted overnight (~ 16 hr) with free access to water and subsequently anesthetized with sodium pentobarbital (40 – 60 mg/kg intraperitoneal). Their abdominal cavity was then exposed and an 8 cm long jejunal segment, beginning 2 cm distal from the Ligament of Treitz, was isolated and both ends cannulated. The proximal canula was attached to a syringe containing pH 6.0 perfusion solution and positioned in a perfusion pump (PHD Ultra, Harvard Apparatus, South Natick, MA). The distal canula was connected to a collection vial.

The perfusion solution contained 145 mM NaCl, 5 mM morpholinoethanesulfonic acid (MES), 5 mM glucose, 3 mM KCl, 1 mM $CaCl_2$, 1 mM NaH_2PO_4, 0.5 mM $MgCl_2$, and either 100 μM Gem or 100 μM V-Gem. To assess drug stability in the intestinal lumen, the perfusion solution containing Gem or V-Gem was perfused through the cannulated segment at 0.1 ml/min for 30 min to achieve steady-state, and then for an additional 60 min with outlet sample collections every 10 min. The concentrations of Gem, dFdU, and V-Gem were determined in inlet and outlet samples using a previously described UPLC assay [18], revalidated for the quantification of an additional analyte, V-Gem (validation data not shown here).

Perfusion studies to explore drug stability in intestinal epithelial cells were also performed by perfusing perfusion solution, containing 10 mM Gem or 10 mM V-Gem, through the cannulated jejunal segment at 0.1 mL/min for 5 min and then immediately collecting a portal blood sample (~ 200 ul). The portal blood sample was collected in a 1.5 mL microcentrifuge tube containing EDTA-K3 and THU, and immediately centrifuged at 3000 g for 4 minutes at 4 °C. A 50 μl aliquot of plasma was then mixed with 200 μl of ice-cold acetonitrile (containing caffeine as an IS) and stored at -20 °C until all samples were collected. Samples were then centrifuged at 17,000 g for 10

min at 4 ℃ and 60 µL of the supernatant collected. The supernatants were then dried in a SpeedVac concentrator for two hours (with heating at 45 ℃ during the first hour) and reconstituted in 80 µL water (plus 0.1% TFA). The reconstituted samples were centrifuged at 17,000 g for 10 min at 4℃ and the supernatants analyzed via UPLC, as described below.

4.3.7 UPLC assay for analysis of portal blood samples

The concentrations of Gem, dFdU, and V-Gem were determined in portal plasma samples using a Waters Acquity H-Class UPLC system (Milford, MA) coupled with a photodiode array detector. Following portal plasma collection and preparation (see above), 15 µl of supernatant was injected onto a 40℃ Acquity HSS T3 column (2.1 x 100 mm), fitted with an HSS T3 VanGuard precolumn (2.1 x 5 mm). Analyte separation was achieved using a gradient elution method combining water (plus 0.1% TFA) and acetonitrile (plus 0.1% TFA) at a flow rate of 0.4 ml/min. The gradient was initiated at 0% acetonitrile, increased to 6% acetonitrile linearly from 0 – 3 min, increased to 15% acetonitrile linearly from 3 – 5 min, increased to 80% acetonitrile linearly from 5 – 7 min, held at 80% acetonitrile from 7 – 8 min, returned to 0% acetonitrile linearly from 8 – 9 min, and held at 0% acetonitrile until the end of the run (12 min). Calibration curves ranging from the lower limit of quantiation to the upper limit of quantitation were generated for V-Gem (0.025 – 5 µM, detection wavelength = 275 nm), Gem (0.1 – 50 µM, detection wavelength = 284 nm), and dFdU (0.1 – 50 µM, detection wavelength = 260 nm) using caffeine (detection wavelength = 275 nm) as the IS. The method was validated with respect to selectivity, showing no endogenous compound interference with analyte detection, linearity ($r^2 > 0.991$), accuracy (average bias of triplicated QC samples < 12%), and precision (relative standard deviation of triplicated QC samples < 7%).

4.3.8 Data analysis

Noncompartmental analysis (NCA) of plasma-concentration time profiles after oral and intravenous dosing was performed using Phoenix WinNonlin 8.2 (Certara, St. Louis, MO). All pharmacokinetic parameters were reported as geometric mean (geometric CV%) except for T_{max}, which was reported as median (min – max). The bioavailability of Gem following oral Gem and V-Gem administrations was calculated as $\frac{AUC_{Gem,Gem\ PO}}{AUC_{Gem,Gem\ IV}} \times \frac{Dose_{IV}}{Dose_{PO}}$ and $\frac{AUC_{Gem,\ V-Gem\ PO}}{AUC_{Gem,\ Gem\ IV}} \times \frac{Dose_{IV}}{Dose_{PO}}$, respectively. When performing calculations with AUC values, AUC_{inf} values were used unless the percent extrapolated was > 25%, in which case $AUC_{0\text{-}6\ hr}$ values were used. All other data were reported as arithmetic mean ± SE, unless otherwise noted. When comparing two groups, statistical differences were evaluated using an unpaired t-test (Prism version 7, GraphPad Software, La Jolla, California). A p value ≤ 0.05 was considered significant.

4.4 Results

4.4.1 LC-MS/MS assay validation for use in pharmacokinetic studies

Selectivity of the assay was demonstrated by injecting blank plasma samples from multiple mice, blank plasma spiked with IS, and blank plasma spiked with the analytes and IS. No significant interference of co-eluting peaks on analysis of the three analytes (*i.e.,* Gem, dFdU, and V-Gem) and two IS (*i.e.,* $^{13}C,^{15}N_{2-}$ Gem and $^{13}C,^{15}N_{2-}$ dFdU) was observed. Next, calibration curves ranging from 0.05 – 100 μM were developed for all analytes and shown to be linear ($r^2 >$ 0.990). As shown in Table 4.2, the method showed excellent accuracy and precision in quantification of all analytes at low, medium, and high concentrations. Finally, sample stability was demonstrated for all analytes during long-term (30 days) storage at -80°C (recovery range: 102 – 111 %) and during short-term (24 hr) storage on the autosampler at 4°C (recovery range: 96.2 – 113 %).

4.4.2 Pharmacokinetics following intravenous and oral Gem administrations

The mean plasma concentration-time profiles of Gem and dFdU are shown following intravenous administration of 76 nmol Gem/g body weight (Figure 4.2) and oral administration of 228 nmol Gem/g body weight (Figure 4.3). Pharmacokinetic parameters for Gem and dFdU are summarized in Table 4.3. Following intravenous administration, Gem reached an initial concentration ($C_0 = C_{max}$) of 67.2 μM and was converted to dFdU, with the T_{max} of dFdU occurring at 30 min. Following oral administration, Gem was rapidly absorbed reaching a maximum concentration (C_{max}) of 9.8 μM at a T_{max} of 30 min. The terminal half-life ($T_{1/2}$) of Gem following intravenous Gem administration (42.5 min) was not different than the $T_{1/2}$ after oral Gem administration (29.8 min) ($p = 0.258$). The $T_{1/2}$ of dFdU was shorter following intravenous Gem administration (106 min), as compared to the $T_{1/2}$ after oral Gem administration (210 min) ($p =$

0.050). Route-dependent differences were observed in the systemic exposure (*i.e.,* AUC) ratios for dFdU/Gem, where the ratio was 1.5 after intravenous Gem dosing but 6.9 after oral Gem dosing.

4.4.3 Pharmacokinetics following intravenous and oral V-Gem administrations

The mean plasma concentration-time profiles of Gem, dFdU, and V-Gem are shown following intravenous administration of 76 nmol V-Gem/g body weight (Figure 4.4) and oral administration of 228 nmol V-Gem/g body weight (Figure 4.5). Pharmacokinetic parameters for Gem, dFdU, and V-Gem are summarized in Table 4.3. Following intravenous V-Gem administration, V-Gem reached an initial concentration ($C_0 = C_{max}$) of 32.7 μM and was rapidly eliminated with a $T_{1/2}$ of 3.7 min. Gem was rapidly formed with a T_{max} occurring at the first sampling time point (2 min) in all mice. Systemic exposure of prodrug following intravenous V-Gem administration was quite small relative to Gem (V-Gem to Gem AUC ratio = 0.13) and dFdU (V-Gem to dFdU AUC ratio = 0.05). Following oral V-Gem administration, the systemic exposure of prodrug was negligible (V-Gem oral to intravenous dose adjusted AUC ratio = 0.006) and Gem was rapidly formed, reaching a C_{max} of 11.1 μM with a T_{max} of 15 min. Again, the $T_{1/2}$ of Gem following intravenous V-Gem administration (46.2 min) was not different than the $T_{1/2}$ following oral V-Gem administration (39.1 min) ($p = 0.406$). However, the $T_{1/2}$ of dFdU was shorter following intravenous V-Gem administration (128 min) as compared to oral V-Gem administration (216 min) ($p < 0.001$). Similar to Gem dosing, the average dFdU to Gem exposure ratio increased from 2.9 to 9.6 following intravenous and oral V-Gem dosing, respectively.

4.4.4 V-Gem activation following intravenous V-Gem administration

As observed in Table 4.3, mean systemic Gem exposure was ≈ 50% lower following V-Gem intravenous administration (801 min x μM) relative to Gem intravenous administration (1628 min x μM) ($p < 0.05$). In contrast, mean systemic dFdU exposure was not different following V-Gem

intravenous administration (2345 min x μM) and Gem intravenous administration (2484 min x μM) ($p = 0.848$).

4.4.5 Comparing systemic Gem and dFdU exposure following oral Gem and V-Gem administrations

As observed in Figure 4.6A, the mean plasma concentration-time profiles of Gem following oral Gem and V-Gem administrations are very similar. In fact, no statistically significant difference in Gem exposure exists following oral Gem administration (893 min x μM) and oral V-Gem administration (814 min x μM) ($p = 0.594$). Moreover, the bioavailability of Gem following oral Gem and V-Gem administrations are 18.3% and 16.7%, respectively. As shown in Figure 4.6B, the concentration-time profiles of dFdU are also similar following oral Gem and V-Gem administrations. Additionally, there is no statistically significant difference in dFdU exposure ($p = 0.084$).

4.4.6 Intestinal stability and absorption of Gem and V-Gem

Single-pass intestinal perfusions of Gem and V-Gem, with analysis of perfusion outlet samples, showed that < 1% of perfused Gem was found in outlet samples as dFdU and < 10% of perfused V-Gem was found in outlet samples as Gem. Furthermore, as shown in Figure 4.7, portal plasma concentrations of Gem, dFdU, and V-Gem were determined following 5 min perfusions of Gem and V-Gem. Following Gem perfusion, dFdU accounted for about 30% of the total drug found in portal plasma. Following V-Gem perfusion, V-Gem accounted for < 12% of the total drug found in portal plasma. Furthermore, total drug concentrations (*i.e.,* Gem + dFdU + V-Gem) in portal plasma were no different following perfusions of either Gem or V-Gem ($p = 0.608$).

4.5 Discussion

With an oral bioavailability in humans of only 10%, gemcitabine's therapeutic application is currently hindered by a reliance on intravenous administration [13]. Recent work using *in situ* intestinal perfusions in mice showed that the intestinal effective permeability of gemcitabine is high at low drug concentrations and rapidly decreases with increasing drug concentration as uptake via high-affinity nucleoside transporters becomes saturated [18]. Importantly, gemcitabine's low systemic exposure following oral dosing was reported when gemcitabine was administered at low doses (≤ 8 mg) unlikely to saturate intestinal uptake [13], implying that first-pass metabolism of gemcitabine via cytidine deaminase (CDA) drives its low bioavailability. This conclusion is further supported by data in human and mouse showing that gemcitabine undergoes extensive presystemic deamination following oral administration, forming the deaminated gemcitabine metabolite dFdU [13, 25]. To decrease first-pass metabolism, and thus increase gemcitabine bioavailability, gemcitabine may be formulated as a prodrug which reduces the ability of CDA to bind and metabolize gemcitabine. For example, an l-valine ester gemcitabine prodrug, 5'-L-valyl-gemcitabine (V-Gem) (Figure 4.1), was previously synthesized and shown to be stable against CDA mediated deamination, relative to gemcitabine, via incubations with recombinant human CDA [19, 22]. Furthermore, V-Gem was shown to be transported by peptide transporter 1 (PEPT1) [19, 23], a low-affinity, high-capacity transporter found on the apical membrane of intestinal enterocytes [21].

By formulating gemcitabine as a prodrug that confers stability against CDA-mediated first-pass metabolism and is targeted to a high-capacity, low-affinity intestinal uptake transporter (*i.e.,* PEPT1), V-Gem may both reduce first-pass gemcitabine metabolism and mitigate the potential for saturation of intestinal gemcitabine uptake. As a result, we decided to characterize the *in vivo*

pharmacokinetic performance of gemcitabine and V-Gem following intravenous and oral administrations in mice as well as the ability of V-Gem to reduce first-pass metabolism and increase drug absorption, relative to gemcitabine. In doing so, our studies revealed for the first time that: 1) V-Gem prodrug undergoes rapid systemic elimination ($T_{1/2} < 4$ min) and has very low oral bioavailability (<1%), 2) oral administration of V-Gem does not increase systemic exposure to gemcitabine, relative to oral gemcitabine administration, 3) V-Gem undergoes extensive first-pass activation in intestinal epithelial cells, and 4) gemcitabine undergoes first-pass metabolism in intestinal epithelial cells.

Using a novel and validated LC-MS/MS assay, the concentration-time profiles of gemcitabine, dFdU, and V-Gem (following V-Gem administration) were determined in mice following intravenous administration of 76 nmol gemcitabine/g body weight, oral administration of 228 nmol gemcitabine/g body weight, intravenous administration of 76 nmol V-Gem/g body weight, and oral administration of 228 nmol V-Gem/g body weight. As shown in Table 4.3, the pharmacokinetic parameters describing gemcitabine disposition following intravenous and oral gemcitabine administrations are in agreement with previously reported values in mice [25]. Additionally, the initial gemcitabine concentration ($C_0 = C_{max}$) following intravenous administration of 76 nmol gemcitabine/g body weight (*i.e.,* 20 mg gemcitabine/kg body weight) in mice was 67.2 μM, replicating the gemcitabine maximum concentration (C_{max}) of 50 – 70 μM following intravenous infusion of 1,250 mg gemcitabine/m^2 in human [26]. It was observed that the metabolite (dFdU) to parent (gemcitabine) exposure ratio was >1 following both intravenous (ratio = 1.5) and oral (ratio = 6.9) gemcitabine administrations, reflecting the extensive conversion of gemcitabine to dFdU and the slow elimination of dFdU, relative to gemcitabine. This ratio was much higher following oral administration due to extensive presystemic conversion of gemcitabine

to dFdU, in accordance with previously published work [25, 27]. Interestingly, in previous studies reporting $T_{1/2}$ values of dFdU in mice, there is substantial variability in both the calculated $T_{1/2}$ and the length of time over which plasma samples were collected [25, 27-29]. Examining the mean concentration-time profile of dFdU in studies where plasma samples were collected for $\geq$ 24 hr following gemcitabine administration [25, 29] suggests that the sampling scheme employed in the current study, which was designed to ensure adequate characterization of the concentration-time profile of gemcitabine, may bias downward estimates of dFdU $T_{1/2}$. Thus, the statistically significant difference in dFdU $T_{1/2}$ following oral gemcitabine administration (210 min) and intravenous gemcitabine administration (106 min) may be due to our sampling schedule being limited to six hours.

Following intravenous V-Gem administration, the prodrug rapidly disappeared from plasma with a $T_{1/2}$ of 3.7 min, while gemcitabine rapidly appeared in plasma, with the gemcitabine T_{max} occurring in the first sample (2 min) for all mice. Two enzymes, RBBP9 and the biphenyl hydrolase like enzyme (BPHL), have previously been shown to catalyze V-Gem activation *in vitro* via V-Gem incubations with these recombinant human enzymes [30, 31]. These studies, however, did not rule out the potential involvement of additional esterase enzymes in V-Gem activation. Interestingly, systemic gemcitabine exposure (AUC_{inf}) was about 50% lower following intravenous V-Gem administration, relative to intravenous administration of an equimolar gemcitabine dose ($p < 0.05$). Total dFdU exposure (AUC_{inf}), however, was not different following intravenous V-Gem and gemcitabine administrations. One potential explanation for this observation is that V-Gem is not completely activated to gemcitabine following intravenous administration but, instead, a portion of the administered V-Gem is first deaminated, forming 5'-L-valyl-dFdU (V-dFdU), and V-dFdU is subsequently cleaved releasing dFdU. Given that

gemcitabine's clearance and first-pass metabolism is driven by CDA-mediated deamination [9, 13], the ability of V-Gem to reduce CDA-mediated deamination was tested and confirmed *in vitro* with recombinant human enzyme [19, 22]. However, it is feasible that V-Gem becomes a substrate of a different deaminase enzyme [32-35], whose activity on V-Gem has not been previously evaluated. It is also possible that V-Gem is stable against human, but not murine CDA. This species difference in CDA substrate specificity seems unlikely, however, as the amino acid residues believed to dictate CDA substrate specific are completely conserved between mouse and human CDA [36]. To confirm the hypothesized V-Gem metabolic scheme, verification of V-dFdU formation *in vivo* would be required. Regardless, the $T_{1/2}$ of gemcitabine and dFdU following V-Gem intravenous administration closely mirrored the corresponding values following gemcitabine intravenous administration.

The mean oral bioavailability of V-Gem was about 0.6% and, thus, systemic exposure to V-Gem following oral administration was negligible. The mean plasma concentration-time profiles of gemcitabine following oral gemcitabine and V-Gem administrations (Figure 4.6A) are very similar, demonstrating that oral administrations of gemcitabine and V-Gem lead to equivalent systemic gemcitabine exposure. Quantitatively, this is evidenced by the fact that systemic gemcitabine exposure (AUC_{inf}) following oral administration of gemcitabine (893 min x μM) and V-Gem (814 min x μM) were not statistically significantly different. In fact, the average gemcitabine exposure following oral V-Gem administration was about 9% lower. Gemcitabine oral bioavailability was 18.3% following oral gemcitabine administration, in line with previously reported values [25], and 16.7% following oral V-Gem administration. Interestingly, the concentration-time profile of dFdU appears to differ slightly following oral administrations of

gemcitabine and V-Gem (Figure 4.6B). However, there was no statistically significant difference in dFdU exposure following oral gemcitabine and V-Gem dosing.

To further understand why oral V-Gem administration did not increase systemic gemcitabine exposure, relative to oral gemcitabine administration, additional intestinal perfusion experiments were performed in mice. Importantly, for V-Gem to undergo PEPT1-mediated uptake and confer resistance against first-pass metabolism, it must be stable in both the stomach and the intestinal lumen. Previous work demonstrated V-Gem stability in pH 1.2 simulated gastric fluid ($T_{1/2}$ > 120 min) [23]. The stability of V-Gem in the intestinal lumen was explored in the current work by perfusing V-Gem through a cannulated jejunal segment in an anesthetized mouse and quantifying the concentration of activated gemcitabine in perfusion outlet samples. These experiments demonstrated that V-Gem underwent some activation in the intestinal lumen, however, < 10% of the perfused V-Gem was found in outlet samples as activated Gem.

Prodrug stability in intestinal epithelial cells was then explored by perfusing V-Gem for 5 min and quantifying the concentration of gemcitabine, dFdU, and V-Gem in portal plasma samples (Figure 4.7). The short perfusion time was selected to minimize the impact of recirculated drug on the estimation of prodrug activation in intestinal epithelial cells. These results show that V-Gem undergoes extensive activation in intestinal epithelial cells as intact prodrug accounted for < 12% of total drug found in portal plasma. This observation is consistent with other work reporting extensive activation of amino acid ester prodrugs in mouse and rat intestinal epithelium [31, 37-39]. Additionally, perfusion experiments were performed showing gemcitabine is quite stable in the intestinal lumen (< 1% of perfused gemcitabine found in outlet samples as dFdU) but undergoes first-pass metabolism in the intestinal enterocytes, as evidenced by the appearance of dFdU in portal plasma, accounting for about 30% of total drug. Thus, the extensive activation of

V-Gem in intestinal epithelial cells diminishes the ability of V-Gem to protect against first-pass gemcitabine metabolism in both the intestine and the liver and, thus, the ability of V-Gem to increase systemic gemcitabine exposure. Importantly, interspecies differences (*i.e.,* mouse vs human) in the activity of various esterases have been reported, suggesting that V-Gem may be more stable in the human intestinal epithelium [40]. However, this seems unlikely given *in vitro* work showing that V-Gem undergoes extensive (> 90%) activation during transit through a Caco-2 cell monolayer [19].

Furthermore, total drug concentrations in portal plasma samples following perfusion of 10 mM gemcitabine and V-Gem were not different, indicating that even at high intestinal concentrations expected to completely saturate nucleoside transporter mediated gemcitabine uptake, partitioning of total drug from the intestinal lumen into portal plasma was not increased by V-Gem. An important caveat to this conclusion, however, is the assumption that no other V-Gem metabolites are present in portal plasma (*e.g.,* V-dFdU). To address this possibility, perfusions with radiolabeled V-Gem could be performed and total drug concentrations in portal blood assayed via total radioactivity.

As alluded to above, the incomplete conversion of V-Gem to gemcitabine, which was hypothesized to occur following intravenous V-Gem administration, could also contribute to the inability of oral V-Gem administration to increase systemic gemcitabine exposure, relative to oral gemcitabine administration. However, it is important to note that incomplete V-Gem activation following intravenous V-Gem administration remains speculative and that V-Gem activation may differ following oral and intravenous administrations (*i.e.,* V-Gem may undergo complete activation following oral but not intravenous administration). Thus, additional studies would be

needed to further explore V-Gem activation *in vivo* and the impact of potential incomplete activation on gemcitabine exposure following oral V-Gem administration.

In conclusion, the *in vivo* performance of a PEPT1-targeted gemcitabine prodrug, V-Gem, was evaluated following intravenous and oral administrations in mice. This work demonstrated that V-Gem is rapidly removed from plasma following intravenous administration and has very low oral bioavailability (< 1%). Furthermore, our studies demonstrate that formulation of gemcitabine as V-Gem did not lead to increased systemic gemcitabine exposure following oral dosing as gemcitabine bioavailability was no different following oral gemcitabine and V-Gem administrations. These results suggest that future prodrug strategies aimed at increasing systemic exposure of gemcitabine following oral dosing should focus on prodrugs with high intestinal effective permeability, good stability during first-pass transit through the intestinal enterocytes and liver, and complete conversion to the active gemcitabine species. Alternatively, future work aimed at enabling oral gemcitabine administration could focus on decreasing first-pass gemcitabine metabolism and, thus, increasing systemic gemcitabine exposure through co-administration of gemcitabine with a cytidine deaminase inhibitor.

Tables and Figures

Table 4.1 Summary of analyte-specific mass spectrometry parameters

Compound	Parent Ion (m/z)	Product Ion (m/z)	Declustering Potential (V)	Entrance Potential (V)	Collision Energy (V)	Collision Cell Exit Potential (V)
Gem	264.0	112.0	60	12	26	13
dFdU	265.0	113.0	60	12	22	13
V-Gem	363.1	264.0	6	8	22	14
$^{13}C,^{15}N_2$-Gem (IS)	267.0	115.0	60	12	26	13
$^{13}C,^{15}N_2$-dFdU (IS)	268.0	116.0	60	12	22	13

Gem, gemcitabine; dFdU, 2',2'-difluorodeoxyuridine; V-Gem, 5'-L-valyl-gemcitabine; IS, internal standard.

Table 4.2 Summary of intra-day and inter-day accuracy and precision of the LC-MS/MS assay for quantification of Gem, dFdU, and V-Gem at low (0.1 μM), medium (5 μM), and high (50 μM) concentrations in mouse plasma

		Intra-day (n=3)		Inter-day (n=9)	
Analyte	**Concentration (μM)**	**Accuracy (%)**	**Precision (CV%)**	**Accuracy (%)**	**Precision (CV%)**
Gem	0.1 / 5 / 50	104 / 108 / 102	3.2 / 2.6 / 6.7	94 / 109 / 103	9.3 / 8.4 / 9.4
dFdU	0.1 / 5 / 50	104 / 108 / 112	4.1 / 3.7 / 4.5	114 / 106 / 102	6.1 / 4.5 / 4.0
V-Gem	0.1 / 5 / 50	107 / 91.1 / 102	2.9 / 12.3 / 6.4	112 / 90 / 108	11.3 / 10.4 / 4.0

Gem, gemcitabine; dFdU, 2',2'-difluorodeoxyuridine; V-Gem, 5'-L-valyl-gemcitabine.

Table 4.3 Pharmacokinetic parameters of Gem, dFdU, and V-Gem following IV (76 nmol/g) and PO (228 nmol/g) administrations of Gem and V-Gem in mice (n = 4)

Treatment	Parameter	Analyte		
		Gemcitabine	**dFdU**	**Prodrug**
Gem IV (76 nmol/g)	$AUC_{0\text{-}6\ hr}$ (min x µM)	1621 (38%)	2218 (54%)	-
	AUC_{inf} (min x µM)	1628 (38%)	2484 (65%)	-
	% Extrapolated	0.4 (40%)	8.2 (88%)	-
	$T_{1/2}$ (min)	42.5 (44%)	106 (32%)	-
	T_{max} (min)	-	30 (30 - 45)	-
	C_{max} (µM)	67.2 (30%)†	15.5 (34%)	-
	CL (mL/hr/g)	2.8 (38%)	-	-
	V_{ss} (mL/g)	1.4 (44%)	-	-
Gem PO (228 nmol/g)	$AUC_{0\text{-}6\ hr}$ (min x µM)	887 (55%)	6091 (15%)	-
	AUC_{inf} (min x µM)	893 (55%)	8613 (22%)	-
	% Extrapolated	0.6 (55%)	26.2 (52%)	-
	$T_{1/2}$ (min)	29.8 (41%)	210 (41%)	-
	T_{max} (min)	30 (15 - 45)	45 (30 - 120)	-
	C_{max} (µM)	9.8 (42%)	35.3 (30%)	-
	F_{oral}	18.3%	-	-
V-Gem IV (76 nmol/g)	$AUC_{0\text{-}6\ hr}$ (min x µM)	794 (23%)	2017 (49%)	103 (101%)
	AUC_{inf} (min x µM)	801 (22%)	2345 (61%)	106 (98%)
	% Extrapolated	0.8 (92%)	11.3 (84%)	1.1 (253%)
	$T_{1/2}$ (min)	46.2 (34%)	128 (38%)	3.7 (33%)
	T_{max} (min)	2 (2 - 2)	22.5 (15 - 30)	-
	C_{max} (µM)	41.6 (26%)	13.9 (31%)	32.7 (139%)†
	CL (mL/hr/g)	-	-	43.1 (98%)
	V_{ss} (mL/g)	-	-	2.4 (145%)
V-Gem PO (228 nmol/g)	$AUC_{0\text{-}6\ hr}$ (min x µM)	806 (27%)	7732 (19%)	1.9 (113%)
	AUC_{inf} (min x µM)	814 (27%)	11,125 (24%)	CND
	% Extrapolated	0.9 (17%)	30.2 (13%)	CND
	$T_{1/2}$ (min)	39.1 (25%)	216 (9%)	CND
	T_{max} (min)	15 (5 - 30)	30 (15 - 30)	3.5 (2 - 5)
	C_{max} (µM)	11.1 (24%)	47.9 (6%)	0.2 (101%)
	F_{oral}	16.7%	-	0.6%

Parameters are reported as geometric mean (geometric CV%), except for T_{max}, which is reported as median (min – max), and oral bioavailability (F_{oral}), which is reported as the dose normalized ratio (oral/IV) of the geometric mean AUC_{inf}. †C_0 reported for C_{max}. CND, could not be determined; IV, intravenous; PO, oral; Gem, gemcitabine; dFdU, 2',2'-difluorodeoxyuridine; V-Gem, 5'-L-valyl-gemcitabine.

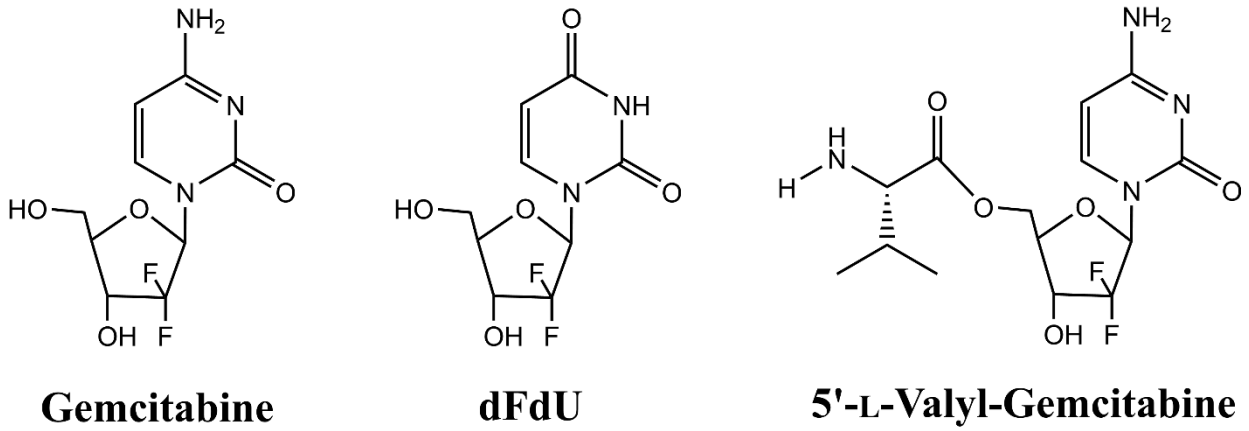

Figure 4.1 Structures of gemcitabine, the deaminated gemcitabine metabolite dFdU, and the gemcitabine prodrug 5'-L-valyl-gemcitabine.

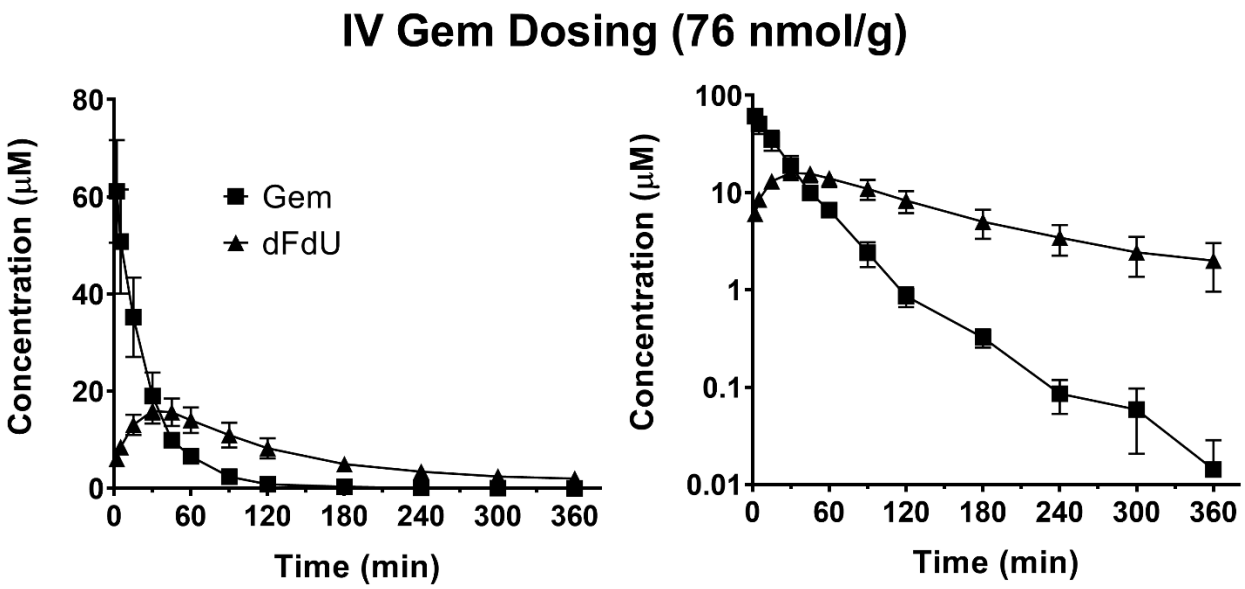

Figure 4.2 Mean plasma concentration-time profiles of Gem and dFdU following intravenous (IV) administration of 76 nmol Gem/g body weight in mice. Data are expressed as mean ± SE (n=4) with the y-axis displayed on linear (left panel) and logarithmic (right panel) scales.

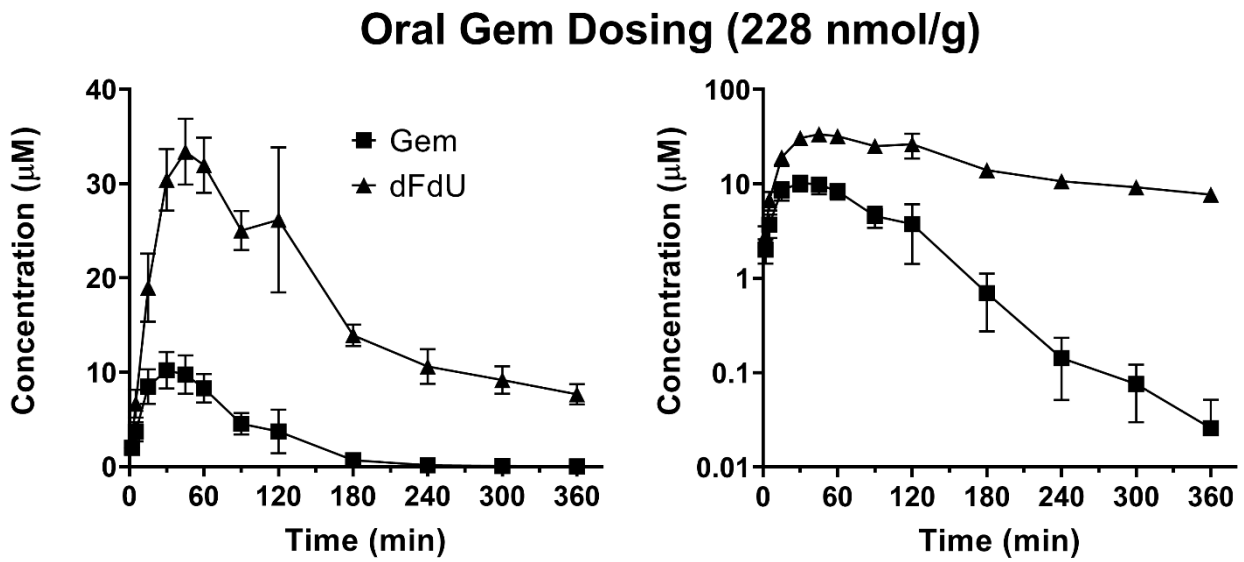

Figure 4.3 Mean plasma concentration-time profiles of Gem and dFdU following oral administration of 228 nmol Gem/g body weight in mice. Data are expressed as mean ± SE (n=4) with the y-axis displayed on linear (left panel) and logarithmic (right panel) scales.

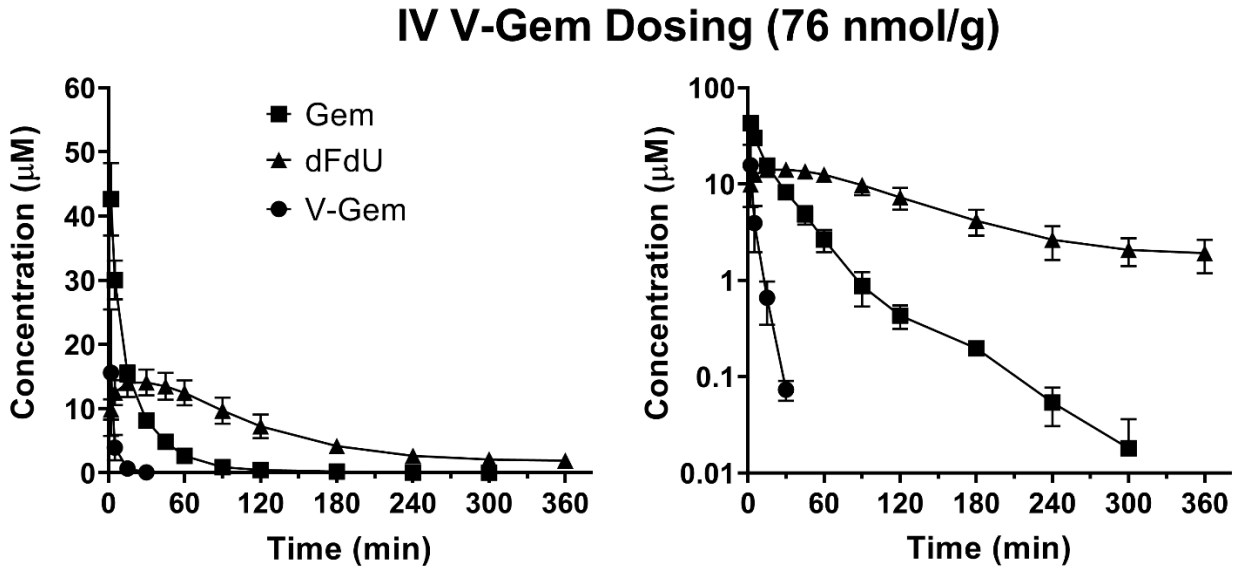

Figure 4.4 Mean plasma concentration-time profiles of Gem, dFdU, and V-Gem following intravenous (IV) administration of 76 nmol V-Gem/g body weight in mice. Data are expressed as mean ± SE (n=4) with the y-axis displayed on linear (left panel) and logarithmic (right panel) scales.

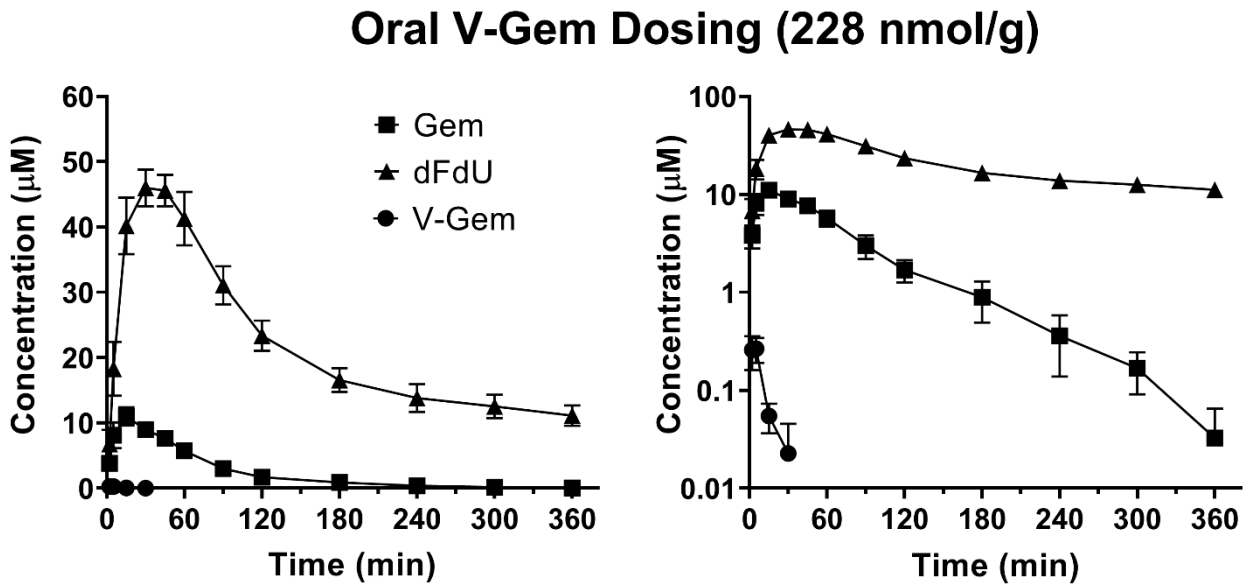

Figure 4.5 Mean plasma concentration-time profiles of Gem, dFdU, and V-Gem following oral administration of 228 nmol V-Gem/g body weight in mice. Data are expressed as mean ± SE (n=4) with the y-axis displayed on linear (left panel) and logarithmic (right panel) scales.

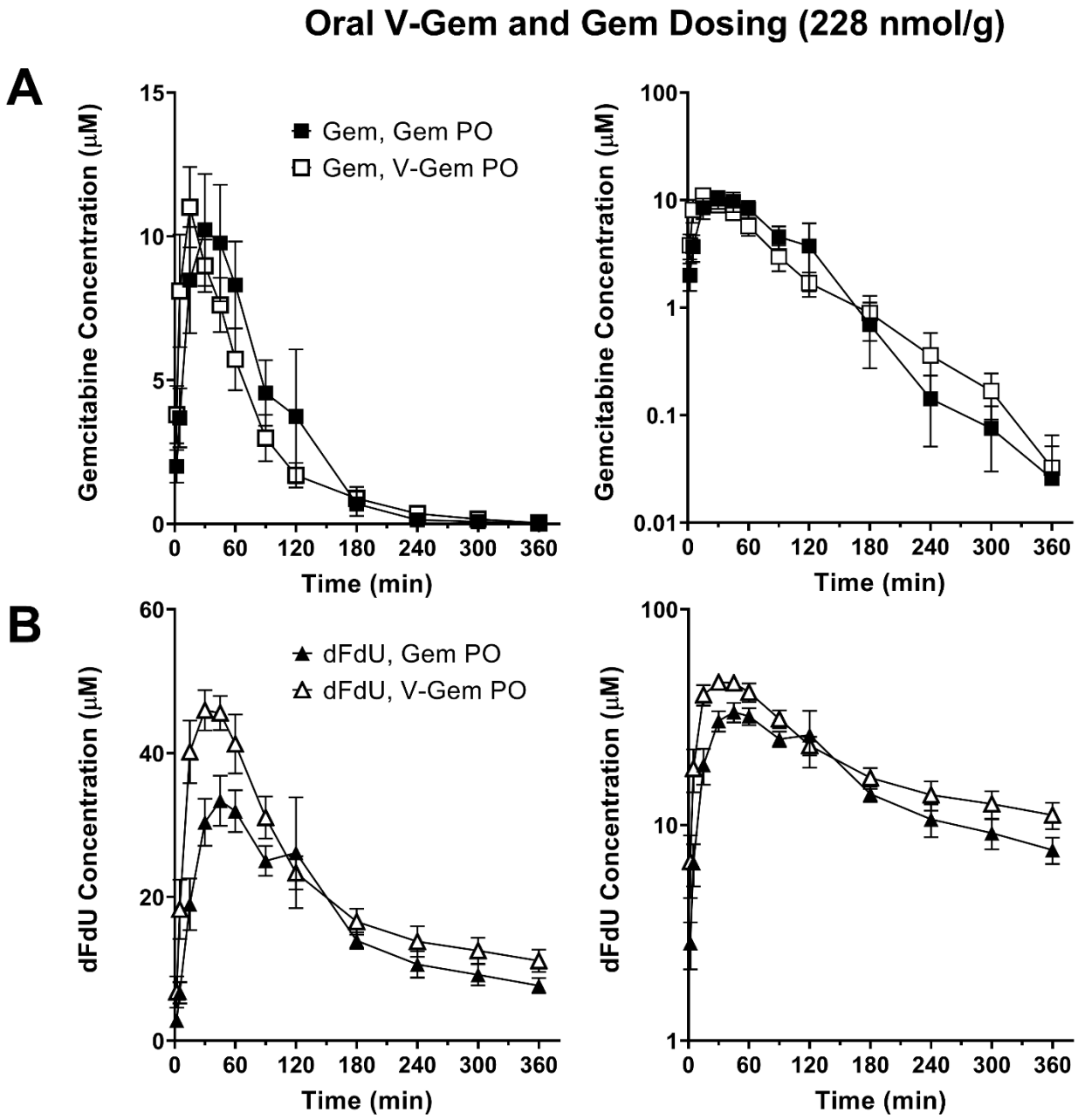

Figure 4.6 Mean plasma concentration-time profiles following oral (PO) administration of 228 nmol/g body weight Gem and V-Gem for (A) Gem and (B) dFdU. Data are expressed as mean ± SE (n=4) with the y-axis displayed on linear (left panel) and logarithmic (right panel) scales.

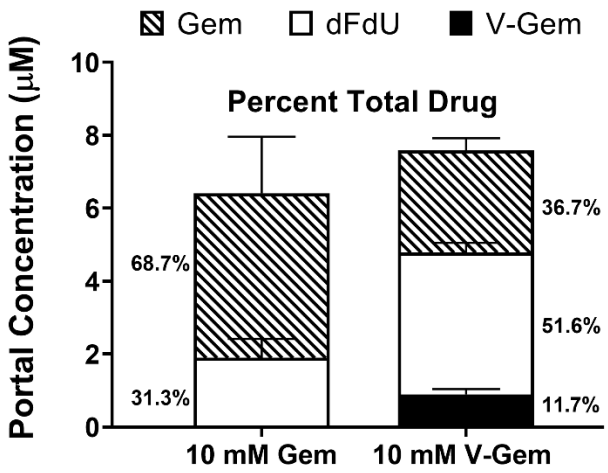

Figure 4.7 Portal plasma concentrations of Gem, dFdU, and V-Gem following 5 min jejunal perfusions of 10 mM Gem and V-Gem. The percent of total drug found as each analyte is also presented. Data are expressed as mean ± SE (n=4). Total drug concentrations were not significantly different following Gem and V-Gem perfusions, as determined by unpaired t-test.

References

[1] Gemzar [package insert]. Eli Lilly and Company, Indianapolis, IN, (2014).

[2] Conti R.M., Bernstein A.C., Villaflor V.M., Schilsky R.L., Rosenthal M.B., and Bach P.B., Prevalence of Off-Label Use and Spending in 2010 Among Patent-Protected Chemotherapies in a Population-Based Cohort of Medical Oncologists, J Clin Oncol. 31 (9) (2013) 1134-1139.

[3] Valle J., Wasan H., Palmer D.H., Cunningham D., Anthoney A., Maraveyas A., Madhusudan S., Iveson T., Hughes S., Pereira S.P., Roughton M., and Bridgewater J., Cisplatin plus gemcitabine versus gemcitabine for biliary tract cancer, N Engl J Med. 362 (14) (2010) 1273-81.

[4] von der Maase H., Sengelov L., Roberts J.T., Ricci S., Dogliotti L., Oliver T., Moore M.J., Zimmermann A., and Arning M., Long-term survival results of a randomized trial comparing gemcitabine plus cisplatin, with methotrexate, vinblastine, doxorubicin, plus cisplatin in patients with bladder cancer, J Clin Oncol. 23 (21) (2005) 4602-8.

[5] Huang P., Chubb S., Hertel L.W., Grindey G.B., and Plunkett W., Action of 2',2'-difluorodeoxycytidine on DNA synthesis, Cancer Res. 51 (22) (1991) 6110-6117.

[6] Huang P. and Plunkett W., Fludarabine- and gemcitabine-induced apoptosis: incorporation of analogs into DNA is a critical event, Cancer Chemother Pharmacol. 36 (3) (1995) 181-188.

[7] Heinemann V., Xu Y.Z., Chubb S., Sen A., Hertel L.W., Grindey G.B., and Plunkett W., Inhibition of ribonucleotide reduction in CCRF-CEM cells by 2',2'-difluorodeoxycytidine, Mol Pharmacol. 38 (4) (1990) 567-572.

[8] Plunkett W., Huang P., Xu Y.Z., Heinemann V., Grunewald R., and Gandhi V., Gemcitabine: metabolism, mechanisms of action, and self-potentiation, Semin Oncol. 22 (4 Suppl 11) (1995) 3-10.

[9] Zhang L., Sinha V., Forgue S.T., Callies S., Ni L., Peck R., and Allerheiligen S.R., Model-based drug development: the road to quantitative pharmacology, J Pharmacokinet Pharmacodyn. 33 (3) (2006) 369-393.

[10] Honeywell R.J., Ruiz van Haperen V.W., Veerman G., Smid K., and Peters G.J., Inhibition of thymidylate synthase by 2',2'-difluoro-2'-deoxycytidine (Gemcitabine) and its metabolite 2',2'-difluoro-2'-deoxyuridine, Int J Biochem Cell Biol. 60 (2015) 73-81.

[11] Veltkamp S.A., Pluim D., van Eijndhoven M.A., Bolijn M.J., Ong F.H., Govindarajan R., Unadkat J.D., Beijnen J.H., and Schellens J.H., New insights into the pharmacology and cytotoxicity of gemcitabine and 2',2'-difluorodeoxyuridine, Mol Cancer Ther. 7 (8) (2008) 2415-2425.

[12] Pauwels B., Korst A.E., Lambrechts H.A., Pattyn G.G., de Pooter C.M., Lardon F., and Vermorken J.B., The radiosensitising effect of difluorodeoxyuridine, a metabolite of gemcitabine, in vitro, Cancer Chemother Pharmacol. 58 (2) (2006) 219-28.

[13] Veltkamp S.A., Jansen R.S., Callies S., Pluim D., Visseren-Grul C.M., Rosing H., Kloeker-Rhoades S., Andre V.A., Beijnen J.H., Slapak C.A., and Schellens J.H., Oral administration of gemcitabine in patients with refractory tumors: a clinical and pharmacologic study, Clin Cancer Res. 14 (11) (2008) 3477-3486.

[14] Cham K., Baker J., Takhar K., Flexman J., Wong M., Owen D., Yung A., Kozlowski P., Reinsberg S., and Chu E., Metronomic gemcitabine suppresses tumour growth, improves perfusion, and reduces hypoxia in human pancreatic ductal adenocarcinoma, Br J Cancer. 103 (1) (2010) 52-60.

[15] Yapp D.T., Wong M.Q., Kyle A.H., Valdez S.M., Tso J., Yung A., Kozlowski P., Owen D.A., Buczkowski A.K., and Chung S.W., The differential effects of metronomic gemcitabine and antiangiogenic treatment in patient-derived xenografts of pancreatic cancer: treatment effects on metabolism, vascular function, cell proliferation, and tumor growth, Angiogenesis. 19 (2) (2016) 229-244.

[16] Tran Cao H.S., Bouvet M., Kaushal S., Keleman A., Romney E., Kim G., Fruehauf J., Imagawa D.K., Hoffman R.M., and Katz M.H., Metronomic gemcitabine in combination with sunitinib inhibits multisite metastasis and increases survival in an orthotopic model of pancreatic cancer, Mol Cancer Ther. 9 (7) (2010) 2068-78.

[17] Dehua Z., Mingming C., and Jisheng W., Meta-analysis of gemcitabine in brief versus prolonged low-dose infusion for advanced non-small cell lung cancer, PLoS One. 13 (3) (2018) e0193814.

[18] Thompson B.R., Hu Y., and Smith D.E., Mechanisms of gemcitabine oral absorption as determined by in situ intestinal perfusions in mice, Biochem Pharmacol. 168 (2019) 57-64.

[19] Song X.Q., Lorenzi P.L., Landowski C.P., Vig B.S., Hilfinger J.M., and Amidon G.L., Amino acid ester prodrugs of the anticancer agent gemcitabine: Synthesis, bioconversion, metabolic bioevasion, and hPEPT1-mediated transport, Mol Pharm. 2 (2) (2005) 157-167.

[20] Drozdzik M., Groer C., Penski J., Lapczuk J., Ostrowski M., Lai Y., Prasad B., Unadkat J.D., Siegmund W., and Oswald S., Protein abundance of clinically relevant multidrug transporters along the entire length of the human intestine, Mol Pharm. 11 (10) (2014) 3547-55.

[21] Smith D.E., Clemencon B., and Hediger M.A., Proton-coupled oligopeptide transporter family SLC15: physiological, pharmacological and pathological implications, Mol Aspects Med. 34 (2-3) (2013) 323-336.

[22] Tsume Y., Drelich A.J., Smith D.E., and Amidon G.L., Potential Development of Tumor-Targeted Oral Anti-Cancer Prodrugs: Amino Acid and Dipeptide Monoester Prodrugs of Gemcitabine, Molecules. 22 (8) (2017) 1322.

[23] Tsume Y., Incecayir T., Song X., Hilfinger J.M., and Amidon G.L., The development of orally administrable gemcitabine prodrugs with D-enantiomer amino acids: enhanced membrane permeability and enzymatic stability, Eur J Pharm Biopharm. 86 (3) (2014) 514-523.

[24] Epling D., Hu Y., and Smith D.E., Evaluating the intestinal and oral absorption of the prodrug valacyclovir in wildtype and huPepT1 transgenic mice, Biochem Pharmacol. 155 (2018) 1-7.

[25] Beumer J.H., Eiseman J.L., Parise R.A., Joseph E., Covey J.M., and Egorin M.J., Modulation of Gemcitabine (2′,2′-Difluoro-2′-Deoxycytidine) Pharmacokinetics, Metabolism, and Bioavailability in Mice by 3,4,5,6-Tetrahydrouridine, Clin Cancer Res. 14 (11) (2008) 3529-3535.

[26] Kuenen B.C., Rosen L., Smit E.F., Parson M.R.N., Levi M., Ruijter R., Huisman H., Kedde M.A., Noordhuis P., Vijgh W.J.F.v.d., Peters G.J., Cropp G.F., Scigalla P., Hoekman K., Pinedo H.M., and Giaccone G., Dose-Finding and Pharmacokinetic Study of Cisplatin, Gemcitabine, and SU5416 in Patients With Solid Tumors, J Clin Oncol. 20 (6) (2002) 1657-1667.

[27] Veltkamp S.A., Pluim D., van Tellingen O., Beijnen J.H., and Schellens J.H., Extensive metabolism and hepatic accumulation of gemcitabine after multiple oral and intravenous administration in mice, Drug Metab Dispos. 36 (8) (2008) 1606-15.

[28] Hao W.H., Wang J.J., Hsueh S.P., Hsu P.J., Chang L.C., Hsu C.S., and Hsu K.Y., In vitro and in vivo studies of pharmacokinetics and antitumor efficacy of D07001-F4, an oral gemcitabine formulation, Cancer Chemother Pharmacol. 71 (2) (2013) 379-388.

[29] Reddy L.H., Khoury H., Paci A., Deroussent A., Ferreira H., Dubernet C., Decleves X., Besnard M., Chacun H., Lepetre-Mouelhi S., Desmaele D., Rousseau B., Laugier C., Cintrat J.C., Vassal G., and Couvreur P., Squalenoylation favorably modifies the in vivo pharmacokinetics and biodistribution of gemcitabine in mice, Drug Metab Dispos. 36 (8) (2008) 1570-7.

[30] Kim I., Song X., Vig B.S., Mittal S., Shin H.-C., Lorenzi P.J., and Amidon G.L., A novel nucleoside prodrug-activating enzyme: substrate specificity of biphenyl hydrolase-like protein, Mol Pharm. 1 (2) (2004) 117-127.

[31] Shenoy V.M., Thompson B.R., Shi J., Zhu H.-J., Smith D.E., and Amidon G.L., Chemoproteomic Identification of Serine Hydrolase RBBP9 as a Valacyclovir-Activating Enzyme, Mol Pharm. 17 (5) (2020) 1706-1714.

[32] Yuan G., Bin J.C., McKay D.J., and Snyder F.F., Cloning and characterization of human guanine deaminase. Purification and partial amino acid sequence of the mouse protein, J Biol Chem. 274 (12) (1999) 8175-80.

[33] Yeung C.Y., Ingolia D.E., Roth D.B., Shoemaker C., Al-Ubaidi M.R., Yen J.Y., Ching C., Bobonis C., Kaufman R.J., and Kellems R.E., Identification of functional murine adenosine

deaminase cDNA clones by complementation in Escherichia coli, J Biol Chem. 260 (18) (1985) 10299-307.

[34] Austin E.A. and Huber B.E., A first step in the development of gene therapy for colorectal carcinoma: cloning, sequencing, and expression of Escherichia coli cytosine deaminase, Mol Pharmacol. 43 (3) (1993) 380-7.

[35] Weiner K.X., Weiner R.S., Maley F., and Maley G.F., Primary structure of human deoxycytidylate deaminase and overexpression of its functional protein in Escherichia coli, J Biol Chem. 268 (17) (1993) 12983-9.

[36] Frances A. and Cordelier P., The Emerging Role of Cytidine Deaminase in Human Diseases: A New Opportunity for Therapy?, Molecular Therapy. 28 (2) (2020) 357-366.

[37] Tao W., Zhao D., Sun M., Wang Z., Lin B., Bao Y., Li Y., He Z., Sun Y., and Sun J., Intestinal absorption and activation of decitabine amino acid ester prodrugs mediated by peptide transporter PEPT1 and enterocyte enzymes, Int J Pharm. 541 (1–2) (2018) 64-71.

[38] Sun Y., Sun J., Shi S., Jing Y., Yin S., Chen Y., Li G., Xu Y., and He Z., Synthesis, transport and pharmacokinetics of 5'-amino acid ester prodrugs of 1-beta-D-arabinofuranosylcytosine, Mol Pharm. 6 (1) (2009) 315-25.

[39] Hu Y., Epling D., Shi J., Song F., Tsume Y., Zhu H.J., Amidon G.L., and Smith D.E., Effect of biphenyl hydrolase-like (BPHL) gene disruption on the intestinal stability, permeability and absorption of valacyclovir in wildtype and Bphl knockout mice, Biochem Pharmacol. 156 (2018) 147-156.

[40] Bahar F.G., Ohura K., Ogihara T., and Imai T., Species difference of esterase expression and hydrolase activity in plasma, J Pharm Sci. 101 (10) (2012) 3979-88.

CHAPTER 5

Future Directions

It was previously believed that gemcitabine's low oral bioavailability was due, at least in part, to inadequate intestinal absorption. However, this dissertation (Chapter 3) demonstrates that gemcitabine undergoes extensive nucleoside transporter-mediated absorption in mouse small intestine, implicating first-pass metabolism as the primary driver of low bioavailability. However, while mice are commonly used as a model system to study nucleoside transporter function in human and previous work concluded that the intestinal expression profile of nucleoside transporter mRNA is similar between mouse and human, translation of these findings to human has not been definitively demonstrated. Conclusive proof that gemcitabine is also extensively absorbed in human is not possible without direct testing in human subjects. However, insights into translating our findings in mice to human could be gained by future work exploring the intestinal expression of nucleoside transporters in mice and human on a protein level, as well as potential differences in gemcitabine transport by orthologous proteins (*e.g.,* human ENT1 vs. mouse ENT1). Such information could be incorporated into a physiologically-based pharmacokinetic (PBPK) model of gemcitabine intestinal absorption, better enabling more accurate quantitative predictions of gemcitabine absorption in human.

The results presented in Chapter 3 also suggest that gemcitabine's oral bioavailability in human could be greatly increased by co-administration with a cytidine deaminase inhibitor. This conclusion is in accordance with previous work in mice showing that co-administration of a cytidine deaminase inhibitor increases gemcitabine's oral bioavailability approximately 4-fold. Importantly, our results further suggest that the fraction of drug absorbed from the intestinal lumen will decrease with increasing dose as uptake via nucleoside transporters becomes saturated. Thus, if this formulation strategy is pursued, gemcitabine may need to be administered via divided doses or given as a controlled-released formulation to limit intestinal drug concentrations (*i.e.,* below saturating concentrations) and maximize the fraction of drug absorbed. The hypothesized inverse relationship between gemcitabine bioavailability and dose (*i.e.,* bioavailability decreases as dose increases) could be tested in mice by determining gemcitabine bioavailability over a range of orally administered doses. Additionally, the aforementioned PBPK model of gemcitabine intestinal absorption, which reflects the dynamic nature of drug absorption (*i.e.,* drug concentrations in the intestinal lumen decrease as drug is absorbed), could provide insights into the relationship between dose and fraction absorbed and guide the development of clinical dosing regimens and formulations (*e.g.,* controlled-release) with acceptable intestinal absorption.

Another strategy to increase gemcitabine's oral bioavailability, formulating gemcitabine as the peptide transporter 1 (PEPT1)-targeted amino acid ester prodrug 5'-L-valyl-gemictabine (V-Gem), was explored in this dissertation (Chapter 4). Oral V-Gem administration did not increase gemcitabine systemic exposure, relative to oral gemcitabine administration, due, in large part, to extensive V-Gem activation in intestinal epithelial cells. Thus, future work developing gemcitabine prodrugs for oral administration should focus on prodrugs which have higher presystemic stability while maintaining adequate intestinal permeability. Importantly, however,

such prodrugs must not be so stable that they are resistant to subsequent systemic activation. This balance between the prodrug's presystemic stability and systemic activation can be manipulated by changing the amino acid moiety in the PEPT1-targeted amino acid ester prodrug (*e.g.,* 5'-L-phenylalanly-gemcitabine), the linkage between the amino acid and gemcitabine (*e.g.,* amino acid amide prodrug), or by changing the prodrug type completely (*e.g.,* a prodrug not targeted to PEPT1).

The results presented in Chapter 4 further suggest that V-Gem may not be completely activated to gemcitabine (*i.e.,* V-Gem is directly converted to both gemcitabine and another V-Gem metabolite(s)) following intravenous administration. Confirmation of this hypothesis would require verification that additional V-Gem metabolite(s) are formed *in vivo.* Given our theory that V-Gem may be directly deaminated, forming valine-dFdU (V-dFdU), plasma samples collected following V-Gem intravenous administration could be analyzed for V-dFdU. Alternatively, a study could be performed in which radiolabeled V-Gem (*e.g.,* [^{3}H] or [^{14}C]) is intravenously administered and drug-related metabolites are identified and quantified in plasma. While synthesizing radiolabeled V-Gem would likely be resource intensive, such a radiolabeled study would greatly ease identification of potential V-Gem metabolites. Furthermore, similar studies could be conducted to explore V-Gem activation following oral administration as V-Gem metabolism may differ following oral and intravenous administration.

Finally, given the large gemcitabine doses administered intravenously (1,000 – 1,250 mg/m^2) and the associated high maximum plasma concentrations (≈ 70 μM), it is possible that this intravenous pharmacokinetic profile will not be able to be replicated when gemcitabine is administered orally. In this case, if gemcitabine is to be administered orally, optimization of the pharmacokinetic profile, and thus the dosing regimen, would be required. Furthermore, even if the

intravenous pharmacokinetic profile is able to be replicated with an oral formulation, there is evidence suggesting that gemcitabine's efficacy and toxicity may be improved by pharmacokinetic profiles often seen with orally administered medications (*e.g.,* sustained plasma exposure at lower concentrations). Given that gemcitabine is only administered to patients intravenously, additional clinical data on the efficacy and toxicity of the pharmacokinetics associated with such dosing regimens would be required.

APPENDICES

APPENDIX A

Individual Data from Chapter 3

Table A.1 The i*n situ* jejunal permeability of gemcitabine at 100 μM in C57BL/6 and BALB/c mice when samples were analyzed by UPLC (following experiments performed in C57BL/6 and BALB/c mice) and by measuring radioactivity (following experiments performed in C57BL/6 mice)

Replicate #	Strain	Analytical Method	P_{eff} (x 10^{-4} cm/s)	Perfused Segment Length (cm)
1	C57BL/6	UPLC	1.18 ± 0.08	5.5
2	C57BL/6	UPLC	1.05 ± 0.05	5.5
3	C57BL/6	UPLC	0.97 ± 0.08	9
4	C57BL/6	UPLC	1.35 ± 0.05	9
AVERAGE	C57BL/6	UPLC	1.14 ± 0.17	
1	C57BL/6	Radioactivity	1.18 ± 0.10	7.5
2	C57BL/6	Radioactivity	0.76 ± 0.13	5.5
3	C57BL/6	Radioactivity	1.19 ± 0.15	7.5
4	C57BL/6	Radioactivity	1.09 ± 0.08	6.5
AVERAGE	C57BL/6	Radioactivity	1.05 ± 0.20	
1	BALB/c	UPLC	1.22 *	5
2	BALB/c	UPLC	0.97 ± 0.14	6
AVERAGE	BALB/c	UPLC	1.09 ± 0.18	

Data are presented as mean ± SD. For each replicate, the mean and SD were calculated using the permeability values determined at each of the six sampling timepoints. The average mean and SD were calculated using the means of the individual replicates. *Individual SD unavailable. P_{eff}, *in situ* jejunal permeability

Table A.2 Concentration-dependent gemcitabine permeability and flux during *in situ* jejunal perfusions in C57BL/6 mice

Replicate #	Concentration (μM)	Peff (x 10^{-4} cm/s)	Flux (pmol/cm^2/s)	Perfused Segment Length (cm)
1	0.5	2.20 ± 0.25	0.110 ± 0.013	7
2	0.5	1.65 ± 0.14	0.082 ± 0.007	6.5
3	0.5	1.66 ± 0.06	0.083 ± 0.003	8
4	0.5	1.19 ± 0.27	0.058 ± 0.013	8
AVERAGE	0.5	1.68 ± 0.41	0.084 ± 0.021	
1	1	1.45 ± 0.13	0.145 ± 0.013	7.5
2	1	1.56 ± 0.18	0.156 ± 0.018	7
3	1	1.63 ± 0.04	0.163 ± 0.004	6.5
4	1	1.75 ± 0.11	0.175 ± 0.011	6.5
AVERAGE	1	1.60 ± 0.12	0.160 ± 0.012	
1	5	1.40 ± 0.12	0.701 ± 0.059	7
2	5	2.20 ± 0.12	1.10 ± 0.06	6
3	5	2.18 ± 0.10	1.09 ± 0.05	5.5
4	5	1.67 ± 0.08	0.834 ± 0.040	6
AVERAGE	5	1.86 ± 0.39	0.931 ± 0.197	
1	10	1.75 ± 0.13	1.75 ± 0.13	6
2	10	1.74 ± 0.03	1.74 ± 0.03	6
3	10	1.88 ± 0.09	1.88 ± 0.09	5
4	10	1.47 ± 0.12	1.47 ± 0.12	8
AVERAGE	10	1.71 ± 0.17	1.71 ± 0.17	
1	25	1.06 ± 0.09	2.66 ± 0.23	6
2	25	0.72 ± 0.02	1.79 ± 0.05	5
3	25	1.34 ± 0.14	3.36 ± 0.35	7
4	25	1.23 ± 0.03	3.04 ± 0.08	6.5
AVERAGE	25	1.09 ± 0.27	2.71 ± 0.68	
1	50	0.78 ± 0.05	3.91 ± 0.25	6.5
2	50	1.20 ± 0.08	6.00 ± 0.39	6.5
3	50	1.11 ± 0.05	5.56 ± 0.25	6
4	50	0.85 ± 0.07	4.24 ± 0.36	7.5
AVERAGE	50	0.985 ± 0.201	4.92 ± 1.01	

1	75	0.835 ± 0.026	6.26 ± 0.20	6.5
2	75	0.684 ± 0.043	5.13 ± 0.32	6.5
3	75	0.842 ± 0.071	6.31 ± 0.53	7
4	75	0.714 ± 0.060	5.35 ± 0.45	7.5
AVERAGE	75	0.769 ± 0.081	5.76 ± 0.61	
1	100	0.831 ± 0.110	8.31 ± 1.10	6
2	100	0.692 ± 0.036	6.92 ± 0.36	6
3	100	0.761 ± 0.063	7.61 ± 0.63	6
4	100	0.743 ± 0.040	7.43 ± 0.40	6
AVERAGE	100	0.757 ± 0.058	7.57 ± 0.58	
1	150	0.498 ± 0.022	7.46 ± 0.34	6.5
2	150	0.520 ± 0.031	7.80 ± 0.46	7
3	150	0.598 ± 0.058	8.97 ± 0.87	7
4	150	0.500 ± 0.067	7.49 ± 1.01	6.5
AVERAGE	150	0.529 ± 0.047	7.93 ± 0.71	
1	250	0.427 ± 0.039	10.68 ± 0.98	5.5
2	250	0.519 ± 0.043	12.98 ± 1.08	7
3	250	0.485 ± 0.049	12.14 ± 1.22	6.5
4	250	0.623 ± 0.077	15.57 ± 1.91	4
AVERAGE	250	0.514 ± 0.082	12.84 ± 2.05	
1	500	0.344 ± 0.060	17.19 ± 2.98	7.5
2	500	0.431 ± 0.028	21.56 ± 1.42	6
3	500	0.418 ± 0.114	20.90 ± 5.71	6
4	500	0.425 ± 0.022	21.25 ± 1.10	6
AVERAGE	500	0.404 ± 0.041	20.22 ± 2.04	
1	750	0.297 ± 0.141	22.26 ± 10.60	7
2	750	0.263 ± 0.096	19.71 ± 7.17	7
3	750	0.416 ± 0.141	31.21 ± 10.58	7
4	750	0.402 ± 0.162	30.16 ± 12.17	6.5
AVERAGE	750	0.344 ± 0.076	25.83 ± 5.72	
1	1250	0.192 ± 0.131	23.97 ± 16.31	6
2	1250	0.197 ± 0.053	24.58 ± 6.68	6.5
3	1250	0.199 ± 0.112	24.90 ± 13.97	6.5
4	1250	0.129 ± 0.019	16.08 ± 2.35	6.5
AVERAGE	1250	0.179 ± 0.034	22.38 ± 4.22	

1	2000	0.185 ± 0.026	36.91 ± 5.17	6
2	2000	0.102 ± 0.087	20.46 ± 17.39	6
3	2000	0.230 ± 0.083	46.02 ± 16.69	7
4	2000	0.081 ± 0.016	16.27 ± 3.16	8
AVERAGE	2000	0.150 ± 0.070	29.91 ± 13.95	

Data are presented as mean ± SD. For individual replicates, mean and SD were calculated using the permeability values determined at each of the six sampling timepoints. The average mean and SD were calculated using the means of the individual replicates. P_{eff}, *in situ* jejunal permeability

Table A.3 Effect of co-perfused nucleoside transporter inhibitors on the *in situ* jejunal permeability of 5 μM gemcitabine in C57BL/6 mice

Replicate #	Inhibitor	P_{eff} (x 10^{-4} cm/s)	Perfused Segment Length (cm)
1	None	1.40 ± 0.12	7
2	None	2.20 ± 0.12	6
3	None	2.18 ± 0.10	5.5
4	None	1.67 ± 0.08	6
AVERAGE	None	1.86 ± 0.39	
1	2 mM thymidine	0.0056 ± 0.0032	7
2	2 mM thymidine	0.0117 ± 0.0012	7
3	2 mM thymidine	0.0101 ± 0.0019	6
4	2 mM thymidine	0.0066 ± 0.0048	6.5
AVERAGE	2 mM thymidine	0.0085 ± 0.0029	
1	Na^+-free buffer	0.055 ± 0.007	7.5
2	Na^+-free buffer	0.065 ± 0.010	6.5
3	Na^+-free buffer	0.070 ± 0.008	6
4	Na^+-free buffer	0.048 ± 0.009	6.5
AVERAGE	Na^+-free buffer	0.059 ± 0.010	
Replicate #	**Inhibitor**	**Peff (x 10^{-4} cm/s)**	**Perfused Segment Length (cm)**
1	None	1.46 ± 0.06	7.5
2	None	1.48 ± 0.08	6.5
3	None	1.42 ± 0.07	8
4	None	1.50 ± 0.11	7
AVERAGE	None	1.47 ± 0.04	
1	2 mM dilazep	0.78 ± 0.16	7.5
2	2 mM dilazep	0.73 ± 0.07	7.5
3	2 mM dilazep	0.61 ± 0.06	7
4	2 mM dilazep	0.82 ± 0.16	5.5
AVERAGE	2 mM dilazep	0.74 ± 0.09	

Data are presented as mean ± SD. For individual replicates, mean and SD were calculated using the permeability values determined at each of the six sampling timepoints. The average mean and SD were calculated using the means of the individual replicates. Experiments with 2 mM thymidine and sodium-free buffer were performed months before those with 2 mM dilazep and, as a result, control values were reported for each set of experiments. P_{eff}, *in situ* jejunal permeability.

Table A.4 Total radioactivity in jejunal tissue and portal venous plasma following *in situ* jejunal perfusion of 5 μM [^{14}C]-gemcitabine in C57BL/6 mice

Replicate #	Inhibitor	Jejunal Tissue Gemcitabine Equivalents (pmol)/ mg tissue	Plasma Gemcitabine Equivalents (pmol)/ mL plasma	Perfused Segment Length (cm)
1	None	10.7	955.2	7.5
2	None	10.2	694.9	6.5
3	None	9.6	674.6	8
4	None	7.5	728.4	7
AVERAGE	None	9.52 ± 1.41	763.3 ± 129.9	
1	2 mM dilazep	10.7	213.8	7.5
2	2 mM dilazep	11.0	318.7	7.5
3	2 mM dilazep	8.3	229.9	7
4	2 mM dilazep	8.7	229.4	5.5
AVERAGE	2 mM dilazep	9.67 ± 1.36	248.0 ± 47.8	

Data are presented as mean ± SD.

Table A.5 Concentration-dependent thymidine- and dilazep-mediated inhibition of gemcitabine flux during *in situ* jejunal perfusion of 5 μM gemcitabine in C57BL/6 mice

Inhibitor	Inhibitor Concentration (μM)	Gemcitabine Flux (pmol/cm^2/s)	% of control
Thymidine	0	0.809	100.0
Thymidine	0.1	0.890	110.0
Thymidine	1	0.759	93.8
Thymidine	10	0.616	76.2
Thymidine	100	0.395	48.8
Thymidine	200	0.249	30.8
Thymidine	300	0.280	34.6
Thymidine	1000	0.081	10.0
Thymidine	2000	0.043	5.3
Dilazep	0	0.809	100.0
Dilazep	0.1	0.820	101.4
Dilazep	1	0.646	79.8
Dilazep	1	0.630	77.9
Dilazep	10	0.811	100.2
Dilazep	50	0.769	95.0
Dilazep	100	0.593	73.2
Dilazep	500	0.506	62.5
Dilazep	1000	0.476	58.9
Dilazep	2000	0.368	45.5
Dilazep	2500	0.364	45.0

Data are presented as mean (n = 1-4).

APPENDIX B

Individual Data from Chapter 4

Table B.1 The plasma concentration – time profiles of gemcitabine and dFdU in C57BL/6 mice following intravenous gemcitabine administration

	ID = GEMIV-WTF1		ID = GEMIV-WTF2	
Time(min)	**Gem (µM)**	**dFdU (µM)**	**Gem (µM)**	**dFdU (µM)**
2	47.1	8.87	58.2	6.22
5	37.6	10.6	41.7	9.80
15	23.5	17.3	34.4	15.9
30	12.3	22.2	15.8	18.1
45	7.40	22.0	10.8	18.9
60	4.41	20.2	7.38	16.6
90	1.27	17.4	2.40	12.7
120	0.551	13.2	0.814	10.3
180	0.407	9.11	0.261	6.30
240	0.126	6.37	0.146	4.43
300	0.160	5.38	0.075	2.66
360	0.057	4.98	BQL	1.84

	ID = GEMIV-WTM1		ID = GEMIV-WTM2	
Time(min)	**Gem (µM)**	**dFdU (µM)**	**Gem (µM)**	**dFdU (µM)**
2	47.3	4.02	AQL	7.73
5	41.1	5.83	82.8	9.19
15	24.4	9.93	58.6	12.2
30	14.6	11.3	33.3	11.0
45	8.41	10.7	13.2	9.55
60	5.18	9.8	9.46	7.13
90	1.62	6.63	4.34	4.76
120	0.657	4.84	1.43	2.34
180	0.162	2.31	0.464	1.36
240	0.0714	1.64	BQL	0.819
300	BQL	0.881	BQL	0.515
360	BQL	0.66	BQL	BQL

Gem, gemcitabine; dFdU, 2',2'-difluorodeoxyuridine; AQL, above the limit of quantification; BQL, below the limit of quantification

Table B.2 Non-compartmental analysis of the gemcitabine and dFdU plasma concentration-time profiles in C57BL/6 mice following intravenous gemcitabine administration

ID	$AUC_{0\text{-}6\ hr}$ (min x µM)	AUC_{inf} (min x µM)	% Extrapolated	$T_{1/2}$ (min)	T_{max} (min)	C_{max} (µM)	CL (mL/hr/g)	V_{ss} (mL/g)	Analyte
GEMIV-WTF1	1211.5	1217.1	0.5%	67.2	-	54.7*	3.75	2.10	Gem
GEMIV-WTF2	1619.6	1625.4	0.4%	53.8	-	72.7*	2.81	1.47	
GEMIV-WTM1	1294.1	1297.5	0.3%	33.4	-	51.9*	3.51	1.65	
GEMIV-WTM2	2718.4	2736.5	0.7%	27.1	-	98.4*	1.67	0.78	
GEMIV-WTF1	3941.8	5148.5	23.4%	168.0	30.0	22.2	-	-	dFdU
GEMIV-WTF2	2909.6	3165.9	8.1%	96.6	45.0	18.9	-	-	
GEMIV-WTM1	1448.9	1539.3	5.9%	95.0	30.0	11.3	-	-	
GEMIV-WTM2	1455.5	1516.7	4.0%	82.4	30.0	12.2	-	-	

*C0 (initial plasma concentration) reported. Gem, gemcitabine; dFdU, 2',2'-difluorodeoxyuridine; $AUC_{0\text{-}6hr}$, area under the plasma concentration-time curve from time 0 to 6 hr; AUC_{inf}, area under the plasma concentration-time curve from time 0 to infinity; $T_{1/2}$, terminal half-life; $T_{max,}$ time of maximum plasma concentration; $C_{max,}$ maximum plasma concentration; CL, clearance; $V_{ss,}$ volume of distribution at steady-state

Table B.3 The plasma concentration – time profiles of gemcitabine and dFdU in C57BL/6 mice following oral gemcitabine administration

	ID = GEMPO-WTF1		ID = GEMPO-WTF2	
Time(min)	**Gem (µM)**	**dFdU (µM)**	**Gem (µM)**	**dFdU (µM)**
2	3.59	4.85	1.39	2.33
5	6.67	10.9	3.06	6.57
15	13.6	29.4	6.06	17.2
30	13.9	39.4	5.90	25.3
45	12.8	40.6	4.89	24.8
60	10.3	37.3	5.06	24.6
90	3.77	26.3	2.21	20.4
120	0.991	19.6	0.703	19.7
180	0.148	13.1	0.151	16.1
240	BQL	10.4	BQL	15.9
300	BQL	9.53	BQL	13.1
360	BQL	8.68	BQL	10.2

	ID = GEMPO-WTM1		ID = GEMPO-WTM2	
Time(min)	**Gem (µM)**	**dFdU (µM)**	**Gem (µM)**	**dFdU (µM)**
2	0.990	1.64	2.03	2.55
5	1.96	4.78	3.06	4.44
15	5.51	12.9	8.75	16.4
30	8.00	25.8	13.1	31.1
45	7.97	30.9	13.4	37.2
60	6.48	30.0	11.4	35.9
90	4.60	23.3	7.64	30.1
120	2.67	16.2	10.6	49.1
180	0.551	11.1	1.93	15.4
240	0.188	8.22	0.381	7.98
300	0.118	7.79	0.184	6.28
360	BQL	5.85	0.103	5.94

Gem, gemcitabine; dFdU, 2',2'-difluorodeoxyuridine; BQL, below the limit of quantification

Table B.4 Non-compartmental analysis of the gemcitabine and dFdU plasma concentration-time profiles in C57BL/6 mice following oral gemcitabine administration

ID	$AUC_{0\text{-}6\ hr}$ (min x µM)	AUC_{inf} (min x µM)	% Extrapolated	$T_{1/2}$ (min)	T_{max} (min)	C_{max} (µM)	CL/F (mL/hr/g)	Analyte
GEMPO-WTF1	1016.7	1020.9	0.4%	19.4	30.0	13.9	13.4	Gem
GEMPO-WTF2	477.3	482.4	1.1%	23.4	15.0	6.1	28.4	
GEMPO-WTM1	775.5	782.3	0.9%	39.9	30.0	8.0	17.5	
GEMPO-WTM2	1647.3	1653.8	0.4%	43.7	45.0	13.4	8.3	
GEMPO-WTF1	6402.9	10342.0	38.1%	314.6	45.0	40.6	-	dFdU
GEMPO-WTF2	6079.0	9994.6	39.2%	266.1	30.0	25.3	-	
GEMPO-WTM1	4952.0	6419.9	22.9%	173.9	45.0	30.9	-	
GEMPO-WTM2	7142.8	8293.4	13.9%	134.3	120.0	49.1	-	

Gem, gemcitabine; dFdU, 2',2'-difluorodeoxyuridine; $AUC_{0\text{-}6hr}$, area under the plasma concentration-time curve from time 0 to 6 hr; AUC_{inf}, area under the plasma concentration-time curve from time 0 to infinity; $T_{1/2}$, terminal half-life; $T_{max,}$ time of maximum plasma concentration; $C_{max,}$ maximum plasma concentration; CL/F, oral clearance

Table B.5 The plasma concentration – time profiles of 5'-L-valyl-gemictabine, gemcitabine, and dFdU in C57BL/6 mice following intravenous 5'-L-valyl-gemictabine administration

	ID =PDIV-WTF1			ID =PDIV-WTF2		
Time(min)	**V-Gem (µM)**	**Gem (µM)**	**dFdU (µM)**	**V-Gem (µM)**	**Gem (µM)**	**dFdU (µM)**
2	7.97	40.7	10.9	13.6	38.8	13.9
5	2.62	31.0	13.7	2.94	25.2	17.4
15	0.577	13.5	14.6	0.259	13.4	20.0
30	0.0856	6.7	14.9	BQL	6.14	19.1
45	BQL	3.02	14.8	BQL	3.02	18.6
60	BQL	1.33	13.2	BQL	1.66	17.1
90	BQL	0.537	12.0	BQL	0.394	14.2
120	BQL	0.304	10.3	BQL	0.202	10.6
180	BQL	0.184	6.25	BQL	0.174	6.34
240	BQL	0.113	4.67	BQL	BQL	4.08
300	BQL	BQL	3.19	BQL	BQL	3.24
360	BQL	BQL	3.35	BQL	BQL	2.95

	ID =PDIV-WTM1			ID =PDIV-WTM2		
Time(min)	**V-Gem (µM)**	**Gem (µM)**	**dFdU (µM)**	**V-Gem (µM)**	**Gem (µM)**	**dFdU (µM)**
2	48.8	58.7	7.11	7.68	32.2	7.55
5	10.8	38.2	10.3	3.25	25.8	8.52
15	1.71	18.6	11.7	0.738	16.4	9.80
30	0.134	10.5	12.7	BQL	9.39	9.57
45	BQL	6.37	11.5	BQL	6.89	8.97
60	BQL	3.39	11.9	BQL	4.18	7.66
90	BQL	0.682	6.82	BQL	1.88	5.75
120	BQL	0.477	4.38	BQL	0.738	3.73
180	BQL	0.211	2.08	BQL	0.218	1.93
240	BQL	0.051	0.943	BQL	0.0510	0.840
300	BQL	BQL	1.07	BQL	0.0721	0.768
360	BQL	BQL	0.781	BQL	BQL	0.548

V-Gem, 5'-L-valyl-gemcitabine; Gem, gemcitabine; dFdU, 2',2'-difluorodeoxyuridine; BQL, below the limit of quantification

Table B.6 Non-compartmental analysis of the 5'-L-valyl-gemcitabine, gemcitabine, and dFdU plasma concentration-time profiles in C57BL/6 mice following intravenous 5'-L-valyl-gemcitabine administration

ID	$AUC_{0\text{-}6\ hr}$ (min x µM)	AUC_{inf} (min x µM)	% Extrapolated	$T_{1/2}$ (min)	T_{max} (min)	C_{max} (µM)	CL (mL/hr/g)	V_{ss} (mL/g)	Analyte
PDIV-WTF1	61.5	62.2	1.0%	5.1	-	16.7*	73.3	5.43	**V-Gem**
PDIV-WTF2	92.2	93.1	1.0%	2.4	-	37.8*	49.0	1.75	
PDIV-WTM1	348.0	348.7	0.2%	4.0	-	133.4*	13.1	0.61	
PDIV-WTM2	57.6	61.9	6.9%	4.0	-	13.6*	73.6	5.72	
PDIV-WTF1	691.6	703.1	1.6%	70.1	2	40.7	-	-	**Gem**
PDIV-WTF2	629.2	637.3	1.3%	32.4	2	38.8	-	-	
PDIV-WTM1	1013.0	1016.0	0.3%	40.5	2	58.7	-	-	
PDIV-WTM2	899.4	904.5	0.6%	49.3	2	32.2	-	-	
PDIV-WTF1	2811.9	3704.4	24.1%	184.7	30	14.9	-	-	**dFdU**
PDIV-WTF2	3159.2	3860.0	18.2%	164.7	15	20.0	-	-	
PDIV-WTM1	1532.4	1646.4	6.9%	101.1	30	12.7	-	-	
PDIV-WTM2	1216.3	1285.4	5.4%	87.4	15	9.8	-	-	

*C0 (initial plasma concentration) reported. V-Gem, 5'-L-valyl-gemcitabine; Gem, gemcitabine; dFdU, 2',2'-difluorodeoxyuridine; $AUC_{0\text{-}6hr}$, area under the plasma concentration-time curve from time 0 to 6 hr; AUC_{inf}, area under the plasma concentration-time curve from time 0 to infinity; $T_{1/2}$, terminal half-life; T_{max}, time of maximum plasma concentration; C_{max}, maximum plasma concentration; CL, clearance; V_{ss}, volume of distribution at steady-state

Table B.7 The plasma concentration – time profiles of 5'-L-valyl-gemictabine, gemcitabine, and dFdU in C57BL/6 mice following oral 5'-L-valyl-gemictabine administration

	ID =PDPO-WTF1			ID =PDPO-WTF2		
Time(min)	**V-Gem (µM)**	**Gem (µM)**	**dFdU (µM)**	**V-Gem (µM)**	**Gem (µM)**	**dFdU (µM)**
2	0.261	3.22	4.40	0.168	5.71	12.4
5	0.297	7.93	16.9	0.309	11.6	27.5
15	0.0708	10.9	39.3	BQL	10.8	46.6
30	0.0908	10.7	49.9	BQL	6.71	38.7
45	BQL	10.1	49.7	BQL	6.03	39.3
60	BQL	8.69	48.1	BQL	3.57	29.8
90	BQL	4.97	35.4	BQL	1.02	22.5
120	BQL	2.18	25.1	BQL	0.401	16.7
180	BQL	0.434	18.1	BQL	0.104	11.1
240	BQL	0.140	18.9	BQL	BQL	8.81
300	BQL	0.146	14.4	BQL	BQL	7.21
360	BQL	BQL	12.0	BQL	BQL	7.13

	ID =PDPO-WTM1			ID =PDPO-WTM2		
Time(min)	**V-Gem (µM)**	**Gem (µM)**	**dFdU (µM)**	**V-Gem (µM)**	**Gem (µM)**	**dFdU (µM)**
2	0.528	5.03	7.86	0.0741	1.25	2.43
5	0.405	10.2	20.9	0.0510	2.68	7.83
15	0.0753	14.6	46.6	0.0722	7.75	28.2
30	BQL	10.2	50.9	BQL	8.29	44.4
45	BQL	8.08	48.9	BQL	6.25	44.4
60	BQL	5.67	46.1	BQL	4.98	41.1
90	BQL	3.15	34.3	BQL	2.82	32.0
120	BQL	2.03	27.3	BQL	2.16	24.3
180	BQL	1.11	18.2	BQL	1.91	18.8
240	BQL	0.300	12.4	BQL	0.997	15.1
300	BQL	0.152	15.1	BQL	0.373	13.4
360	BQL	BQL	14.6	BQL	0.130	10.8

V-Gem, 5'-L-valyl-gemcitabine; Gem, gemcitabine; dFdU, 2',2'-difluorodeoxyuridine; BQL, below the limit of quantification

Table B.8 Non-compartmental analysis of the 5'-L-valyl-gemcitabine, gemcitabine, and dFdU plasma concentration-time profiles in C57BL/6 mice following oral 5'-L-valyl-gemcitabine administration

ID	$AUC_{0\text{-}6\ hr}$ (min x µM)	AUC_{inf} (min x µM)	% Extrapolated	$T_{1/2}$ (min)	T_{max} (min)	C_{max} (µM)	Analyte
GEMPO-WTF1	4.15	CND	CND	CND	5	0.30	**V-Gem**
GEMPO-WTF2	0.88	CND	CND	CND	5	0.31	
GEMPO-WTM1	4.33	CND	CND	CND	2	0.53	
GEMPO-WTM2	0.88	CND	CND	CND	2	0.07	
GEMPO-WTF1	989.4	997.6	0.8%	38.9	15	10.9	**Gem**
GEMPO-WTF2	547.9	552.0	0.8%	27.8	5	11.6	
GEMPO-WTM1	938.2	948.4	1.1%	46.8	15	14.6	
GEMPO-WTM2	830.1	838.7	1.0%	46.0	30	8.3	
GEMPO-WTF1	8823.9	13047.7	32.4%	244.0	30	49.9	**dFdU**
GEMPO-WTF2	5900.4	7905.3	25.4%	194.9	15	46.6	
GEMPO-WTM1	8709.8	13273.4	34.4%	216.7	30	50.9	
GEMPO-WTM2	7881.7	11187.1	29.5%	212.1	30	44.4	

V-Gem, 5'-L-valyl-gemcitabine; Gem, gemcitabine; dFdU, 2',2'-difluorodeoxyuridine; CND, could not be determined; $AUC_{0\text{-}6hr}$, area under the plasma concentration-time curve from time 0 to 6 hr; AUC_{inf}, area under the plasma concentration-time curve from time 0 to infinity; $T_{1/2}$, terminal half-life; $T_{max,}$ time of maximum plasma concentration; $C_{max,}$ maximum plasma concentration

APPENDIX C

Mechanisms of Gemcitabine Oral Absorption as Determined by *In Situ* Intestinal Perfusions in Mice

Biochemical Pharmacology 168 (2019) 57–64

Contents lists available at ScienceDirect

Biochemical Pharmacology

journal homepage: www.elsevier.com/locate/biochempharm

Mechanisms of gemcitabine oral absorption as determined by *in situ* intestinal perfusions in mice

Brian R. Thompson, Yongjun Hu, David E. Smith*

Department of Pharmaceutical Sciences, College of Pharmacy, University of Michigan, Ann Arbor, MI, USA

ARTICLE INFO

Keywords:
Concentrative nucleoside transporters
Equilibrative nucleoside transporters
Gemcitabine
Intestinal permeability
Saturation kinetics

ABSTRACT

Gemcitabine is a widely used chemotherapeutic drug that is administered via intravenous infusion due to a low oral bioavailability of only 10%. This low oral bioavailability is believed to be the result of gemcitabine's low intestinal permeability and oral absorption, followed by significant presystemic metabolism. In the present study, we sought to define the mechanisms of gemcitabine intestinal permeability, the potential for saturation of intestinal uptake, and the transporter(s) responsible for mediating the oral absorption of drug using *in situ* single-pass intestinal perfusions in mice. Concentration-dependent studies were performed for gemcitabine over 0.5–2000 μM, along with studies of 5 μM gemcitabine in a sodium-containing buffer ± thymidine (which can inhibit concentrative (i.e., CNT1 and CNT3) and equilibrative (i.e., ENT1 and ENT2) nucleoside transporters) or dilazep (which can inhibit ENT1 and ENT2), or in a sodium-free buffer (which can inhibit CNT1 and CNT3). Our findings demonstrated that gemcitabine was, in fact, a high-permeability drug in the intestine at low concentrations, that jejunal uptake of gemcitabine was saturable and mediated almost exclusively by nucleoside transporters, and that jejunal flux was mediated by both high-affinity, low-capacity (K_m = 27.4 μM, V_{max} = 3.6 pmol/cm^2/s) and low-affinity, high-capacity (K_m = 700 μM, V_{max} = 35.9 pmol/cm^2/s) transport systems. Thus, CNTs and ENTs at the apical membrane allow for gemcitabine uptake from the lumen to enterocyte, whereas ENTs at the basolateral membrane allow for gemcitabine efflux from the enterocyte to portal venous blood.

1. Introduction

Gemcitabine (2′,2′-difluoro-2′-deoxycytidine; dFdC) is a pyrimidine nucleoside analogue used in the treatment of various solid tumors [1–4]. Gemcitabine distribution and cellular uptake is mediated by the action of two evolutionarily unrelated transporter families: the concentrative nucleoside transporters (CNTs) and the equilibrative nucleoside transporters (ENTs), belonging to the solute carrier families 28 and 29, respectively [5,6]. Specifically, gemcitabine is a substrate of the pyrimidine selective transmembrane transporter CNT1 and the broadly selective purine and pyrimidine transmembrane transporters CNT3, ENT1, and ENT2 [7,8]. CNT1 and CNT3 function as concentrative and unidirectional sodium:substrate cotransporters, whereas ENT1 and ENT2 function as equilibrative and bidirectional sodium-independent transporters [9]. It has also been demonstrated that CNT3 can function as a proton:substrate cotransporter, albeit with altered transport activity and substrate specificity [10].

Following cellular uptake, gemcitabine undergoes phosphorylation events forming the active metabolites gemcitabine diphosphate (dFdCDP) and triphosphate (dFdCTP) [11]. dFdCTP is incorporated into DNA in place of the natural substrate deoxycytidine triphosphate, preventing chain elongation [12] and leading to apoptosis [13]. dFdCDP inhibits ribonucleotide reductase, depleting the pool of deoxynucleotide triphosphates and increasing dFdCTP incorporation into DNA [14]. Additional self-potentiating mechanisms have also been described [15].

Due to a low oral bioavailability of only 10% [16], gemcitabine is administered as an intravenous infusion, typically over 30 min at a dose of 1000–1250 mg/m^2 once per week [17]. The factors limiting gemcitabine's oral bioavailability have been explored in humans and mice.

Abbreviations: CNT1, concentrative nucleoside transporter 1; CNT3, concentrative nucleoside transporter 3; CNTs, concentrative nucleoside transporters; dFdC, 2′,2′-difluoro-2′-deoxycytidine (or gemcitabine); dFdCDP, gemcitabine diphosphate; dFdCTP, gemcitabine triphosphate; dFdU, 2′,2′-difluoro-2′-deoxyuridine; ENT1, equilibrative nucleoside transporter 1; ENT2, equilibrative nucleoside transporter 2; ENTs, equilibrative nucleoside transporters; IC50, half maximal inhibitory concentration; Peff, effective permeability; UPLC, ultra-performance liquid chromatography

* Corresponding author at: University of Michigan, College of Pharmacy, 428 Church Street, Ann Arbor, MI 48109-1065, USA.
E-mail address: smithb@med.umich.edu (D.E. Smith).

https://doi.org/10.1016/j.bcp.2019.06.013
Received 8 April 2019; Accepted 12 June 2019
Available online 14 June 2019
0006-2952/

APPENDIX D

Pharmacokinetics of Gemcitabine and its Amino Acid Ester Prodrug following Intravenous and Oral Administrations in Mice

Biochemical Pharmacology 180 (2020) 114127

Contents lists available at ScienceDirect

Biochemical Pharmacology

journal homepage: www.elsevier.com/locate/biochempharm

Pharmacokinetics of gemcitabine and its amino acid ester prodrug following intravenous and oral administrations in mice

Brian R. Thompson[a], Jian Shi[b], Hao-Jie Zhu[b], David E. Smith[a,*]

[a] Department of Pharmaceutical Sciences, College of Pharmacy, University of Michigan, Ann Arbor, MI 48109, USA
[b] Department of Clinical Pharmacy, College of Pharmacy, University of Michigan, Ann Arbor, MI 48109, USA

ARTICLE INFO

Keywords:
Bioavailability
Gemcitabine
PEPT1
Prodrug

ABSTRACT

Gemcitabine is an intravenously administered anti-cancer nucleoside analogue. Systemic exposure following oral administration of gemcitabine is limited by extensive first-pass metabolism via cytidine deaminase (CDA) and potentially by saturation of nucleoside transporter-mediated intestinal uptake. An amino acid ester prodrug of gemcitabine, 5′-l-valyl-gemcitabine (V-Gem), was previously shown to be a substrate of the intestinally expressed peptide transporter 1 (PEPT1) and stable against CDA-mediated metabolism. However, preliminary studies did not evaluate the *in vivo* oral performance of V-Gem as compared to parent drug. In the present study, we evaluated the pharmacokinetics and *in vivo* oral absorption of gemcitabine and V-Gem following intravenous and oral administrations in mice. These studies revealed that V-Gem undergoes rapid systemic elimination (half-life < 1 min) and has a low oral bioavailability (<1%). Most importantly, the systemic exposure of gemcitabine was not different following oral administration of equimolar doses of gemcitabine (gemcitabine bioavailability of 18.3%) and V-Gem (gemcitabine bioavailability of 16.7%). Single-pass intestinal perfusions with portal blood sampling in mice revealed that V-Gem undergoes extensive activation in intestinal epithelial cells and that gemcitabine undergoes first-pass metabolism in intestinal epithelial cells. Thus, formulation of gemcitabine as the prodrug V-Gem does not increase systemic gemcitabine exposure following oral dosing, due, in part, to the instability of V-Gem in intestinal epithelial cells.

1. Introduction

Gemcitabine (2′,2′-difluoro-2′-deoxycytidine; dFdC) is a nucleoside analogue approved for use in the treatment of pancreatic, non-small cell lung, ovarian, and breast cancer [1]. It is also used off-label for treatment of other cancer types such as biliary tract and bladder cancer [2–4]. Gemcitabine exerts its anti-cancer activity through incorporation of gemcitabine triphosphate into growing DNA strands, inhibiting DNA synthesis [5] and leading to apoptosis [6]. Various self-potentiating mechanisms, including gemcitabine diphosphate inhibition of ribonucleotide reductase [7], have been reported to augment gemcitabine cytotoxicity [8]. Gemcitabine is rapidly cleared from plasma (half-life = 42 – 94 min), mainly via cytidine deaminase (CDA)-mediated deamination of gemcitabine to 2′,2′-difluoro-2′-deoxyuridine (dFdU) [9]. The *in vivo* activity of dFdU is currently unclear, although some work has suggested it may contribute to gemcitabine cytotoxicity [10,11] and radiosensitization [12].

Gemcitabine has a low oral bioavailability of about 10% [13] and is, thus, administered via intravenous infusion, typically once per week at a dose of 1000 – 1250 mg/m^2 [1]. However, oral administration is generally preferred as it is more patient friendly, less invasive, and reduces the costs and complications associated with intravenous drug administration. Furthermore, oral gemcitabine administration would allow for greater flexibility in designing dosing schedules, enabling both metronomic gemcitabine dosing (*i.e.,* frequent low dose administration) and dosing which replicates gemcitabine pharmacokinetics following a prolonged intravenous infusion. There is evidence that such dosing schedules may lead to improvements in efficacy and/or reductions in toxicity [14–17].

Given the advantages of oral gemcitabine administration, much

Abbreviations: $AUC_{0\text{-}6hr}$, area under the plasma concentration–time curve from time 0 to 6hr; AUC_{inf}, area under the plasma concentration–time curve from time 0 to infinity; CDA, cytidine deaminase; C_0, initial plasma concentration at time 0; C_{max}, maximum plasma concentration; dFdU, 2′,2′-difluoro-2′-deoxyuridine; Gem, gemcitabine; NT, nucleoside transporters; PEPT1, peptide transporter 1; THU, tetrahydrouridine; $T_{1/2}$, half-life; T_{max}, time to reach the maximum plasma concentration; V-Gem, 5′-l-valyl-gemcitabine; V_{ss}, volume of distribution steady-state

* Corresponding author at: University of Michigan, College of Pharmacy, 428 Church Street, Ann Arbor, MI 48109-1065, USA.
E-mail address: smithb@med.umich.edu (D.E. Smith).

https://doi.org/10.1016/j.bcp.2020.114127
Received 13 May 2020; Received in revised form 23 June 2020; Accepted 25 June 2020
Available online 27 June 2020

APPENDIX E

Chemoproteomic Identification of Serine Hydrolase RBBP9 as a Valacyclovir-Activating Enzyme

molecular pharmaceutics

pubs.acs.org/molecularpharmaceutics Article

Chemoproteomic Identification of Serine Hydrolase RBBP9 as a Valacyclovir-Activating Enzyme

Vikram M. Shenoy,* Brian R. Thompson, Jian Shi, Hao-Jie Zhu, David E. Smith, and Gordon L. Amidon*

Cite This: *Mol. Pharmaceutics* 2020, 17, 1706−1714 Read Online

ACCESS | Metrics & More | Article Recommendations | Supporting Information

ABSTRACT: Prodrug discovery and development in the pharmaceutical industry have been hampered by a lack of knowledge of prodrug activation pathways. Such knowledge would minimize the risks of prodrug failure by enabling proper selection of preclinical animal models, prediction of pharmacogenomic variability, and identification of drug−drug interactions. Technologies for annotation of activating enzymes have not kept pace with the growing need. Activity-based protein profiling (ABPP) has matured considerably in recent decades, leading to widespread use in the pharmaceutical industry. Here, we report the extension of competitive ABPP (cABPP) to prodrug-activating enzyme identification in stable isotope-labeled cell lysates using a modified fluorophosphonate probe. Focusing on the antiviral ester prodrug valacyclovir (VACV), we identified serine hydrolase RBBP9 as an activating enzyme in Caco-2 cells via shotgun proteomics, validating the activity via the selective inhibitor emetine (EME). Kinetic characterization of RBBP9 revealed a catalytic efficiency ($k_{cat}{\cdot}K_M^{-1}$ = 104 $mM^{-1}{\cdot}s^{-1}$) comparable to that of BPHL, the only known VACV-activating enzyme prior to this work. EME incubation in wild-type and *Bphl*-knockout jejunum and liver lysates demonstrated the near-exclusivity of VACV activation by RBBP9 in the intestine. Additionally, these studies showed that RBBP9 and BPHL are the two major and coequal VACV-activating enzymes in the liver. Single-pass intestinal perfusions of VACV ± EME in mice showed EME coperfusion significantly inhibited the intestinal activation of VACV, implying the *in vivo* relevance of RBBP9-mediated VACV activation. We envision that others might use the cABPP approach in the future for global, rapid, and efficient discovery of prodrug-activating enzymes.

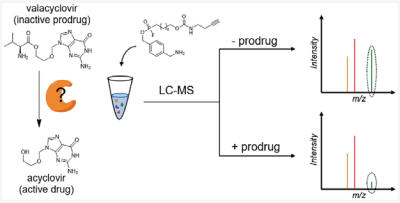

KEYWORDS: *prodrug-activating enzymes, valacyclovir, Caco-2, retinoblastoma binding protein 9 (RBBP9), activity-based protein profiling, biphenyl hydrolase-like (BPHL)*

INTRODUCTION

Prodrugs, latent chemical derivatives of drugs requiring *in vivo* activation to take effect, are often implemented as a late-stage strategy in drug development to improve drug candidates with excellent *in vitro* activity but poor *in vivo* performance. In most cases, enzymes are responsible for prodrug activation, yet their specific identities are rarely known. Prodrug-activating enzyme (PAE) identification is crucial for prodrug development as it enables the proper selection of preclinical animal models as well as prediction of pharmacogenomic variability and drug/food interactions. However, traditional PAE identification approaches like activity-guided fractionation are laborious, leaving much room for improvement.

Activity-based protein profiling (ABPP),[1] in which covalent active-site directed enzyme inhibitors attached to analyzable moieties are used to quantify or identify enzyme activities directly in complex proteomes, has recently been adapted to address this problem.[2] The activity-based probes (ABPs) utilized in ABPP can only inhibit enzymes with an accessible catalytic pocket, allowing for detection of competitive inhibitors and even substrates, such as prodrugs, by competitive ABPP (cABPP). The reactive portion of ABPs is often derived from mechanism-based inhibitors, making them selective for mechanistic enzyme classes but otherwise nonselective within that class, obviating the need for purified enzymes or tailored substrate assays.

Esters are the most prevalent choice for prodrug derivatization due to their synthetic simplicity and ease of activation by one of many nonspecific esterases in drug-metabolizing tissues such as the intestines, liver, and bloodstream.[3] Despite this, ester PAEs are relatively under-

Received: February 8, 2020
Revised: March 19, 2020
Accepted: March 20, 2020
Published: March 20, 2020

https://dx.doi.org/10.1021/acs.molpharmaceut.0c00131
Mol. Pharmaceutics 2020, 17, 1706−1714